ISSN 1408-7073

RMZ

MATERIALS AND GEOENVIRONMENT

MATERIALI IN GEOOKOLJE

Volume 53 Letnik

Ljubljana, November 2006

No. 3 Št.

RMZ - Materials and Geoenvironment
RMZ - Materiali in geookolje

Old title: Rudarsko-metalurški zbornik (Mining and Metallurgy Quarterly),
ISSN 0035-9645, 1952-1997.

Is issued quarterly by the *Faculty of Natural Science and Engineering, Ljubljana,* the *Institute for Mining, Geotechnology and Environment Ljubljana* and *Premogovnik Velenje, Velenje.*
Izdaja *Naravoslovnotehniška fakulteta Univerze v Ljubljani, Inštitut za rudarstvo, geotehnologijo in okolje Ljubljana in Premogovnik Velenje,* štirikrat letno.
Financially supported also by Ministry of Education, Science and Sport of Republic of Slovenia.
Pri financiranju revije sodeluje *Ministrstvo za šolstvo, znanost in šport Republike Slovenije.*

Editorial Office (Uredništvo):
Barbara Bohar Bobnar
Iztok Anželj
Nives Vukič
Digital Layout (Priprava za tisk):
Tomaž Sterniša s.p., Ljubljana
Print (Tisk): R-TISK d.o.o, Ljubljana

RMZ - Materials and Geoenvironment
Aškerčeva cesta 12, p.p. 312
1001 Ljubljana, R. Slovenija
Telefon: +386 (0)1 470 45 00
Telefaks: +386 (0)1 470 45 60

Indexation bases of RMZ-M&G: CA SEARCH-Chemical Abstracts, METADEX, GeoRef, Energy Science and Technology, PASCAL. Main of 23 bases registrated
Baze v katerih je RMZ-M&G indeksiran: CA SEARCH-Chemical Abstracts, METADEX, GeoRef, Energy Science and Technology, PASCAL. Najpomembnejši med 23 registriranimi

Naklada 300 izvodov. Printed in 300 copies.
Online Journal/Elektronska revija: http://www.rmz-mg.com
Letna naroč za posameznike: 4.000,00 SIT, za inštitucije: 8.000,00 SIT
Yearly subscribtion 20 EUR, institutions 40 EUR

Tekoči račun pri Novi Ljubljanski banki, d.d. Ljubljana:
UJP 01100-6030708186
Davčna številka: 24405388

ISSN 1408-7073

RMZ - MATERIALS AND GEOENVIRONMENT

PERIODICAL FOR MINING, METALLURGY AND GEOLOGY

RMZ - MATERIALI IN GEOOKOLJE

REVIJA ZA RUDARSTVO, METALURGIJO IN GEOLOGIJO

RMZ-M&G, Vol. 53, No. 3 pp. 285-417 (2006)

Ljubljana, November 2006

Historical Review

More than 80 years have passed since in 1919 the University Ljubljana in Slovenia was founded. Technical fields were joint in the School of Engineering that included the Geologic and Mining Division while the Metallurgy Division was established in 1939 only. Today the Departments of Geology, Mining and Geotechnology, Materials and Metallurgy are part of the Faculty of Natural Sciences and Engineering, University of Ljubljana.

Before War II the members of the Mining Section together with the Association of Yugoslav Mining and Metallurgy Engineers began to publish the summaries of their research and studies in their technical periodical Rudarski zbornik (Mining Proceedings). Three volumes of Rudarski zbornik (1937, 1938 and 1939) were published. The War interrupted the publication and not untill 1952 the first number of the new journal Rudarsko-metalurški zbornik - RMZ (Mining and Metallurgy Quarterly) has been published by the Division of Mining and Metallurgy, University of Ljubljana. Later the journal has been regularly published quarterly by the Departments of Geology, Mining and Geotechnology, Materials and Metallurgy, and the Institute for Mining, Geotechnology and Environment.

On the meeting of the Advisory and the Editorial Board on May 22nd 1998 Rudarsko-metalurški zbornik has been renamed into "RMZ - Materials and Geoenvironment (RMZ - Materiali in Geookolje)" or shortly RMZ - M&G.

RMZ - M&G is managed by an international advisory and editorial board and is exchanged with other world-known periodicals. All the papers are reviewed by the corresponding professionals and experts.

RMZ - M&G is the only scientific and professional periodical in Slovenia, which is published in the same form nearly 50 years. It incorporates the scientific and professional topics in geology, mining, and geotechnology, in materials and in metallurgy.

The wide range of topics inside the geosciences are wellcome to be published in the RMZ - Materials and Geoenvironment. Research results in geology, hydrogeology, mining, geotechnology, materials, metallurgy, natural and antropogenic pollution of environment, biogeochemistry are proposed fields of work which the journal will handle. RMZ - M&G is co-issued and co-financed by the Faculty of Natural Sciences and Engineering Ljubljana, and the Institute for Mining, Geotechnology and Environment Ljubljana. In addition it is financially suported also by the Ministry of Education Science and Sport of Slovenian Government.

Editor in chief

Table of Contents - Kazalo

Time - Dependent Processes in Rocks

Časovno odvisni procesi v kamninah

Jakob Likar[1], Gregor Vesel[1], Evgen Dervarič[2], Gregor Jeromel[2]

[1]Faculty of Natural Sciences and Engineering , University of Ljubljana,
Aškerčeva 12, 1000 Ljubljana, Slovenia;
E-mail: jakob.likar@ntf.uni-lj.si, gregor.vesel@ntf.uni-lj.si
[2]Velenje Lignite Mines, Partizanska 78, 3320 Velenje, Slovenia:
E-mail: evgen.dervaric@rlv.si, gregor.jeromel@rlv.si

Received: November 02, 2006 **Accepted**: November 14, 2006

Abstract: Time-dependent transformations in rocks, which occur primarily as a consequence of their natural properties, are a significant factor in the analysis of deformations developing during the construction of underground structures and afterwards. The excavation method used and the method of supporting an underground structure depend to a considerable degree on the intensity of the time development of deformations and their size.
The contribution analyzes the basic rheological models used for computational analyses of time-dependent displacements in the linings of underground structures using the so-called friendly cross sections, and provides a comparison between the measured and calculated displacement values. The exposure of a complex rock structure, which is a frequent occurrence in the construction of underground structures such as, for example, tunnels, is explained using back analyses. These are significant both from the perspective of proper selection of construction technology, and in cases when it is necessary to decide on the basic orientations to be used in the method of supporting a specific underground facility.

Izvleček: Časovno odvisne spremembe v kamninah, ki so posledica predvsem njihovih naravnih lastnosti, so pomemben dejavnik pri analizi deformacij, ki se razvijejo v času gradnje podzemnega prostora in po njej. Od intenzivnosti časovnega poteka razvoja deformacij in njihovih velikosti, je v veliki meri odvisen način izkopa in podpiranja podzemnega prostora.
V prispevku so analizirani osnovni reološki modeli, ki se uporabljajo za računske analize časovno odvisnih pomikov ostenj podzemnih prostorov s t.i. prijaznimi prečnimi profili in narejena primerjava med izmerjenimi in izračunanimi vrednostmi pomikov. Izpostavljenost kompleksne hribinske zgradbe, ki je pogosto primer pri gradnji podzemnih prostorov, kot npr. predorov, je pojasnjena s povratnimi analizami. Te so pomembne tako v pogledu pravilne izbire tehnologije gradnje, kakor tudi takrat, ko se je potrebno odločiti o osnovnih usmeritvah načina podpiranja določenega podzemnega objekta.

Key words: rheological models, time-dependent deformations, viscoelasticity, Permian-Carboniferous rocks
Ključne besede: reološki modeli, časovno odvisne deformacije, viskoelestičnost, permokarbonske kamnine

Scientific paper

INTRODUCTION

As is often the case in rock mechanics, a question that frequently arises with rheological models is how far we can go in applying various theories, developed on the basis of the elasticity or elastoplasticity theory, for the evaluation of actual occurrences in complex natural materials. Deformation occurrences in nature, including rocks, are often considerably more complicated than we can actually describe. That is why any progress towards such occurrences is encouraging and will pave the way for the scientific explanation of such processes.

A knowledge of time-dependent processes in rocks is highly significant from the engineering aspect. In our case, we have in mind those processes involving the time development of stress changes and deformations in the vicinity of underground structures. These processes, which are of long duration and may last for several days or even decades, affect the transformation and redistribution of stresses in the vicinity of the underground structures. One of the consequences of this is an increased load on the supporting system and the reduced stability of the structure, which in extreme cases may even lead to collapse.

Analyzing time-dependent processes in rocks and preparing evaluations of possible effects on the stability of an underground structure are of extreme importance in planning the construction schedule, selecting the appropriate supporting method, and ensuring the long-term stability of the structure. To determine or describe these processes, we frequently make use of various rheological models that are linked to individual parameters which can be determined on the basis of various procedures. These parameters may be determined in laboratories or with the help of back analyses, which is shown in this contribution. This paper is divided into an introductory theoretical part presenting basic information on time-dependent processes in rocks, and a practical part in which back analyses are used to determine the parameters of a simple linear, viscoelastic rheological model, which may be used to describe the time development of deformations while taking into account specific assumptions.

RHEOLOGICAL CHARACTERISTICS OF ROCKS

When calculating deformations in rocks in the vicinity of underground structures, equations are often used in which time does not appear as a variable and we have to content ourselves with so-called final deformations. Such cases are quite frequent and this method of calculating deformations may be completely satisfactory for the needs of standard dimensioning. However, one should be aware that no phenomena in nature is only of a momentary character, and that time is a parameter which can to a great degree influence the final result in rheologically sensitive rocks. In equations uniting the stresses and deformations of a deformable body, the introduction of an independent time variable leads to complicated mutual relations resulting in quite unfriendly mathematical solutions. Yet this method provides us with more detailed insight into the time development of deformations, which is of great significance in the construction of underground facilities with long-term use. There are some known cases in which insufficient attention was devoted to the investigation of such phenomena, neither in the period of designing a specific

structure, nor during the course of its construction. The long-term effects of such actions appeared even after ten or more years. The consequences of these influences were numerous rehabilitation works on facilities, in some cases even demolitions.

Today, the systematic investigation of time-dependent phenomena in rocks using numerical procedures and analyses enables better comparative analyses, particularly as regards considering no homogenity and anisotropy, which are frequently present in rocks. The rheology of rocks deals primarily with the following sub areas, which are thematically and conceptually oriented towards:

- searching for and analyzing the causes of the occurrence of time-dependent processes,
- the development and testing of rheological models and influential parameters for describing such processes,
- the method of determining influential parameters,
- searching for mathematical combinations presenting time-dependent processes, etc.

Causes of time changes in stress and deformations

The stresses and deformations occurring in the vicinity of underground facilities may change over time for various reasons. The most frequent among these are changes in loads or rock pressures occurring in and affecting rocks. Such cases occur, e.g. due to flowing strata waters (abundant precipitation, drainage), changes in the geometry of an excavated area (excavation round or gradual, phase construction of a specific type of facility), changes in size and additional loads on an area (construction of new structure in the immediate vicinity), changes in the deformation properties of rocks (weathering), and similar.

A specific example of time-dependent changes in rock stresses and deformations is represented by the viscose properties of rocks. The viscose behavior of rocks causes the material to gradually deform under constant load, depending on the time period, which may last several decades. This phenomenon is also known as creep, whose causes may be explained by two principal factors, i.e. rock mass yielding and the formation of cracks. Some rocks, such as rock salt, tar sands, compact shales, etc. creep at relatively small deviatory stresses, despite their uncracked or undamaged, intact base. In the case of rock salt, the creep process includes movement of dislocations and intercrystalline sliding; in unconsolidated clayey rocks, the creep process includes water migration and movements of clayey particles; bituminous rocks, such as tar sands, are characterized by rock mass yielding, which occurs in particular at higher temperatures. Even solid rocks such as granite and limestone may creep as the result of deviatory stress activity, resulting in the formation and growth of new cracks. A change in deviatory stress may cause changes in the crack network because, after the initial closing of cracks, the old cracks will expand once again and new cracks will appear. A specific example of time-dependent deformations is also rock swelling, which is characteristic of anhydrite, certain types of shales, grey clay, etc... All these factors cause rocks in the phase of additional load to undergo both momentary and delayed deformation, the latter of which is time-dependent. This kind of rock is therefore referred to as viscoelastic or viscoplastic,

provided the process occurs in a plastic area. Similar to elasticity, rocks can show different forms of nonlinearity, yet the majority of viscoelasticity theories are based on the treatment of rocks as a linear, viscoelastic material.

Creep, Dilatation and Compression

Two principal factors essentially influence the mode of deformation and, in the final phase, the collapse of the rock mass. One of these is determined by the geotechnical properties of rocks, while the other depends on the size and speed of loading. Both processes are time-dependent, which means that for a realistic definition of rocks, time is a crucial factor to be considered in constitutive equations presenting the association between deformations and stresses.

A typical time-dependent phenomenon found primarily in low-bearing-capacity and soft rocks is creep. Creep is defined as the irreversible deformation of rock mass in the period leading up to its collapse. In general, deformations resulting from creep depend primarily on three main parameters: time, temperature and stress.

The influence of time on the development of time deformations is evident from the creep curve, i.e. as time versus a specific axial deformation, which is schematically shown in Figure 1. As is evident in this figure, the initial elastic deformation is followed by primary creep with a decreasing speed of deformations, then secondary creep, where the change in deformations is constant and tertiary creep, where the speed of deformations increases until final collapse.

Temperature has a negative influence on the development of time deformations, as a rising temperature will increase the speed of creeping. An even greater influence on the development of time deformations is shown by load speed, which is reflected in the following facts:

- comparatively speaking, a higher load speed causes smaller deformations,
- a higher load speed gives a higher peak stress in smaller collapse deformations,
- the yield limit and creep phenomenon already occur at very small loads.

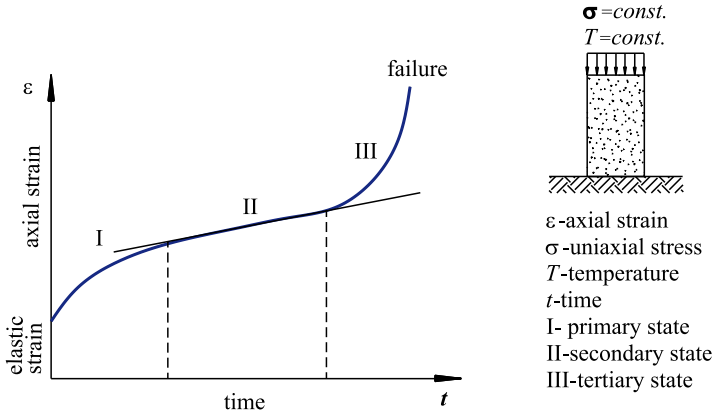

Figure 1. Typical time dependent creep curve
Slika 1. Značilna oblika krivulje lezenja

How the volume of a rock mass will deform in the creep phase depends on the stress state dominating the rock. This is because the volume deformation of a sample may be positive (compression) or negative (dilatation). In an area with smaller stresses, the volume diminishes (contracts) due to the contracting or closing of micro cracks and pores. Areas with higher stresses will witness the irreversible growth of volume, as new micro cracks begin to form and the existing ones begin to expand.

The compressibility and dilatation area obtained using the triaxial test is presented in Figure 2. In this figure, area D_c represents the compression area, and area D_d represents the dilatation area. The boundary between the two areas is called the dilatation limit.

Another interesting figure in addition to the above-mentioned is Figure 3, which shows the development of volume deformations during an unconfined pressure test on a rock sample. The decreasing volume is evident in the first nonlinear part due to the closing of micro cracks and pores. This is followed by the second, almost linear part between stresses *C* and *I*, with a reversible volume deformation. The last, nonlinear part is characterized by the opening and expansion of micro cracks, i.e. dilatation.

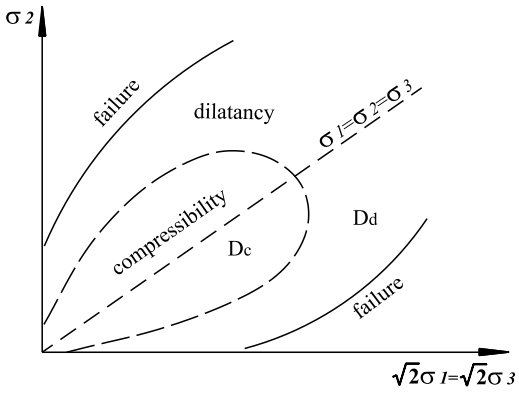

Figure 2. Domains of compressibility and of dilatancy
Slika 2. Območje stiskanja in dilatacije

Creep, Dilatation and Compression in the Vicinity of Tunnels

Knowledge of the dilatation and compression areas in the vicinity of underground structures is of essential importance in their design and construction. Two parameters significantly influence the size and distribution of an individual area. These are: the relation between the horizontal and vertical stress components (σ_h/σ_v), and the effect of the primary supporting system. On the basis of laboratory tests and field measurements, we have arrived at the following conclusions on the behavior of rocks in the vicinity of tunnels and other underground structures:

- a rock is much more unstable when it is $\sigma_h \neq \sigma_v$ than when it is $\sigma_h = \sigma_v$,
- the dilatation area diminishes substantially if the σ_h/σ_v ratio is higher and if the supporting is taken into account,
- creep is more rapid in the direction of the smallest soil pressure component,
- the convergence size depends on the σ_h/σ_v ratio, the height of the overburden, and the functioning of the supporting system.

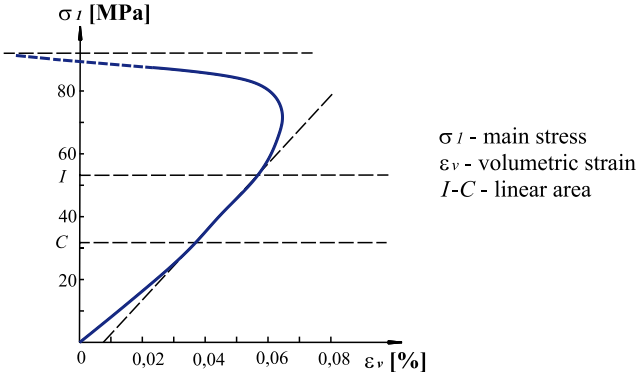

Figure 3. Stress strain curve showing dilatancy
Slika 3. Razvoj volumskih deformacij pri enoosnem tlačnem preiz-

Why is it important to have a knowledge of time-dependent deformations?

In the construction of underground structures, a knowledge of time-dependent deformations will enable the following:

- to select the proper rigidity of supporting,
- to determine the sequence of excavations and supporting,
- to predict a suitable time for incorporating the interior lining,
- to determine the course of increasing load on the supporting,
- to predict the period of eventual rehabilitation of the structure,
- to forecast the long-term stable shape and size of the underground structure,
- to determine the required over profile of the excavation,
- to determine the areas where collapse may occur due to excessive deformations, etc.

All the above-mentioned may be determined with some certainty, if, of course, we are able to correctly assess or forecast the time development of deformations. In doing so we shall have to consider the effect of interactions between the rock mass and supporting, as we are dealing with two materials (rock mass and supporting) that are both time-dependent, but do not behave in the same way in a specific time interval. In this contribution, we shall deal only with time-dependent processes in rocks that can be described using various rheological elements interconnected in various models. Burger's linear viscoelastic rheological model is presented in more detail below.

BURGER'S RHEOLOGICAL MODEL

The dependence of normal specific deformations on time, also referred to as creep curves, which are obtained in laboratory or field investigations, may be described using various rheological models. In this case we shall limit ourselves to linear viscoelastic rheological models comprised of two basic rheological elements. These are Hook's spring and Newton's vessel, which are interconnected in various ways and, through these interconnections, determine various rheological models. Several basic linear viscoelastic rheological

models are known, such as Maxwell's, Kelvin's, Generalized Maxwell's, Generalized Kelvin's, and Burger's model. The last mentioned is the most broadly accepted model in rock mechanics, as it best describes and presents the development of rock deformations in dependence of time.

Burger's rheological model is obtained as a consecutive link of Maxwell's and Kelvin's rheological models, as shown in Figure 4. One can see that the model has four rheological elements, whose notation is as follows:

- G_1: shear modulus, which controls the size of delayed elasticity,
- G_2: shear modulus, which defines the size of instantaneous elastic deformation,
- η_1: dynamic viscosity, which determines the stage of delayed elasticity,
- η_2: dynamic viscosity, which describes the stage of viscose yielding,
- γ_1, γ_2, γ_3: shear strains.

The response of time deformations with respect to the instantaneous and constantly active shear load τ, begins with the instantaneous elastic shear strain γ_1, followed by the exponentially diminishing shear strain γ_2, which then approaches the asymptote and continues into the constantly growing shear strain γ_3.

In addition to the shear stress τ, the sample may also be burdened with a normal load σ. By increasing (decreasing) this load, the sample measures the axial specific deformations ε, which is the laboratory procedure for determining the parameters of Burger's model. In this procedure, the cylindrical rock sample is subjected to a uniaxial pressure load by means of an instantaneous load σ_1, during which the time development of specific axial deformations ε_1 are measured. This is observed for as long as the creep curve does not approach the asymptote. The load is then increased and the procedure of strain measurement is repeated. The test is performed in several load stages, and for each stage a characteristic creep curve is obtained, as shown in Figure 5.

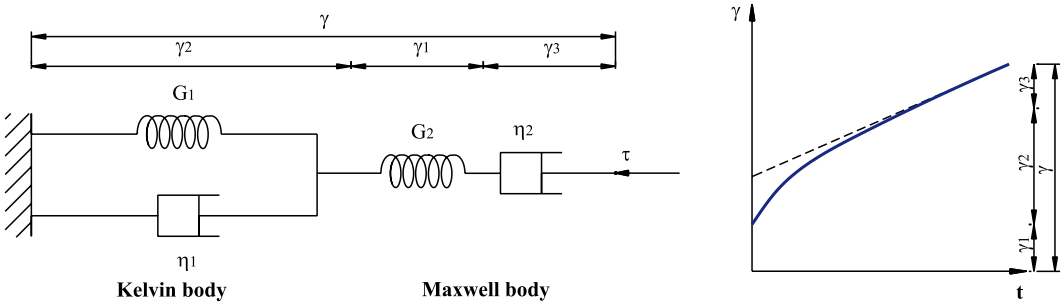

Figure 4. Burger`s rheological model and a diagram of shear strains γ versus time *t*
Slika 4. Burgerjev reološki model in diagram strižnih specifičnih deformacij γ v odvisnosti od časa *t*

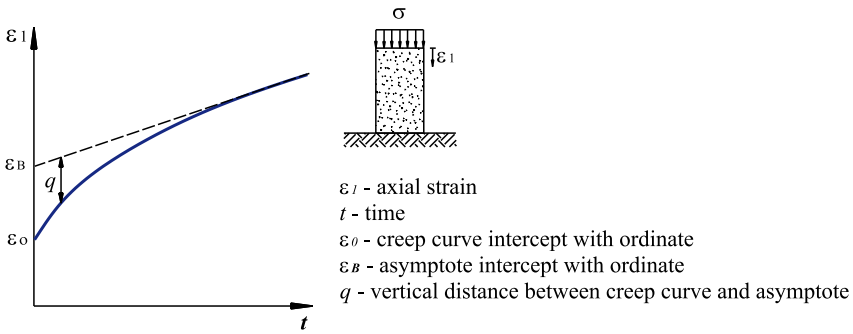

Figure 5. Time dependent curve of the axial strains
Slika 5. Krivulja osnih specifičnih deformacij v odvisnosti od časa *t*

The size of axial specific deformations by time $\varepsilon_1(t)$ for the relevant Burger's model, burdened with constant axial load σ_1, is presented using the equation:

$$\varepsilon_1(t) = \frac{2\sigma_1}{9K} + \frac{\sigma_1}{3G_2} + \frac{\sigma_1}{3G_1} - \frac{\sigma_1}{3G_1} \cdot e^{-(G_1 \cdot t/\eta_1)} + \frac{\sigma_1}{3\eta_2} \cdot t \tag{1}$$

In this equation, the compression module K is independent of time and is calculated using the equation $K = \sigma_1 / 3(\varepsilon_1 + 2\varepsilon_3)$. The sizes of axial ε_1 and transversal ε_3 strains are determined using resistance strain gages. The remaining parameters G_1, G_2, η_1 and η_2 are determined with the help of Figure 5 and the equations presented below. In this diagram, one can see that in time t=0, the curve bisects the ordinate at point ε_0, whereas in time $t \to \infty$ the curve approaches the asymptote, which has a gradient $\sigma_1 / 3\eta_2$ and bisects the ordinate at point ε_B. On the basis of this data, the following three parameters can be calculated:

$$\varepsilon_0 = \sigma_1 \left(\frac{2}{9K} + \frac{1}{3G_2} \right) \Rightarrow G_2 \tag{2}$$

$$\varepsilon_B = \sigma_1 \left(\frac{2}{9K} + \frac{1}{3G_2} + \frac{1}{3G_1} \right) \Rightarrow G_1 \tag{3}$$

$$\frac{\sigma_1}{3\eta_2} \Rightarrow \eta_2 \tag{4}$$

If, in the above diagram, the distance between the curve and the asymptote is designated by q, then at a given moment of time t the semi logarithmic diagram log q may be drawn in dependence of time t. In this diagram (Figure 5) we obtain a straight line, which is presented by the equation:

$$\log q = \log\left(\frac{\sigma_1}{3G_1}\right) - \frac{G_1}{2{,}3\cdot\eta_1}\cdot t \qquad (5)$$

The first part of the given equation represents the intersection point of the line and the ordinate, which gives value G_1, and the second part of the equation represents the line gradient, which gives value η_1.

$$\frac{G_1}{2{,}3\cdot\eta_1} \quad \Rightarrow \quad \eta_1 \qquad (6)$$

In practice, the rheological model shown above can be satisfactorily used in the majority of cases to describe the curve of so-called secondary creep all the way up to the limit of tertiary creep. If we wish to describe the process of time-dependent creep in rocks, taking into account the plastic deformations, a more complex model will need to be selected, which may also be obtained by connecting additional rheological elements. The deficiency of the linear viscoelastic rheological model is primarily in the fact that it cannot be used to describe the dilatational and compressive specific deformations linked to collapse mechanisms in rocks. In such cases, the elastic viscoplastic rheological model may be used to describe time occurrences in the plastic area as well.

Analysis of time-dependent deformations during tunnel construction in compressive low-bearing-capacity rocks

In the text below, the behaviour of a tunnel during its construction, which took place in rheologically highly sensitive rocks (Figure 6) with varying geotechnical properties, is compared with a computer model of the time development of displacements in the tunnel tube walls. A typical example of such rocks are Permian-Carboniferous layers, which are comprised primarily of

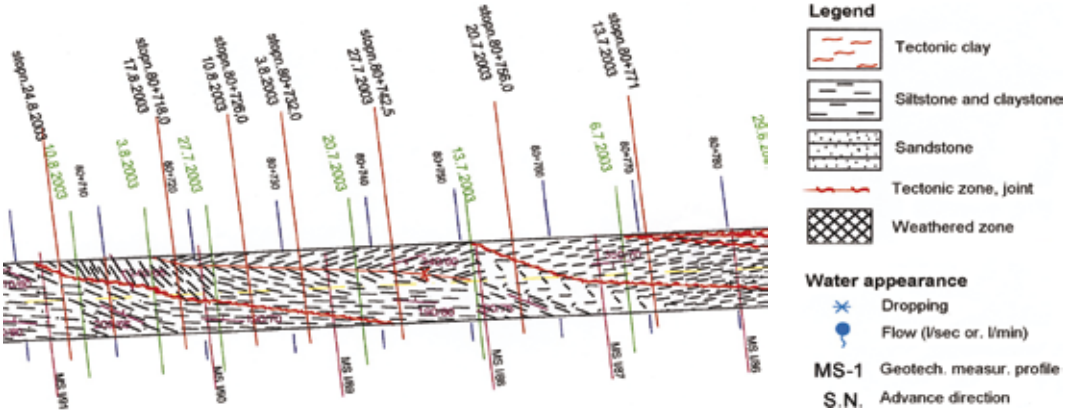

Figure 6. Geological site conditions of the covered area
Slika 6. Geološka sestava analiziranega območja

molded shaley claystones, tectonic clay and siltstones intercalated with various clay minerals, which in reality provide a physical basis for the interpretation of more or less intensive creep.

The description of time deformations is performed using an appropriate rheological model, but one should bear in mind that we are dealing with two time-dependent systems in interaction. These are the rock strata base as the principal medium, and the primary lining comprised of sprayed concrete and other supporting elements, such as rock bolts, steel supports, etc. In the case discussed, only the rheological properties of the rock mass have been taken into account, while the supporting system is treated as an elastic structural element comprised of sprayed concrete or supports.

In the analyzed practical example, equations were used within the scope of a simple analytical method, the so-called closed form solutions[1]. With the help of these equations and measured displacements of the roof measuring point in the tunnel tube, the rheological parameters of surrounding rocks in the analyzed profile were determined by means of a back analysis.

The procedure used in the above-mentioned analysis is based on the use of Burger's model and the Generalized Maxwell's model. Because the parameters of surrounding rocks were not known for the above-mentioned two models, a back analysis was used. Taking into account the actual variability and structural damage of Permian-Carboniferous rocks, and indirectly also the interwoven ness of their individual lithological types, the employed method of determining parameters has, in comparison with classical methods (laboratory, in situ with dilatometer or load plate), several advantages. These are the following:

- problem of acquiring adequate samples for conducting creep tests is eliminated,
- dependence of creep parameters on the structure of tested samples is also excluded, and
- application of laboratory-measured values of creep parameters on the broader rock mass areas is not necessary.
-

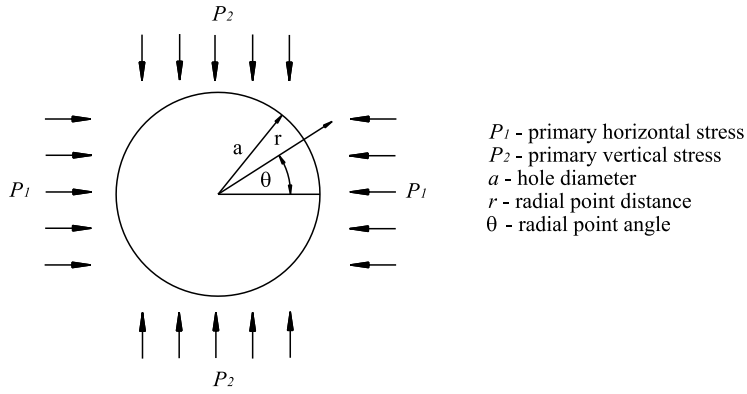

Figure 7. Cross section of an unlined tunnel tube
Slika 7. Shematski prikaz stanja pred vgradnjo primarne obloge v predorsko cev

The back analysis was conducted by dividing the curve of measured displacements in the analyzed profile into three parts, each of which was examined separately. For the entire displacement curve we therefore obtained:

- initial displacements occurring immediately after excavation (using Kirsch's equation for circular opening, Figure 7).
- displacements occurring in the period from the excavation of the calotte until the incorporation of the complete primary lining of the tunnel (using equations for describing the creep of rocks around the unsupported tunnel, Figure 7).
- displacements occurring after the completed incorporation of primary lining along the entire circumference of the tunnel tube (using equations for describing the creep of rocks around the supported tunnel, Figure 8).

For the curve of measured displacements, we took the measured vertical displacements in the left (south) tunnel tube, on the west part of the Trojane tunnel, at cross sections 86, 87, 88 and 89. Relevant data are available in the Report on geological and geotechnical monitoring of the Trojane tunnel excavation no.151[4]. It should be mentioned that an initial displacement u_0 was added to the measured displacements. This displacement is of the same size as the one used in the curve of calculated displacements. However, it is not included in the measured values, as it occurs before the incorporation of measuring points in the analyzed measuring profile. The equations used for the calculation of displacements are presented in[1] and have the following form:

Initial displacement:

$$u_0 = \frac{p\,a}{2G} \tag{7}$$

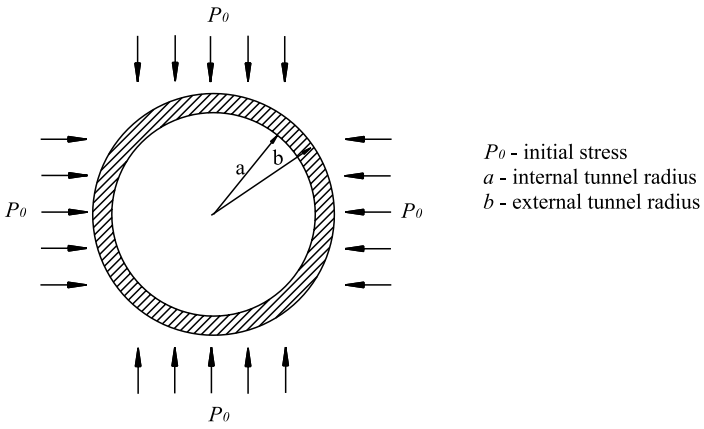

Figure 8. Cross section of a lined tunnel tube
Slika 8. Prikaz predorske cevi z vgrajeno primarno oblogo

An unlined tunnel displacement:

$$u_r(t)=\left[A+B\left(\frac{1}{2}-\frac{a^2}{4r^2}\right)\right]\left(\frac{1}{G_2}+\frac{1}{G_1}-\frac{1}{G_1}\ e^{-(G_1 t/\eta_1)}+\frac{t}{\eta_2}\right) \tag{8}$$

$$A=\frac{p_1+p_2}{4}\frac{a^2}{r} \tag{9}$$

$$B=(p_1-p_2)\frac{a^2}{r}\cos 2\theta \tag{10}$$

A lined tunnel displacement:

$$p_b(t)=p_0\left(1+Ce^{r_1 t}+De^{r_2 t}\right) \tag{11}$$

$$C=\frac{\eta_2}{G_1}r_2\left(\frac{r_1\left(1+\eta_1/\eta_2\right)+G_1/\eta_2}{(r_1-r_2)}\right) \tag{12}$$

$$D=\frac{\eta_2}{G_1}r_1\left(\frac{r_2\left(1+\eta_1/\eta_2\right)+G_1/\eta_2}{(r_2-r_1)}\right) \tag{13}$$

$$\eta_1 Bs^2+\left[G_1 B+\left(1+\frac{\eta_1}{\eta_2}\right)\right]s+\frac{G_1}{\eta_2}=0\Rightarrow r_1,r_2 \tag{14}$$

$$B=\frac{1}{G'}\left(\frac{(1-2\nu')b^2+a^2}{b^2-a^2}\right) \tag{15}$$

$$u_r=-\frac{b^2 r p_b\left(1-2\nu'+a^2/r^2\right)}{2G'\left(b^2-a^2\right)}\qquad for\quad a\le r\le b \tag{16}$$

$$u_r=-\frac{b^2}{r}p_b\left(\frac{(1-2\nu')b^2+a^2}{2G'\left(b^2-a^2\right)}\right)\qquad for\quad r\ge b \tag{17}$$

With the help of back analyses and the iteration of various parameters, η_1, η_2, G_1 and G_2, we obtained diagrams showing the measured and calculated vertical displacements of roof measuring points in the above-mentioned measuring cross profiles.

On the basis of calculations performed, diagrams shown (Figure 9) and relevant analyses, we may summarize as follows:

- The curve of measured values may be easily followed until approx. day 13, when the primary lining in the tunnel tube was completed. From here on the supported tunnel equation was used, in which we observed a sharp rise in displacements in dependence of time, followed by rapid stabilization.

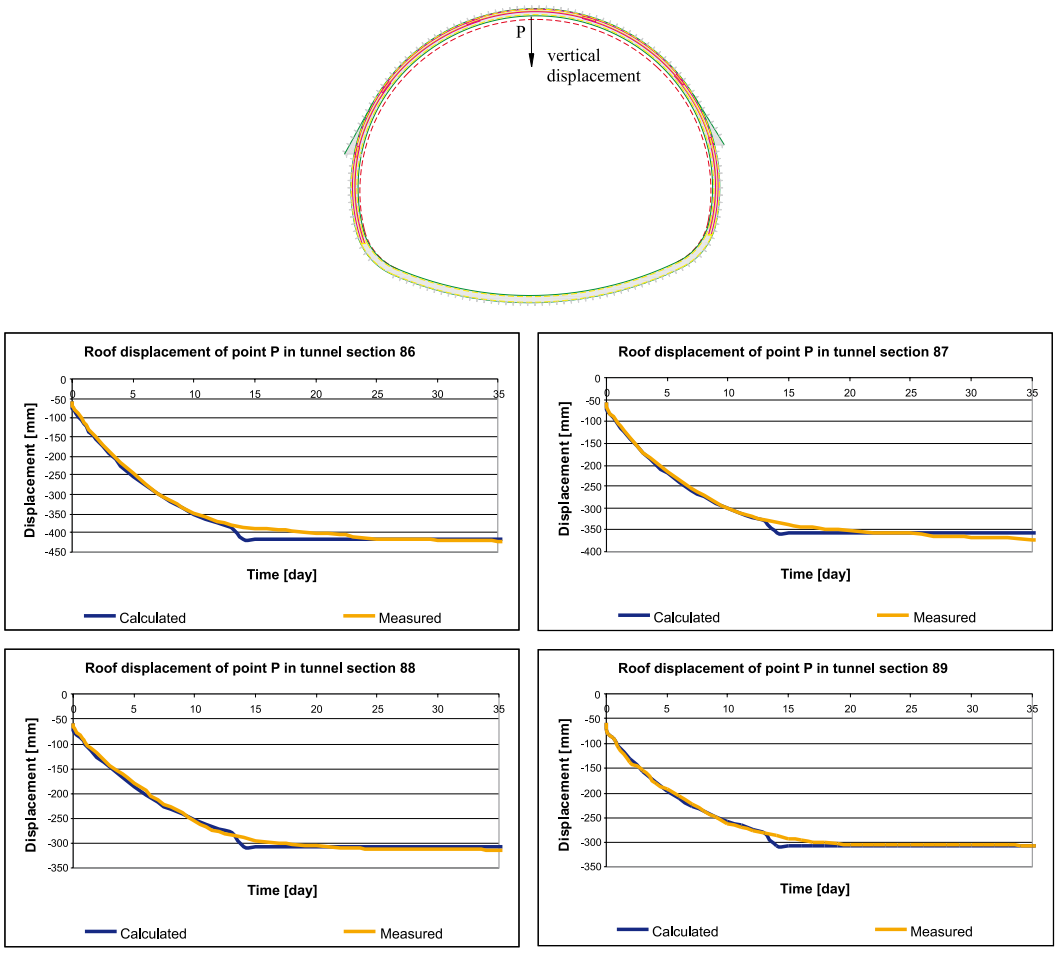

Figure 9. Comparison between measured and calculated vertical displacements of a roof point
Slika 9. Primerjava med izmerjenimi in izračunanimi pomiki stropne točke

- Since the phase of support creeping of primary lining was not taken into account in the supported tunnel equation, which means that its constant solidity and rigidity is assumed from the moment of incorporation, the description of displacements in this phase is not entirely realistic because a certain average value was used. This equation is thus applicable in cases when a tunnel is supported by prefabricated, reinforced concrete segments, which are frequently used in construction works where TBM machines (for cutting the entire tunnel profile) are used.
- The average values of rheological parameters for the above-mentioned profiles are: G_1=5,5MPa, G_2=115MPa, η_1=65000MPa·min, η_2=5,05·10^{8}MPa·min. It should be mentioned that the average maximum displacements in the analyzed area were approx. 360 mm.
- The established values of rheological parameters were considerably lower than those normally obtained in laboratory tests. It should be taken into account that the excavation of the tunnel tube was performed in a rock mass with low strength and deformability properties, which indirectly called for the immediate incorporation of supporting elements.
- It is evident from the measuring data that the curves of measured time-dependent displacement are of varying shape and size in the observed time period. This is due to the geological composition and structure of surrounding rocks, which are characterized by rapid changes both as regards the content of individual lithological components and the position of rock strata. In the given case, it was thus practically impossible to obtain representational rheological parameters of existing rocks in the laboratory.
- Based on the above-mentioned, we may conclude that describing the time development of deformations in rocks depends on a large number of influential factors which are difficult to include in calculations or whose interrelations are hard to determine. The procedure used in the given case may be suitable for the preparation of preliminary analyses of more simple cases of creep, which by their complexity do not surpass the cross section of an underground structure or the structure of the rock mass. Part of the complexity of a specific problem may be solved by means of numerical methods, which are available within the scope of complex software applications.

CONCLUSIONS

- Time-dependent processes in rocks which, depending on natural conditions, are more or less intensive play a significant role in the construction of underground structures. These processes indirectly influence the design and execution of construction works, including the supporting method, and have a long-term effect on the stability of the structure.
- Typical time-dependent occurrences in rocks often have the character of creeping soft and low-bearing-capacity rocks or rock mass containing soils.

- Typical rock masses with distinctive rheological properties are also Permian-Carboniferous layers, which can be found in several areas throughout Slovenia, such as in the Karavanke mountains, Idrija, Mežica, Trojane, Ljubljana (Golovec hill, Šentvid), and elsewhere.
- The presented practical example of the use of viscoelastic rheological models in the calculation of time-dependent displacements of tunnel tube walls has opened the question of the applicability of such calculations in practice.
- The analyzed comparisons between measured and calculated values of displacements professionally justify the presented calculation methods alongside sufficiently known simplifications and assumptions.
- Quick calculations coupled with practical experience are adequate bases for rough estimates of the method of primary supporting of underground structures being built in rheologically sensitive rocks.
- In describing the creeping of rock masses, it would be necessary to use, for supported underground structures, a more detailed equation that would also take into account the creep of a support system made of sprayed concrete cement or any other time-dependent support system.

Povzetek

Časovno odvisni procesi v kamninah

Poznavanje časovno odvisnih procesov v kamninah, je z inženirskega vidika zelo pomembno. V mislih imamo procese, ki zajemajo časovni razvoj napetosti in deformacij v hribinah in okolici podzemnih objektov. Ti procesi, ki so dolgotrajni in se lahko odvijajo več dni ali celo desetletij, vplivajo na spremembe in prerazporeditve napetosti v hribinah v katerih so zgrajeni podzemni prostori. Posledice tega so med drugim povečanje obremenitev podpornega sistema oz. zmanjšanje stabilnosti objekta, kar v skrajnem primeru lahko privede celo do porušitve.

Dejavnike, ki povzročajo omenjene spremembe napetosti in deformacij v kamninah gre pripisati različnim vzrokom. Med najpogostejše štejemo spremembe obtežb ali hribinskih pritiskov, ki delujejo v kamninah in so lahko posledica pretakanje vode, spremembe geometrije izkopanega prostora, preperevanja in podobno. Drugi pomembni dejavnik, ki prav tako povzroča časovno odvisne procese v kamninah pa je lezenje, čigar vzroke lahko razložimo s tremi glavnimi vplivi. To so plastično tečenje hribinskih mas, širjenje vezanih in nastajanje novih razpok ter nabrekanje. Vsi ti dejavniki povzročajo, da kamnine v fazi dodatne obremenitve, poleg trenutne deformacije, kažejo tudi zakasnelo – časovno odvisno deformacijo, ki je lahko različno velika tako po obsegu kot tudi po času trajanja. Kamnine ali širše gledano hribine, ki imajo te lastnosti, imenujemo viskoelastične oz., v kolikor se ti procesi odvijajo v plastičnem območju, tudi viskoplastične.

Poznavanje časovno odvisnih sprememb deformacijsko napetostnega polja v okolici podzemnih objektov, je z vidika načrtovanja in gradnje podzemnih objektov velikega pomena, saj nam omogoča pravilnejšo izbiro togosti podporja, določitev zaporedja izkopa in podpiranja, napovedovanje primernega časa vgradnje notranje obloge, določiti potek naraščanja obremenitve podporja, določiti potreben nadprofil izkopa prostora, itd.

Eno od pomembnih področij znanstvene vede, ki je se ukvarja s časovno odvisnimi procesi v hribinah, je tudi razvoj in preizkušanje reoloških modelov, s katerimi opisujemo časovno odvisne napetostno deformacijske spremembe v hribinskih sistemih. V pričujočem delu smo se omejili na linearne viskoelastične reološke modele, med katerimi je Burgerjev model dobro uporaben v mehaniki kamnin.

Ta model je določen z zaporedno vezavo Maxwellovega in Kelvinovega reološkega modela. Lastnosti modela podajata dva elastična in dva viskoelastična parametra G_1, G_2, η_1 in η_2, katere določimo s pomočjo krivulje lezenja, dobljene na osnovi laboratorijskih oz. in-situ raziskav. Poznavanje omenjenih parametrov, lahko uporabimo za napovedovanje časovnega razvoja deformacij hribine, izpostavljene določenemu napetostnemu stanju ali spremembi napetosti.

Ker je določitev viskoelastičnih parametrov v laboratoriju oz. in-situ v posameznih primerih lahko vprašljiva, se v ta namen pogostokrat poslužujemo povratne analize, kjer se na osnovi poznanih oz. izmerjenih vrednosti npr. pomikov določenih točk ostenja podzemnega prostora, z iteriranjem poišče iskane realne vrednosti. Ta način dela je prikazan tudi v pričujočem prispevku, kjer smo s pomočjo povratne analize poiskali viskoelastične parametre za Burgerjev in posplošeni Maxwellov model. Navedena reološka modela se uporabljata za napovedovanje časovnega razvoja deformacij nepodprtega in podprtega predora krožnega prereza.

Enačbe omenjenih modelov so podane v[1] in spadajo v kategorijo t.i. preprostih analitičnih enačb zaprte oblike. Ker gre za analitične enačbe, ki opisujejo dogajanje v okolju, ki je izjemno kompleksno in odvisno od številnih parametrov, seveda ni za pričakovati popolnega ujemanja med napovedanimi in izmerjenimi vrednostmi. V pričujočem prispevku je obdelana tematika, ki obravnava v kolikšni meri so omenjene enačbe za napovedovanje časovnega razvoja deformacij nepodprtega in podprtega predora uporabne ter kolikšne so vrednosti viskoelastičnih parametrov analiziranega območja.

Analizirano območje, skozi katero je potekala gradnja predora sestavljajo permokarbonske kamnine, med katerimi prevladujejo pregneteni skrilavi glinavci, tektonska glina in meljevci z različnimi vsebnostmi mineralov glin. Omenjene kamnine imajo izrazite reološke lastnosti in jih lahko srečamo širom Slovenije, kot npr. v Karavankah, Idriji, Mežici, Trojanah, Ljubljani (Golovec, Šentvid) in drugod.
Povratna analiza je potekala tako, da smo s pomočjo iteriranja dosegli ujemanje med krivuljo izračunanih in krivuljo izmerjenih pomikov. Krivuljo izračunanih pomikov smo dobili kot vsoto treh različnih pomikov, katere podajajo tri različne enačbe. To so začetni elastični pomik, viskoelastični pomik nepodprtega predora in viskoelastični pomik podprtega predora. Za krivuljo poz-

nanih vrednosti pa smo privzeli izmerjene vertikalne pomike ostenja predora v štirih zaporednih prečnih profilih na analiziranem odseku predorske cevi.

Na osnovi primerjave rezultatov in oblike krivulj lahko ugotovimo, da enačba časovnih deformacij nepodprtega predora lepo sledi izmerjenim pomikom, dočim pri uporabi enačbe podprtega predora pride do manjšega odstopanja. Vzrok slednjemu je dejstvo, da imamo v našem primeru opravka z dvema časovno odvisnima materialoma, to je hribino in podporjem. Ker v enačbi podprtega predora ni upoštevana faza lezenja podporja oz. primarne obloge, kar pomeni, da je privzeta njegova konstantna trdnost in togost od trenutka vgradnje, opisovanje pomikov za to fazo ni povsem realno, saj upoštevamo določeno povprečno vrednost. Enačba za izračun pomikov podprtega dela predora je zato bolj uporabna v primeru podpiranja predora s prefabriciranimi armirano betonskimi segmenti, kateri se pogosto uporabljajo pri gradnjah z uporabo strojev za rezanje celotnega profila predora (TBM).

Absolutne velikosti viskoelastičnih parametrov imajo precej nižje vrednosti, kot jih dobimo iz laboratorijskih preiskav. Upoštevati je potrebno dejstvo, da je izkop predorske cevi potekal v izjemno heterogeni hribini z nizkimi trdnostnimi in deformabilnostnimi lastnostmi, kar je posredno narekovalo takojšnjo vgradnjo podpornih elementov. Poleg tega je omenjeno dejstvo povezano tudi z geološko sestavo in strukturo okoliških hribin, za katere je značilno hitro spreminjanje tako glede zastopanosti posameznih litoloških členov, kot tudi glede lege hribinskih plasti.

Iz vsega podanega lahko povzamemo, da je opisovanje časovnega razvoja deformacij v hribinah povezano z velikim številom vplivnih dejavnikov, ki jih je v izračunih težko v popolnosti zajeti in poiskati njihove medsebojne povezave. Postopek, ki je bil uporabljen v obravnavanem primeru, je uporaben za izdelavo preliminarnih analiz enostavnejših primerov lezenja, ki po svoji kompleksnosti ne presegajo niti oblike prečnega profila podzemnega prostora niti strukture hribinske zgradbe. Del kompleksnosti določenega problema, ki je prisoten pri analiziranju časovno odvisnih pojavov pri gradnji podzemnih prostorov, je rešljiv z numeričnimi metodami, ki so danes na voljo v sklopu zahtevnih programskih orodij.

References

[1] Richard E. Goodman: Introduction to Rock Mechanics, 2nd edition, New York, 1989;
[2] N. Cristescu: Rock Rheology, Dordrecht, 1989;
[3] B.H.G Brady & E.T. Brown: Rock Mechanics For Underground Mining, 2nd edition, Dordrecht, 2004;
[4] Geološka in geotehnična spremljava izkopa predora Trojane; Izvajalec del: Grassetto S.p.A,-151 poročilo, Ljubljana, 2003;

Možnost izvedbe visokotlačnega podzemnega skladišča zemeljskega plina na območju Rudnika Senovo

High Pressure Storage of Gas in Area of Coal Mine Senovo

Željko Vukelić[1], Željko Sternad[2], Vladimir Vukadin[2], Franc Čadež[2], Marjan Hudej[3], Ivan Pečovnik[3]

[1]Naravoslovnotehniška fakulteta, Aškerčeva 12 Oddelek za geotehnologijo in rudarstvo, 1000 Ljubljana, Slovenija; E-mail: zeljko.vukelic@ntf.uni-lj.si
[2]Inštitut za rudarstvo, geotehnologijo in okolje, Slovenčeva 93, 1000 Ljubljana, Slovenija; E-mail: zeljko.sternad@i-rgo.si, vladimir.vukadin@i-rgo.si
[3]RGP, Rudarska 6, 3320 Velenje, Slovenija; E-mail: marjan.hudej@rlv.si, ivan.pecovnik@rlv.si

Received: November 05, 2006 **Accepted**: November 14, 2006

Povzetek: V članku smo predstavili možnost izgradnje podzemnega skladišča zemeljskega plina (PSZP) v karbonatnih kamninah na področju rudnika Senovo. Področje je bilo geološko preiskano. Izvedenih je bilo pet strukturnih vrtin do maksimalne globine 279 m. Jedro iz vrtin je bilo popisano s poudarkom na stratigrafiji, razpokah, tektonskih prelomov, RQD …., vzeto pa je bilo veliko število vzorcev za laboratorijske preiskave. V vrtinah smo izvedli geofizikalne, presiometrične in hidrogeološke preiskave. S preiskavami smo potrdili območje (cca. 16,000 m^2), kjer je pod globino površine 150 m, možno izdelati do štiri komore za podzemno skladišče zemeljskega plina.

Abstract: A paper for underground storage of gas (PSZP) in carbonate rocks was carried out in the area belonging to the Senovo mine. The area was geological surveyed and in addition five structural boreholes were drilled up to the depth of 279 m. The cores were logged with emphasis on stratigraphy, layering, rock joints, tectonic zones, RQD and addition characteristics samples were taken for the laboratory investigations. In boreholes geophysical, pressiometric and hydrogeological investigations were also carried out. The results of the investigations have revealed the occurence of a rock volume (area of 16.000 m^2) of 150 m where the geological and geotechnical conditions are appropriate for construction of several (up to 4) gas chambers for underground storage of gas.

Ključne besede: podzemno skladišče zemeljskega plina (PSZP), karbonatne kamnine, prevlečena podzemna komora
Key words: underground storage of gas (PSZP), carbonate rocks, The Lined Rock Cavern

Uvod

Slovenski plinovodni sistem ima skladišča zemeljskega plina zakupljena v tujini. Termoelektrarna Brestanica (TEB) je eden večjih porabnikov zemeljskega plina v Sloveniji , s svojim načinom delovanja kot tipična konična elektrarna z velikimi urnimi in dnevnimi odjemi, pa povzroča v relativno majhnem plinovodnem omrežju precejšnje težave, posebno še v zimskem času. Takrat se pojavljajo zaradi velikega odjema plina

Scientific paper

tudi omejitve pri obratovanju TEB. Tako smo v letu 2005 pričeli s terenskimi in laboratorijskimi raziskavami na področju Rudnika Senovo v zapiranju. Raziskave so vsebovale geološko kartiranje površine, strukturno vrtanje petih globokih vrtin na jedro, terenske geotehnične meritve v vrtinah (presiometer, geofizikalne meritve, hidrogeološke meritve) in laboratorijske preiskave jedra vrtin za določitev njihovih geomehanskih parametrov. Na območju , kjer smo opravili raziskave prevladujejo apnenci, dolomiti in breče. Z opravljenimi raziskavami smo potrdili možnost izgradnje visokotlačnega podzemnega skladišča zemeljskega plina (PSZP) po tehnologiji LRC (Lined Rock Cavern). Pri PSZP se najprej izdelajo trije pristopni tuneli v treh različnih nivojih. Po izvedbi pristopnih tunelov se prične z izkopom podzemne komore projektiranih dimenzij. Nato se izvede jekleni plašč komore (debelina plašča obloge je 10 - 15 mm). Prostor med hribino in jeklenim plaščem se zalije z betonom. Podzemna komora je s površino povezana z vertikalnim jaškom v katerem so cevi za polnjenje, hlajenje in praznenje plina iz podzemnega skladišča. Na površini je objekt s pripadajočo elektro-strojno opremo, ki zavzema površino 350 m x 300 m. Tehnologija izgradnje je povzeta po projektu PSZP na Švedskem, kjer tako skladišče že obratuje s tem, da je skladišče izdelano v granitnih kamninah.

Opis tehnologije LRC podzemnega skladišča plina

Na švedskem so od leta 1960 intenzivno raziskovali možnost za izgradnjo visokotlačnega podzemnega skladišča plina.[1] Raziskave so bile usmerjene predvsem v možnost skladiščenja v globokih vodonosnikih in opuščenih vrtinah za nafto in plin. Ker se je izkazalo, da v omenjenih variantah ni možno skladiščiti plina, so zadnjih dvajset let intenzivno raziskovali v smeri LRC (The Lined Rock Cavern – z oblogo prevlečen podzemni prostor/ skladišče). Tako danes obratuje podzemno skladišče v Skallenu od začetka leta 2003.

LRC demonstracijski projekt je izveden blizu obalnega mesta Halmstad na severozahodnu Švedske. Objekt leži blizu glavnega plinovoda, ki poteka ob zahodni obali Švedske in ima odlično izhodišče za oskrbo trga s plinom. Gradnja skladišča se je pričela leta 1998.

Načrtovanje LRC podzemnega skladišča in izgradnja skladišča

Podzemna komora izkopa je bila načrtovana s strani strokovnjakov NCC iz Göteborga v sodelovanju z investitorjema Sydkraft in Gaz de France. Projekt je izveden na podlagi več letne študije, ki je definirala LRC (angl. Lined Rock Cavern, sl. Prevlečena podzemna komora) koncept. Načrt podzemnega skladišča je bil skrbno pregledan in odobren s strani švedskega pooblaščenega vladnega organa. Obenem so LRC koncept revidirali strokovnjaki ameriškega Ministrstva za energijo in ga predstavili kot možno opcijo za ameriško tržišče. Rezultati revizije so vzdržali presojo o izvedljivosti projekta in so predstavljeni v letnih poročilih ameriškega Ministrstva za energijo (U.S. Department of Energy,2001; U.S. Department of Energy,2002).

PSZP je izdelano v granitnih kamninah. Izvedba skladišča, od podzemne gradnje, pa do inštalacije elektro-strojne opreme,

Preglednica 1. Dimenzije podzemne komore
Table 1. Dimension of storage cavern

Skupni volumen plina	**10 MNm^3**
Volumen skladišča	**40 000 m^3**
Premer skladišča	**37 m**
Višina skladišča	**50 m**
Tlak	**200 bar**
Globina skladišča pod površino	**115 m**
Čas polnjenja skladišča	**20 dni**
Čas praznjenja skladišča	**10 dni**

je trajala približno 4 leta. Ker je šlo v tem primeru za razvojni projekt je gradnja trajala nekoliko dlje kot bi bilo to pri običajni izgradnji tovrstnega skladišča (predvidoma dve leti). Pri podzemnem skladišču plina se najprej izdela pristopni tunel, ki je povezan s tremi pristopnimi tuneli v treh različnih nivojih. Tuneli so namenjeni za transport materiala med izgradnjo podzemne komore. Po izvedbi pristopnih tunelov se prične z izkopom podzemne komore projektiranih dimenzij (slika 1, preglednica 1). Na površini je objekt s pripadajočo elektro-strojno opremo, ki zavzema površino 350 x 300 m.

Izdelava podzemne komore oziroma podzemnega skladišča se je pričela z izkopom dostopnih tunelov. Tuneli in komora so izkopani v gnajsu. Najprej je bila izkopana zgornja kalota komore. Nato so nadaljevali z izkopom do dna komore. Izkop se je izvajal z miniranjem. Po končanem izkopu komore so na stene pritrdili drenažen cevi in jih zaščitili z brizganim betonom.

Po izkopu komore so pričeli znotraj komore z montažo prosto stoječe jeklene obloge - posode. Jeklena obloga je varjena in je sestavljena iz prefabriciranih jeklenih plošč povprečne debeline 12 mm. Izjemen poudarek je bil na izvedbi varjenja in kvaliteti jeklene obloge. Zvari jeklenih plošč so bili 100 % pregledani z neporušitvenimi metodami. Vso varjenje in kontrola zvarov je bila opravljen do zaključka izdelave obloge. Vertikalna dvigala so bila uporabljena za dviganje posode.

Zadnja faza izgradnje PSZP je bilo polnjenje prostora med jekleno oblogo in steno izkopane komore z betonom. Uporabljen je bil kvaliteten beton, ki ga ni bilo potrebno vibrirati. Posoda se je naponila z vodo tako, da se je vzpostavilo hidrostatično ravnovesje med samim polnjenjem prostora med jekleno oblogo in steno izkopane komore z betonom.

Podzemna komora je povezana s površino v vertikalnim jaškom, ki je bil izvrtan. V jašku so jeklene cevi za polnjenje in praznjenje skladišča plina. Oprema za vtiskanje plina v podzemno skladišče je enaka opremi kot se uporablja pri podzemnih skladiščih plina, ki so izdelani v opuščenih rudnikih soli.

PSZP je vodeno iz kontrolne sobe, ki je na površini in bo v bodoče povezano s centralnim kontrolnim objektom plinovodnega omrežja v Malmöju na Švedskem.

Izgradnja PSZP je bila končana poleti 2002. Po izgradnji so pričeli s testiranjem podzemnega skladišča in obremenjevanjem komore s tlakom do 22 MPa. Izvajali so monitoring hribine in jeklene obloge podzemnega skladišča med obremenilnimi testi. Preliminarne raziskave so pokazale, da so deformacije hribine in jeklene obloge nekoliko nižje kot so jih predvideli pri načrtovanju objekta.

V začetku leta 2003 so vključili podzemno skladišče plina v plinovodno omrežje Švedske.

GEOLOŠKE RAZMERE V OKOLICI RUDNIKA SENOVO V ZAPIRANJU

Podatki pridobljeni z geološkim kartiranjem ter geološkim popisom jedra vrtin, potrjujejo

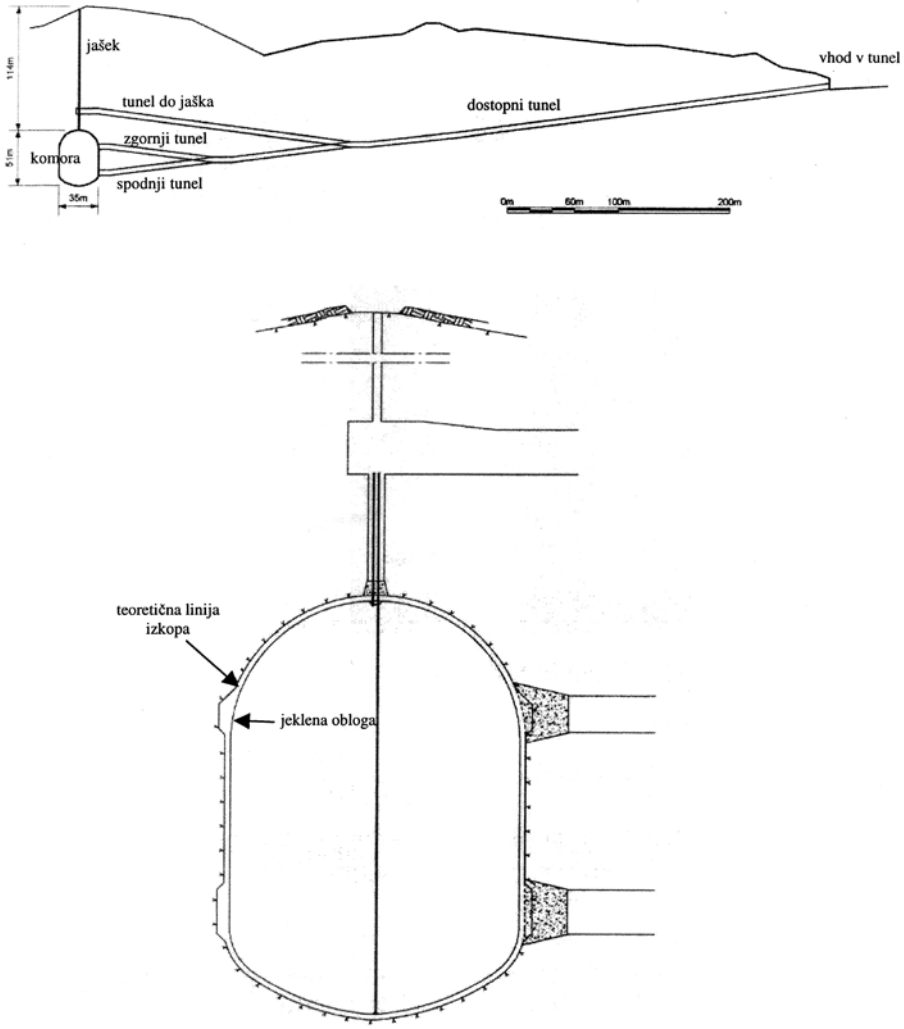

Slika 1. Shematski prikaz podzemnega skladišča zemeljskega plina PSZP (C. NOREN &, 2006)[3]
Figure 1. Layout of storage cavern PSZP

nastopanje apnencev in dolomitov na vzhodnem območju Rudnika Senovo.[2,4]

V vrtinah se pretežno menjavajo sivi do temno sivi apnenci in dolomiti s sivorumenimi brečami. V apnencih in dolomitih se često pojavljajo tanke nekaj mm do nekaj cm debele pole zelenkastih laporjev. Kamnine so zato plastovite. Breče imajo peščeno karbonatno vezivo, kjer je vezivo peščeno lapornato, te breče hitreje razpadajo in imajo slabše geomehanske karakteristike. Prehodi med apnenci in dolomiti so mestoma zvezni mestoma pa so vezani na cone breč. Kamnino presekata navadno 2 sistema razpok, ki jih običajno zapolnjuje kalcit, redkeje se v njih pojavlja lapor. Nekatere žilice so izvotljene, v njih nastopajo drobni kristalčki. Prostorski odnosi med plastovitostjo in dvema sistemoma razpok, ki presekata plasti pod skoraj pravim kotom so lepo vidni na sliki 2.

Na površju smo ugotavljali zelo spremenljive vpade, ki so posledica sedimentacijskih razmer, lokalno pa tudi posledica gubanja majhnega merila. V vrtinah se večinoma pojavljajo zmerni do strmi vpadi med 45 in 90º. Že omenjene razpoke so običajno približno pravokotno orientirane med seboj in na plastovitost. Širina diskontinuitet je med 1mm do nekaj centimetrov, njihova medsebojna oddaljenost pa se spreminja od 0,1 do 1 dm in več.

Mestoma se pojavlja tudi tektonska breča, kjer so kosi apnenca, dolomita in laporja sprijeti v meljasto peščeni osnovi. Tektonsko pretrto jedro smo v krajših odsekih opazovali v vrtinah V-4, V-5 in V-2, kjer pripada manjšim lokalnim prelomom. Večji prelom pa povzemamo z rudniške geološke karte, to je Reštanjski prelom, ki se nahaja na vzhodnem robu karte, ob njem pa so bile oligocenske plasti premaknjene za cca 200 m proti severozahodu.

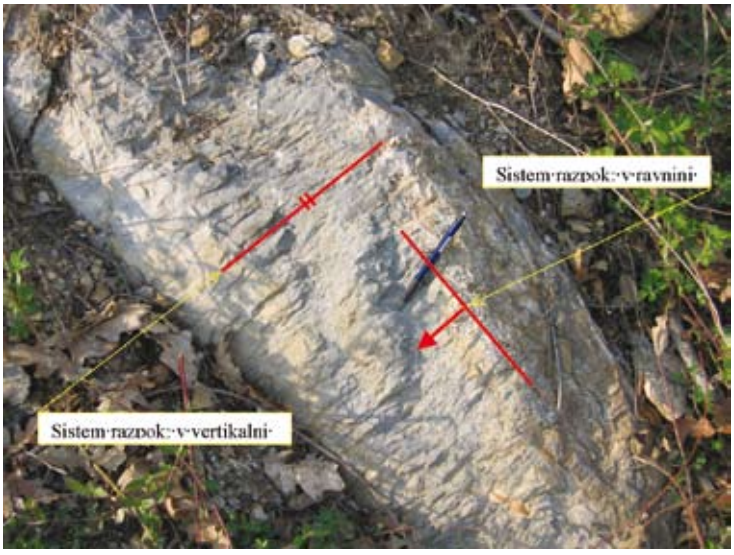

Slika 2. Plast apnenca na površini z dvema sistemoma razpok
Figure 2. Layer of limestone with two crack system

Potencialno primeren odsek za izvedbo podzemne komore, se na podlagi raziskav v vrtini V-1, in nato posledično na ostalih vrtinah, nahaja med globino 196 m in 276 m. V tem delu se zgoraj pojavljajo apnenci spodaj pa dolomiti, ki so močneje razpokani, pogostejše so v njih tudi tanke laporne pole. Razpoke imajo subvertikalno do položno lego, zapolnjene so s kalcitom, ponekod tudi z laporjem. Povprečna vrednost enoosne tlačne trdnosti za ta odsek je znašala 55 MPa, RQD 47 %. Za primerjavo povejmo, da ima odsek nad tem, to je med 143 in 196 m vrednosti σ = 23 MPa, RQD = 29 %. Vrednost RMR za predlagani odsek tako znaša 48, GSI 40. Po vrednosti RMR uvrščamo ta del v III. skupino s srednjo kvaliteto hribine. Za zgornji odsek so vrednosti RMR/GSI 37/30, kar je po RMR IV skupina s slabo kvaliteto hribine.

TERENSKE PREISKAVE

Vse vrtine so bile geološko-geotehnično popisane, pri čemer smo poleg litologije popisovali razpoke: njihovo usmeritev, debelino, polnilo in pogostnost. Izmerjen je bil RQD jedra, posebaj pa smo izdvojili pojavljanje pretrtih con ter pojave različnih mineralov (pirit, železovi oksidi in hidroksidi, ter kalcit). Iz vrtin so bili odvzeti vzorci za laboratorijske preiskave, v samih vrtinah pa so bile izvedene različne geotehnične in hidrogeološke preiskave.

Presiometrske preiskave

Presiometrske preiskave so bile izvedene v vrtinah V2 in V4. Rezultati so pokazali, da se moduli elastičnosti (E_0) v vrtini V2 gibljejo v razponu od 0.103 GPa do 44,9 GPa, ter od 0,295 GPa do 71,36 GPa v vrtini V4.

Nižje vrednosti so značilne za apneno-dolomitne breče z glinasto-lapornim vezivom, glinavce in laporje, ter močno razpokane kamnine, višje vrednosti pa za kompaktne dolomite, apnence in breče s karbonatnim vezivom.

Za močneje razpokane kamnine in kamnine z nižjim modulom elastičnosti je značilno, da je razbremenilni modul (E_{ur}) do 10 krat višji od obremenilnega, za kompaktne kamnine pa je razbremenilni modul 2-3 krat višji.

Primerjava rezultatov meritev elastičnih modulov s presiometrom (E_0) in modulov izmerjenih v laboratoriju (E), kaže da so razponi in velikostni red izmerjenih vrednosti podobne. Direktna primerjava med izmerjenima moduloma je bila možna le v vrtini V2 in sicer na globini 192,5, kjer se pojavljajo brečasti karbonati z različnim vezivom. Vrednost izmerjena s presiometrom znaša 8,3 GPa, v laboratoriju pa smo dobili vrednost 66,9 GPa.

Vzrok za tolikšno odstopanje je v dejstvu, da smo s presiometrom izmerili elastični modul hribine, pri čemer na rezultat posredno vplivajo prostorske variacije, kot so razpokanost, spremembe litologije itd... Vpliv prostorskih variacij je na laboratorijskem vzorcu bistveno manjši zaradi česar je modul višji.

S presiometričnimi meritvami se bolj približamo dejanskemu modulu kompaktne kamnine z razbremenilnim modulom, (E_{ur}), ki v tem primeru znaša 42,6 GPa, kar je veliko bližje laboratorijski vrednosti. Del rezultatov preiskav iz vrtineV4 so povzeti v preglednici 2.

Preglednica 2. Rezultati presiometrskih meritev v vrtini V4
Table 2. Pressiometric tests in well V4

Zap.št.	Vrtina	Globina	E0	Eur(1)	Eur(2)	H	H/V	Eo/Eur
		m	obremenilni GPa	razbremenilni GPa	razbremenilni GPa	MPa		
1	V4	163,5	71,36			2,63	0,60	0,00
2	V4	164,5	10,85	40,81		2,49	0,56	3,76
3	V4	165,5	51,71	76,65		2,50	0,56	1,48
4	V4	166,5	3,82	31,70		2,54	0,57	8,30
5	V4	167,5	26,10	61,66		2,70	0,60	2,36
6	V4	168,5	2,74	19,25		2,47	0,54	7,03
7	V4	196,5	0.29	0,85	1,2	3.03	0,57	2,92
8	V4	197,5	0,91	3,13	1,9	4,70	0,88	3,45
9	V4	198,5	3,17	7,20	5,0	4,09	0,76	2,27
10	V4	199,5	1,80		8,5	2,90	0,54	0,00

Geofizikalne meritve

Na območju predvidene izgradnje PSZP so bile izvedene tudi geofizikalne preiskave in sicer seizmični crosshole ter geoelektrični crosshole med obstoječimi raziskovalnimi vrtinami. Izmerjene so bile 2 seizmični in 2 geoelektrični preslikavi. Cilj preiskav je bil ugotoviti morebitne anomalne cone v pretežno karbonatni kamnini, ki jih

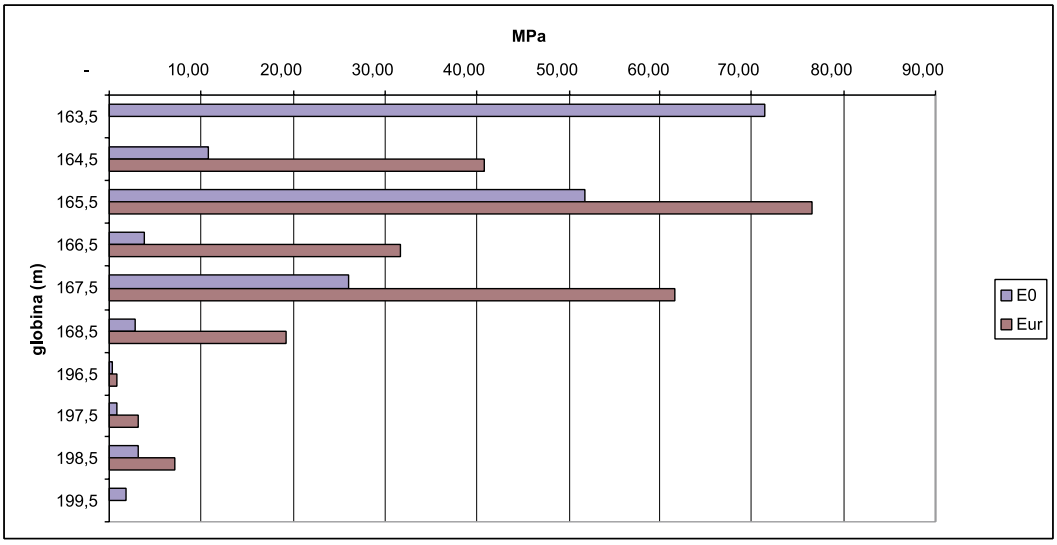

Slika 3. Rezultati presiometrskih meritev v vrtini V4
Figure 3. Pressiometric tests in well V4

Preglednica 3. Rezultati nalivalnih preizkusov v vrtinah V2, V3 in V4
Table 3. Groundwater tests in wells V2, V3 and V4

Vrtina V2:

Datum izvedbe	Globina izvedbe (m)	Izračunan K (m/s)
22. 2. 2006	90,3 – 99,3	**$1{,}64*10^{-6}$**
12. 3. 2006	150 – 172	**$9{,}38*10^{-5}$**
16. 3. 2006	201 - 213	**$5{,}31*10^{-5}$**

Vrtina V3:

Datum izvedbe	Globina izvedbe (m)	Izračunan K (m/s)
11. 4. 2006	146 - 152	**$1{,}41*10^{-5}$**
18. 4. 2006	174 - 186	**$1{,}35*10^{-5}$**

Vrtina V4:

Datum izvedbe	Globina izvedbe (m)	Izračunan K (m/s)
18. 4. 2006	154 - 160	**$2{,}58*10^{-5}$**

povzročajo nekatere plasti klastičnih usedlin, predvsem laporni in skrilavi sedimenti. Z geofizikalnimi preiskavami nismo ugotavili obstoja večjih prelomnih con.

Hidrogeološke preiskave

V okviru hidrogeoloških preiskav smo v vrtinah V2, V 3 in V4 izvedli nalivalne preizkuse v različnih globinah. Poleg tega pa smo izvedli serijo meritev nivoja gladine podtalnice. Rezultati nalivalnih preizkusov, ki so prikazani v preglednici 3 so bili ovrednoteni po različnih metodah (po HVORSLEV-u in po SCHNEEBELLI-ju). Na osnovi izmerjenih vrednosti lahko preiskovane kamnine uvrstimo med srednje prepustne s koeficienti prepustnosti med 10^{-5} in 10^{-6} m/s.

LABORATORIJSKE PREISKAVE

V okviru laboratorijskih preiskav smo na vzorcih odvzetih iz vrtin opravili naslednje preiskave:

- enoosne tlačne trdnosti (σ_c);
- enoosne natezne trdnosti (σ_t);
- prostorninske teže(γ);
- modula elastičnosti (E);
- poissonovega koeficienta (ν).

Rezultati laboratorijskih preiskav v vrtini V4 so podani v preglednici 4.

Preglednica 4. Rezultati laboratorijskih preiskav v vrtini V4
Table 4. Laboratory tests in well V4

Zap. št.	Vzorec			Prostorninska teža suhega materiala	Trdnost zemljine		Modul elastičnosti	Poissonov količnik
	Vrtina	Interval globine	Material		Enoosna tlačna VALJ	Enoosna natezna VALJ		
	ozn.	m		γ kN/m³	σ_c MPa	σ_t MPa	E MPa	ν -
1	V - 4	27,0 - 27,3	apnen skrilavec	23,5	58,9			
2		45.3 - 45.5	apnenec	26,6	73,5	4,3	85080	0,16
3		72,1 - 72,4	tektonska breča	22,7	1,00			
4		82.4 - 82.7	brečast apnenec	26,4	51,80	2,4	54330	0,2
5		100,1 - 100,4	apnenec z meljevcem	26,2	7,7	1,4		
6		106,5 -106,8	apnenec z meljevcem	25,8	22,3	2,1		
7		111,0 - 111,3	tektoniziran meljevec	22,3	1,4	0,3		
8		126,2 - 126,6	apnenec	26,4	65,9	3,3	86670	0,28
9		129,8 - 130,0	apnenec	26,0	42,6	2,7		
10		131,3 - 131,9	apnenec	26,5	71,9	2,9	98520	0,11
11		133,4 - 133,7	apnenec	26,2	62,8	5,5	80000	0,22
12		134,0 - 134,3	apnenec	26,0	76,4	6,8	61150	0,27
13		143,0 - 143,3	apnenec z meljevcem	25,0	7,8	1,4		
14		146,1 - 146,3	apnenec z laporjem	25,7	22,4	2,1		
15		150,0 -150,3	apnenec	26,5	58,2	4,3		
16		150,5 - 150,9	apnenec	26,3	49,0	5,1		
17		152,0 - 152,2	apnenec	26,5	70,1	4,7	53600	0,12
18		159,0 - 159,3	brečast apnenec	26,3	57,8	6,5		
19		174,5 - 174,9	apnenec	26,1	25,9	4,7		
20		178,5 - 178,9	apnenec	26,6	41,9	7,2		
21		191,4 - 191,8	breča z vložki gline	24,0	1,8	0,2		

ZAKLJUČEK

Z izvedenimi raziskavami smo natančneje omejili blok karbonatnih kamnin na površini, s petimi vrtinami in odvzetimi vzorci pa raziskali geološke in geotehnične razmere na obravnavanem prostoru. Preliminarne preiskave kažejo, da so geološko-geotehnične razmere v izdvojenem območju, čigar površina znaša cca 16.000 m^2 (230 x 75 m), primerne za izdelavo večjh (do štirih) komor dimenzij premera cca. 24 m in višine cca. 45 m, pod površjem nad globino cca. 150 m v plasteh apnenca, dolomita in breče.[4] Skladišče bi bilo lahko zgrajeno za tlak 15 do 20 MPa. Po podatkih kartiranj in geofizikalnih meritev se različne plasti hitro menjajo med seboj, z geomehanskega stališča pa ni bistvenih razlik med njimi. Območja ne seka nobena večja tektonska cona. Vrednosti RMR (vrednosti 40 do 50 - Slika 5)[3] uvrščajo ta del v srednji razred po kvaliteti hribine. Za optimalno določitev parametrov PSZP bo potrebno opraviti analizo na podlagi načrtovanja, ki je prikazana na sliki 4.

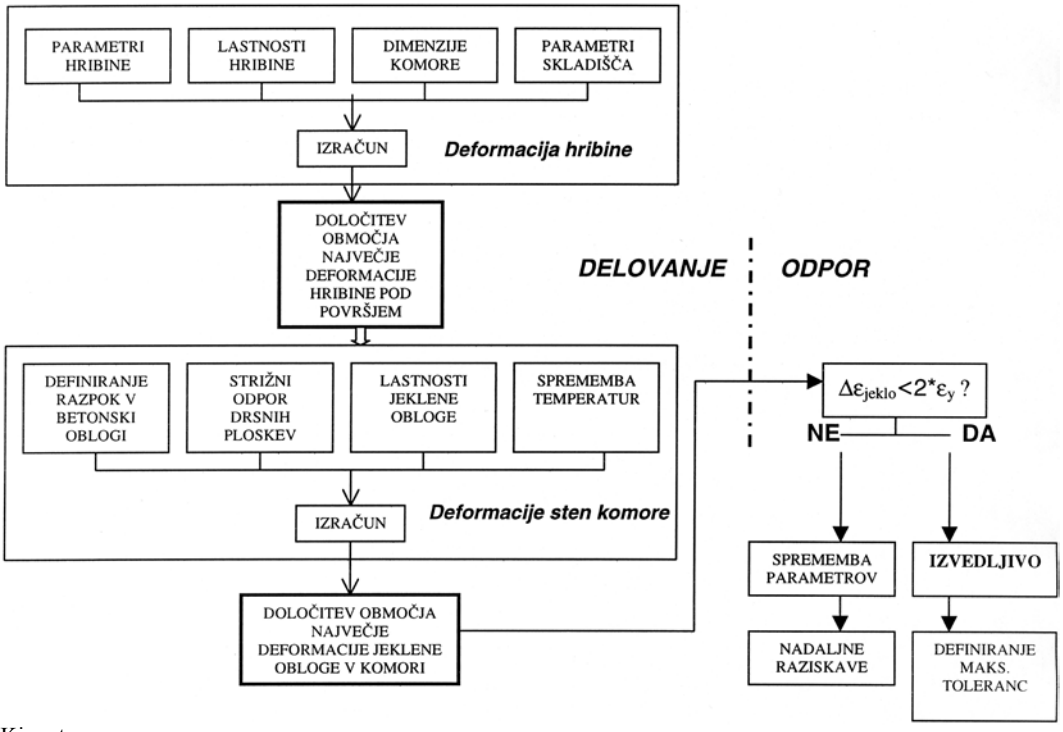

Kjer sta:
- $\Delta\varepsilon_{jeklo}$ velikost deformacije
- ε_y elastična deformacija

Slika 4. Načrtovanje za PSZP[1,2]
Figure 4. Layout of PSZP project

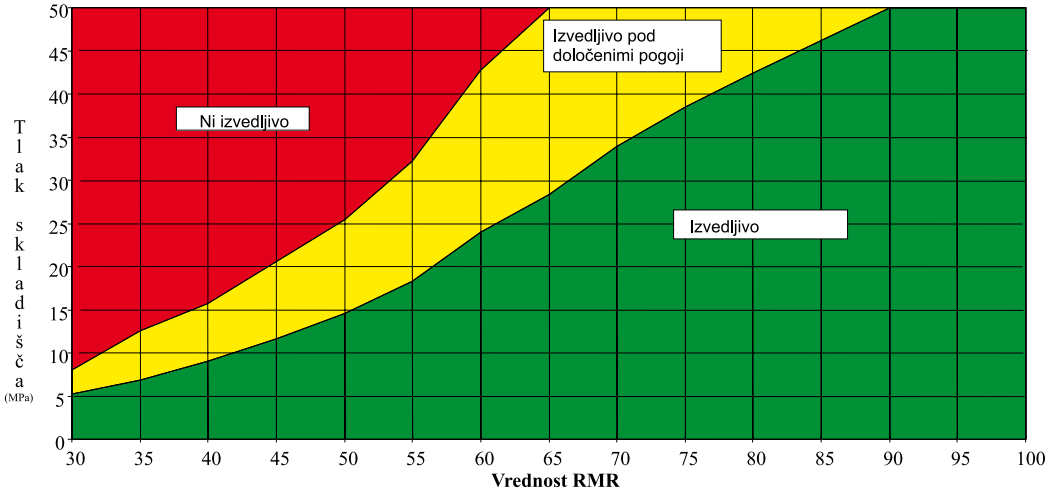

Slika 5. Izvedljivost PSZP v odvisnosti od RMR. (Noren, 2006)[3]
Figure 5. Layout of geological feasibility

Conclusions

High Pressure Storage of Gas in Area of Coal Mine Senovo

Investigations confirm that the rock mass quality is main factor for determining the maximum size for the cavern and maximum pressure. The rock mass at the proposed site consists of dolomites and limestone and is has been classified as Poor to Fair rock (RMR). It is concluded that a cavern with span of 24 m and height of 45 m is feasible. It is also concluded to consider storage pressure between 15 to 20 MPa. Underground 150 m is possible to construct 4 caverns in area of 230 m x 75 m.

Literatura:

[1] J. Johanson: High Pressure Storage of Gas in Lined Rock Cavern, 2003, Stockholm, Švedska
[2] Ž. Vukelić s soavtorji: Študija možnosti izgradnje visokotlačnega skladišča zemljskega plina v Rudniku Senovo, 2004, Naravoslovnotehniška fakulteta, Oddelek za geotehnologijo in rudarstvo;
[3] C. Noren & ..:Underground Storage of Natural Gas in Lined Rock Cavern in Brestanica Area 2006, NCC, Stockholm, Švedska
[4] Ž. Sternad s soavtorji: Končno poročilo o geološko-geotehničnih razmerah na področju PSZP Zakov/Senovo, 2006, RGP, Velenje

Assessment of surface deformation with simultaneous adjustment with several epochs of leveling networks by using nD relative pedaloid

Ocena deformacij-s simultano izravnavo več terminskih izmer z nD relativnim pedaloidom

Milivoj Vulić[1], Ana Vehovec[2]

[1]Faculty of Natural Science and Engineering,
University of Ljubljana, Aškerčeva cesta 12, SI-1000 Ljubljana, Slovenia;
E-mail: milivoj.vulic@ntf.uni-lj.si
[2] DDC svetovanje inženiring, Kotnikova 40, 1000 Ljubljana, Slovenia;
E-mail: ana.vehovec@ddc.si

Received: November 02, 2006 **Accepted:** November 14, 2006

Abstract: Relative error hyperellipsoid, 3D relative error pedaloid and 2D relative pedal curve are discussed.

Izvleček: V članku govori o 3D relativnem pedaloidu pogreškov in 2D relativni pedali.

Key words: Adjustment by parameter variation, nD relative error hyperellipsoid and hyperellipsoid, 3D relative error ellipsoid, 2D relative ellipse.
Ključne besede: Posredna izravnava, nD relativni hiperelipsoid pogreškov in hiperelipsoid, 3D relativni elipsoid pogreškov, 2D relativni elipsoid.

Introduction

Consequence of underground extraction of coal is surface alteration. Negative consequences of mining are reflected above all as ground deformation, field landslides, formation of lakes, climate changes due to alteration of landscape, influence on subterranean waters and thermal springs, seismic effects of subterranean blasting.

Ground subsidence is the most intensive above extraction fields but can also be observed on the edge fields. That is the reason for planning local observation networks, by which expanse of deformation can be determined. Observation of networks is important because of closeness of outbuildings and other buildings.

With simultaneous adjustment of several epochs of measurements, the field deformation can be determined.

Theoretical basis of adjustment by parameter variation in geodetic leveling network

Ultimate aim for adjustment of geodetic networks are point coordinates. Definitive

Scientific paper

or most probable point coordinates can not be obtained by direct mathematical processing of measured quantities (angles, lengths, height differences, etc.), they can be only determined by process of adjustment. This process is possible only if the number of measured data is greater then necessarily needed.

In the leveling network adjustment one point with known absolute height should be given (or assumed). This holds for adjustment by parameter (height coordinate) variation.

In the adjustment there are three types of quantities:

- given quantities (constant values, which don't change by adjustment),
- measured quantities,
- unknown quantities.

By adjustment unknown quantities are determined from given quantities through series of measured quantities on condition that the sum of squares of their residuals is minimal. With observation equation coefficients a_i, b_i,...u_i, and absolute terms f_i. Coefficients are partial derivatives of functional relation between given, measured and unknown quantities. Their values depend on configuration and size of network. Absolute terms can be symbolically expressed as f_i = *approximate – measured*. Approximate values are computed from approximate coordinates.
The adjustment is done considering:

$$\mathbf{v}^T \mathbf{Q}_{ll}^{-1} \mathbf{v} = \min \quad \text{or} \quad \mathbf{v}^T \mathbf{P} \mathbf{v} = \min \qquad \text{(a)}$$

v residuals,
$\mathbf{Q}_{ll}$ correlation matrix of measured quantities,
P weight matrix of measured quantities.

Observation equations can be written in matrix form:

$$\begin{bmatrix} v_1 \\ v_2 \\ \vdots \\ v_i \end{bmatrix} = \begin{bmatrix} a_1 & b_1 & \cdots & u_1 \\ a_2 & b_2 & \cdots & u_2 \\ \vdots & \vdots & \ddots & \vdots \\ a_i & b_i & \cdots & u_i \end{bmatrix} * \begin{bmatrix} x \\ y \\ \vdots \\ t \end{bmatrix} + \begin{bmatrix} f_1 \\ f_2 \\ \vdots \\ f_i \end{bmatrix} \qquad \text{(b)}$$

Or shortly:

v vector of residuals,
A design matrix of observation equations,
x unknowns vector,
f vector of absolute terms.

Coefficient matrix of normal equations **N** reads:

$$\mathbf{v} = \mathbf{A} \cdot \mathbf{x} + \mathbf{f} \qquad \text{(c)}$$

$$\mathbf{N} = \mathbf{A}^T \mathbf{P} \mathbf{A} = \begin{bmatrix} [paa] & [pab] & \cdots & [pau] \\ [pba] & [pbb] & \cdots & [pbu] \\ \vdots & \vdots & \ddots & \vdots \\ [pua] & [pub] & \cdots & [puu] \end{bmatrix} \qquad \text{(d)}$$

$$\mathbf{P} = \mathbf{diag}\begin{bmatrix} p_1 & p_2 & \cdots & p_i \end{bmatrix} \qquad \text{(e)}$$

When measurements are of the same accuracy then $\mathbf{P} = p\mathbf{I}$, where **I** is unit matrix.
Vector of absolute terms of normal equations **n**:

$$\mathbf{n} = \mathbf{A}^{\mathbf{T}} \mathbf{P} \mathbf{f} = \begin{bmatrix} [paf] \\ [pbf] \\ \vdots \\ [puf] \end{bmatrix} = \mathbf{A}^{\mathbf{T}} p\mathbf{I} f = p\mathbf{A}^T f \qquad \text{(f)}$$

Vector of unknowns is:

$$\mathbf{x} = -\mathbf{N}^{-1}\mathbf{n} = -\left(\mathbf{A}^T\mathbf{P}\mathbf{A}\right)^{-1}\mathbf{A}^T\mathbf{P}\mathbf{f} = -\mathbf{N}^{-1}\mathbf{A}^T\mathbf{P}\mathbf{f} \tag{g}$$

Then vector of residuals can be calculated:

$$\mathbf{v} = \mathbf{A}\cdot\mathbf{x} + \mathbf{f} \tag{h}$$

Relative error curve

Relative error curve does not depend on the network datum or coordinate origin.

nD relative hyperpedaloid and hyperellipsoid

$\underset{n,n}{\mathbf{Q}}_{hyperellipsoid}$ in equation (9) can be written as product of unit matrix **I**, matrix $Q_{\Delta_i\xi\Delta_j\xi}$:

$$\underset{n,n}{\mathbf{Q}}_{hyperellipsoid} = \begin{bmatrix} \ddots & \vdots & \ddots \\ \cdots & Q_{\Delta_i\xi\Delta_j\xi} & \cdots \\ \ddots & \vdots & \ddots \end{bmatrix}_{n,n} = \underset{n,2n}{\begin{bmatrix} \mathbf{I}_{n,n} & -\mathbf{I}_{n,n} \end{bmatrix}} \underset{2n,2n}{\begin{bmatrix} \mathbf{Q}_{\xi\xi SS} & \mathbf{Q}_{\xi\xi SV} \\ \mathbf{Q}_{\xi\xi SV} & \mathbf{Q}_{\xi\xi VV} \end{bmatrix}_{n,n}} \underset{2n,2}{\begin{bmatrix} \mathbf{I}_{n,n} \\ -\mathbf{I}_{n,n} \end{bmatrix}} =$$

$$= \underset{n,2n}{\begin{bmatrix} \mathbf{I}_{n,n} & -\mathbf{I}_{n,n} \end{bmatrix}} \underset{2n,n}{\begin{bmatrix} \mathbf{Q}_{\xi\xi SS} & -\mathbf{Q}_{\xi\xi SV} \\ \mathbf{Q}^T_{\xi\xi SV} & -\mathbf{Q}_{\xi\xi VV} \end{bmatrix}_{n,n}} = \underset{n,n}{\begin{bmatrix} \mathbf{Q}_{\xi\xi SS} & -\mathbf{Q}_{\xi\xi SV} & -\mathbf{Q}^T_{\xi\xi SV} & +\mathbf{Q}_{\xi\xi VV} \end{bmatrix}_{n,n}} \tag{i}$$

But also:

$$\underset{n,n}{\mathbf{Q}}_{hyperellipsoid} = \begin{bmatrix} \ddots & \vdots & \ddots \\ \cdots & Q_{\Delta_i\xi\Delta_j\xi} & \cdots \\ \ddots & \vdots & \ddots \end{bmatrix}_{n,n} = \begin{bmatrix} \ddots & \vdots & \ddots \\ \cdots & Q_{i\xi_S j\xi_S} - Q_{i\xi_S j\xi_V} - Q_{i\xi_S j\xi_V} + Q_{i\xi_V j\xi_V} & \cdots \\ \ddots & \vdots & \ddots \end{bmatrix}_{n,n} \tag{j}$$

or

$$Q_{\Delta_i\xi\Delta_j\xi} = Q_{i\xi_S j\xi_S} - Q_{i\xi_S j\xi_V} - Q_{i\xi_S j\xi_V} + Q_{i\xi_V j\xi_V} \tag{k}$$

And after addition:

$$Q_{\Delta_i\xi\Delta_j\xi} = Q_{i\xi_S j\xi_S} - 2Q_{i\xi_S j\xi_V} + Q_{i\xi_V j\xi_V} \tag{l}$$

3D relative pedaloid and ellipsoid

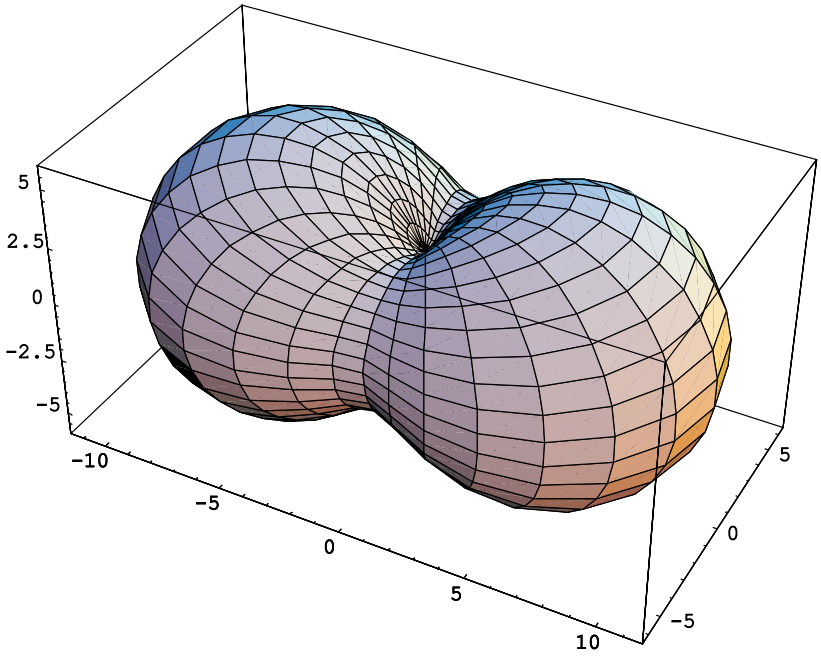

Figure 1. 3D relative ellipsoid
Slika 2. 3D relativni elipsoid

The elements of relative error ellipsoid $\mathbf{Q}_{ellipsoid\ SV}$ are linear combination of matrix **Q** elements:

$$\mathbf{Q}_{ellipsoid\ SV} = \begin{bmatrix} Q_{\Delta Z \Delta Z} & Q_{\Delta Z \Delta Y} & Q_{\Delta Z \Delta X} \\ Q_{\Delta Z \Delta Y} & Q_{\Delta Y \Delta Y} & Q_{\Delta Y \Delta X} \\ Q_{\Delta Z \Delta X} & Q_{\Delta Y \Delta X} & Q_{\Delta X \Delta X} \end{bmatrix} =$$

$$= \begin{bmatrix} 1 & 0 & 0 \\ 0 & 1 & 0 \\ 0 & 0 & 1 \end{bmatrix} - \begin{bmatrix} 1 & 0 & 0 \\ 0 & 1 & 0 \\ 0 & 0 & 1 \end{bmatrix} \begin{bmatrix} \begin{bmatrix} Q_{Z_S Z_S} & Q_{Z_S Y_S} & Q_{Z_S X_S} \\ Q_{Z_S Y_S} & Q_{Y_S Y_S} & Q_{Y_S X_S} \\ Q_{Z_S X_S} & Q_{Y_S X_S} & Q_{X_S X_S} \end{bmatrix} & \begin{bmatrix} Q_{Z_S Z_V} & Q_{Z_S Y_V} & Q_{Z_S X_V} \\ Q_{Y_S Z_V} & Q_{Y_S Y_V} & Q_{Y_S X_V} \\ Q_{X_S Z_V} & Q_{X_S Y_V} & Q_{X_S X_V} \end{bmatrix} \\ \begin{bmatrix} Q_{Z_S Z_V} & Q_{Y_S Z_V} & Q_{X_S Z_V} \\ Q_{Z_S Y_V} & Q_{Y_S Y_V} & Q_{X_S Y_V} \\ Q_{Z_S X_V} & Q_{Y_S X_V} & Q_{X_S X_V} \end{bmatrix} & \begin{bmatrix} Q_{Z_V Z_V} & Q_{Z_V Y_V} & Q_{Z_V X_V} \\ Q_{Z_V Y_V} & Q_{Y_V Y_V} & Q_{Y_S X_V} \\ Q_{Z_V X_V} & Q_{Y_V X_V} & Q_{X_V X_V} \end{bmatrix} \end{bmatrix} \begin{bmatrix} 1 & 0 & 0 \\ 0 & 1 & 0 \\ 0 & 0 & 1 \end{bmatrix} - \begin{bmatrix} 1 & 0 & 0 \\ 0 & 1 & 0 \\ 0 & 0 & 1 \end{bmatrix} \quad \text{(m)}$$

After right multiplication:

$$\mathbf{Q}_{ellipsoid\ SV} = \begin{bmatrix} Q_{\Delta Z\Delta Z} & Q_{\Delta Z\Delta Y} & Q_{\Delta Z\Delta X} \\ Q_{\Delta Z\Delta Y} & Q_{\Delta Y\Delta Y} & Q_{\Delta Y\Delta X} \\ Q_{\Delta Z\Delta X} & Q_{\Delta Y\Delta X} & Q_{\Delta X\Delta X} \end{bmatrix} =$$

$$= \begin{bmatrix} 1 & 0 & 0 \\ 0 & 1 & 0 \\ 0 & 0 & 1 \end{bmatrix} - \begin{bmatrix} 1 & 0 & 0 \\ 0 & 1 & 0 \\ 0 & 0 & 1 \end{bmatrix} \begin{bmatrix} \begin{bmatrix} Q_{Z_S Z_S} & Q_{Z_S Y_S} & Q_{Z_S X_S} \\ Q_{Z_S Y_S} & Q_{Y_S Y_S} & Q_{Y_S X_S} \\ Q_{Z_S X_S} & Q_{Y_S X_S} & Q_{X_S X_S} \end{bmatrix} - \begin{bmatrix} Q_{Z_S Z_V} & Q_{Z_S Y_V} & Q_{Z_S X_V} \\ Q_{Y_S Z_V} & Q_{Y_S Y_V} & Q_{Y_S X_V} \\ Q_{X_S Z_V} & Q_{Y_S X_V} & Q_{X_S X_V} \end{bmatrix} \\ \begin{bmatrix} Q_{Z_S Z_V} & Q_{Y_S Y_V} & Q_{X_S Z_V} \\ Q_{Z_S Y_V} & Q_{Y_S Z_V} & Q_{X_S Y_V} \\ Q_{Z_S X_V} & Q_{Y_S X_V} & Q_{X_S X_V} \end{bmatrix} - \begin{bmatrix} Q_{Z_V Z_V} & Q_{Z_V Y_V} & Q_{Z_V X_V} \\ Q_{Z_V Y_V} & Q_{Y_V Y_V} & Q_{Y_V X_V} \\ Q_{Z_V X_V} & Q_{Y_V X_V} & Q_{X_V X_V} \end{bmatrix} \end{bmatrix} \tag{n}$$

And after left multiplication:

$$\mathbf{Q}_{ellipsoid\ SV} = \begin{bmatrix} Q_{\Delta Z\Delta Z} & Q_{\Delta Z\Delta Y} & Q_{\Delta Z\Delta X} \\ Q_{\Delta Z\Delta Y} & Q_{\Delta Y\Delta Y} & Q_{\Delta Y\Delta X} \\ Q_{\Delta Z\Delta X} & Q_{\Delta Y\Delta X} & Q_{\Delta X\Delta X} \end{bmatrix} = \begin{bmatrix} Q_{Z_S Z_S} & Q_{Z_S Y_S} & Q_{Z_S X_S} \\ Q_{Z_S Y_S} & Q_{Y_S Y_S} & Q_{Y_S X_S} \\ Q_{Z_S X_S} & Q_{Y_S X_S} & Q_{X_S X_S} \end{bmatrix} -$$

$$- \begin{bmatrix} 2Q_{Z_S Z_V} & Q_{Z_S Y_V} + Q_{Y_S Z_V} & Q_{Z_S X_V} + Q_{X_S Z_V} \\ Q_{Y_S Z_V} + Q_{Z_S Y_V} & 2Q_{Y_S Y_V} & Q_{Y_S X_V} + Q_{X_S Y_V} \\ Q_{X_S Z_V} + Q_{Z_S X_V} & Q_{X_S Y_V} + Q_{Y_S X_V} & 2Q_{X_S X_V} \end{bmatrix} + \begin{bmatrix} Q_{Z_V Z_V} & Q_{Z_V Y_V} & Q_{Z_V X_V} \\ Q_{Z_V Y_V} & Q_{Y_V Y_V} & Q_{Y_V X_V} \\ Q_{Z_V X_V} & Q_{Y_V X_V} & Q_{X_V X_V} \end{bmatrix} \tag{o}$$

Matrices in equation (15) are added up (or subtracted) and final value of matrix $\mathbf{Q}_{ellipsoid\ SV}$ is obtained:

$$\mathbf{Q}_{ellipsoid\ SV} = \begin{bmatrix} Q_{\Delta Z\Delta Z} & Q_{\Delta Z\Delta Y} & Q_{\Delta Z\Delta X} \\ Q_{\Delta Z\Delta Y} & Q_{\Delta Y\Delta Y} & Q_{\Delta Y\Delta X} \\ Q_{\Delta Z\Delta X} & Q_{\Delta Y\Delta X} & Q_{\Delta X\Delta X} \end{bmatrix} =$$

$$= \begin{bmatrix} Q_{Z_S Z_S} - 2Q_{Z_S Z_V} + Q_{Z_V Z_V} & Q_{Z_S Y_S} - Q_{Z_S Y_V} - Q_{Y_S Z_V} + Q_{Z_V Y_V} & Q_{Z_S X_S} - Q_{Z_S X_V} - Q_{X_S Z_V} + Q_{Z_V X_V} \\ Q_{Z_S Y_S} - Q_{Z_S Y_V} - Q_{Y_S Z_V} + Q_{Z_V Y_V} & Q_{Y_S Y_S} - 2Q_{Y_S Y_V} + Q_{Y_V Y_V} & Q_{Y_S X_S} - Q_{Y_S X_V} - Q_{X_S Y_V} + Q_{Y_V X_V} \\ Q_{Z_S X_S} - Q_{Z_S X_V} - Q_{X_S Z_V} + Q_{Z_V X_V} & Q_{Y_S X_S} - Q_{Y_S X_V} - Q_{X_S Y_V} + Q_{Y_V X_V} & Q_{X_S X_S} - 2Q_{X_S X_V} + Q_{X_V X_V} \end{bmatrix} \tag{p}$$

2d relative error pedaloid and ellipse

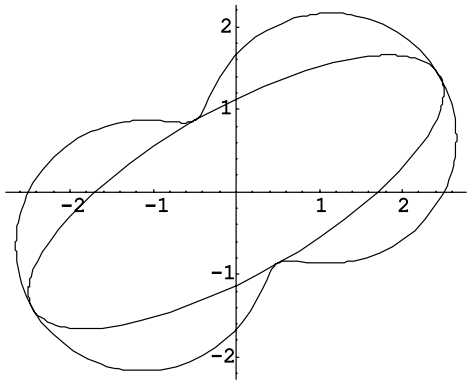

Figure 3. 2D relative pedaloid and ellipsoid
Slika 4. 2D relativni pedaloid in elipsoid

By the analogy of relative ellipsoid, relative error ellipse is:

$$\mathbf{Q}_{ellipse\ SV} = \begin{bmatrix} Q_{\Delta Y \Delta Y} & Q_{\Delta Y \Delta X} \\ Q_{\Delta Y \Delta X} & Q_{\Delta X \Delta X} \end{bmatrix} = \\ = \begin{bmatrix} 1 & 0 & -1 & 0 \\ 0 & 1 & 0 & -1 \end{bmatrix} \begin{bmatrix} Q_{Y_S Y_S} & Q_{Y_S X_S} & Q_{Y_S Y_V} & Q_{Y_S X_V} \\ Q_{Y_S X_S} & Q_{X_S X_S} & Q_{X_S Y_V} & Q_{X_S X_V} \\ Q_{Y_S Y_V} & Q_{X_S Y_V} & Q_{Y_V Y_V} & Q_{Y_V X_V} \\ Q_{Y_S X_V} & Q_{X_S X_V} & Q_{Y_V X_V} & Q_{X_V X_V} \end{bmatrix} \begin{bmatrix} 1 & 0 \\ 0 & 1 \\ -1 & 0 \\ 0 & -1 \end{bmatrix} \tag{q}$$

$$\mathbf{Q}_{ellipse\ SV} = \begin{bmatrix} Q_{\Delta Y \Delta Y} & Q_{\Delta Y \Delta X} \\ Q_{\Delta Y \Delta X} & Q_{\Delta X \Delta X} \end{bmatrix} = \\ = \begin{bmatrix} Q_{Y_S Y_S} - Q_{Y_S Y_V} & Q_{Y_S X_S} - Q_{X_S Y_V} & Q_{Y_S Y_V} - Q_{Y_V Y_V} & Q_{Y_S X_V} - Q_{Y_V X_V} \\ Q_{Y_S X_S} - Q_{Y_S X_V} & Q_{X_S X_S} - Q_{X_S X_V} & Q_{X_S Y_V} - Q_{Y_V X_V} & Q_{X_S X_V} - Q_{X_V X_V} \end{bmatrix} \begin{bmatrix} 1 & 0 \\ 0 & 1 \\ -1 & 0 \\ 0 & -1 \end{bmatrix} \tag{r}$$

$$\mathbf{Q}_{ellipse\ SV} = \begin{bmatrix} Q_{\Delta Y \Delta Y} & Q_{\Delta Y \Delta X} \\ Q_{\Delta Y \Delta X} & Q_{\Delta X \Delta X} \end{bmatrix} = \\ = \begin{bmatrix} Q_{Y_S Y_S} - 2Q_{Y_S Y_V} + Q_{Y_V Y_V} & Q_{Y_S X_S} - Q_{X_S Y_V} - Q_{Y_S X_V} + Q_{Y_V X_V} \\ Q_{Y_S X_S} - Q_{Y_S X_V} - Q_{X_S Y_V} + Q_{Y_V X_V} & Q_{X_S X_S} - 2Q_{X_S X_V} + Q_{X_V X_V} \end{bmatrix} \tag{s}$$

For given point:

$$\mathbf{Q}_{ellipse\ SV} = \begin{bmatrix} Q_{\Delta Y \Delta Y} & Q_{\Delta Y \Delta X} \\ Q_{\Delta Y \Delta X} & Q_{\Delta X \Delta X} \end{bmatrix} = \begin{bmatrix} Q_{Y_V Y_V} & Q_{Y_V X_V} \\ Q_{Y_V X_V} & Q_{X_V X_V} \end{bmatrix} \quad \text{(t)}$$

Summary

Multi epochs adjustment by parameter variation is simple enough, besides that the points subsidence is calculated directly. In this article nD hyperpedaloid and hyperellipsoid, error ellipse and error ellipsoid were formulated.

Their execution was shown. Their characteristic is that they do not depend on coordinate origin.

Reference

Mihajlović, K., Vračarić, K., Geodezija III. *Građevinski fakultet Beograd, Beograd*, 1985.

Mihajlović, K., Vračarić, K., Geodezija I. *Građevinski fakultet Beograd, Beograd*, 1989.

Mihajlović, K., Geodezija II (2. deo), *Naučna knjiga, Beograd*, 1978.

Mihajlović, K., Geodezija: Izravnanje geodetskih mreža. *Građevinski fakultet Beograd, Beograd*, 1992.

Todorović, R. T., Uvod v rudarsko škodo II. *Naravoslovnotehniška fakulteta, Oddelek za geotehnologijo in rudarstvo, Ljubljana,* 1996.

Todorović, R. T., O relativni elipsi pogreškov. *Rudarsko-metalurški zbornik.* 1994: 41, 169-174.

Zaključek

Ocena deformacij s simultano izravnavo več terminskih izmer z nD relativnim pedaloidom

Posredna izravnava več terminskih izmer je dokaj enostavna, poleg tega pa se ugrezke izračunava neposredno. V članku so predstavljeni nD hiperpedaloid in hiperelipsoid, elipsa pogreškov in elipsoid pogreškov. Prikazana je bila njihova izpeljava. Zanje je značilno, da so neodvisni od koordinatnega izhodišča.

Maximum Entropy Theory by Using the Meandering Morphological Investigation

Levent Yilmaz

Technical University of Istanbul, Hydraulic Division, Civil Engineering Department, Maslak, 80626, Istanbul, Turkey.; E-mail: lyilmaz@itu.edu.tr

Received: November 02, 2006 **Accepted**: November 14, 2006

Abstract: Based on the principle of maximum entropy the primary morphologic equation is derived, and then the equations for hydraulic geometry of longitudinal profile and cross-section are established. For V-shaped cross-sections the relevant morphologic equations which are derived are compared with the existing empirical and semi-empirical formulae. They show good agreement with the prototypes.

Key words: Principle of maximum entropy, hydraulic geometry, morphologic equation

Introduction

Einstein (1950) once pointed out that entropy theory is the first theory for overall science. The principle of maximum entropy has been extensively applied in many domains of natural science. In view of this fact, to apply the principle of maximum entropy is adopted to deal with characteristics of alluvial channels capable of carrying given water and sediment load in meandering boundary layers without causing excessive aggradation and degradation.

Width adjustment may take place over a wide range of scales in time and space at meandering channels. In the past engineering analyses of channel width have tended to concentrate on prediction of the equilibrium width for stable channels.

Most commonly the regime; extremal hypothesis, and rational (mechanistic) approaches are used. By meandering channels, more recently, attention has switched to channels that are adjusting their morphology either due to natural instability or in response to changes in meandering watershed land use, river regulation, or channel engineering.

Characterizing and explaining the time-dependent behavior of width in such channels requires and understanding of the fluvial hydraulics of unstable channels, especially in the near-bank regions. Useful engineering tools are presented, and gaps requiring further field and laboratory research are identified. Finally, this research will consider the mechanics of bank retreat due to flow erosion and deposition at meandering bends, mass failure under gravity, and bank advance due to sedimentation and berm building. It will be demonstrated that, while rapid progress is being made, most existing analyses of bank mechanics are still at the stage of being research tools that are not yet suitable for design applications.

Scientific paper

Most mathematical models, however, neglect time- dependent channel width adjustments and do not simulate processes of bank erosion or deposition at meandering channels. Although changes in channel depth caused by aggradation or degradation of the river bed can be simulated, changes in width cannot. Meandering channel morphology usually changes with time, and adjustment of both width and depth, in addition to changes in planform, roughness, and other attributes are the rule rather than the exception (LEOPOLD ET AL., 1964; SIMON AND THORNE, 1996). As a result, the ability to model and predict changes in river morphology and their engineering impacts is limited. The meandering river width adjustments can seriously impact floodplain dwellers, riparian ecosystems, bridge crossings, bank protection works, and other riverside structures, through bank erosion, bank accretion, or bankline abandonment by the active river channel, which are very important for sustainable development of European Mediterranean countries. Considerable research effort has recently been directed towards improving this situation.

The objectives of the river width adjustment research were as follows:

- Review the current understanding of the fluvial processes and bank mechanics involved in river width adjustment
- Evaluate methods (including regime analysis, extremal hypotheses and rational, mechanistic approaches) for predicting equilibrium river width
- Assess the present capability to quantify and model width adjustment
- Identify current needs to advance both state-of-the-art research and the solution of real world problems faced by practicing engineers

To achieve these objectives, river width adjustments may occur due to a wide range of morphological changes and channel responses. Widening can occur by erosion of one or both banks without substantial incision (EVERITT, 1968; BURKHAM, 1972; HEREFORD, 1984; PIZZUTO, 1992). Widening in sinuous channels may occur when outer bank retreat, due to toe scouring, exceeds the rate of advance of the opposite bank, due to alternate or point bar growth (NANSON AND HICKIN, 1983: PIZZUTO, 1994) while, in braided rivers, bank erosion by flows deflected around growing braid bars is a primary cause of widening (LEOPOLD AND WOLMAN, 1957; BEST AND BRISTOW, 1993; THORNE ET AL., 1993). In degrading streams, widening often follows incision of the channel when the increased height and steepness of the banks causes them to become unstable. Bank failures can cause very rapid widening under these circumstances (THORNE ET AL., 1981; LITTLE ET AL., 1982; HARVEY AND WATSON, 1986; SIMON, 1989). Widening in coarse-grained, aggrading channels can occur when flow acceleration due to a decreasing cross-sectional area, coupled with current deflection around growing bars, generates bank erosion (SIMON AND THORNE, 1996). Morphological adjustments involving channel narrowing are equally diverse. Rivers may narrow through the formation of in-channel berms, or benches at the margins.

Berm/bench growth often occurs when bed levels stage following a period of degradation and can eventually create a new, low-elevation floodplain and establish a narrower, quasi-equilibrium channel (WOODYER, 1968; HARVEY AND WATSON, 1986; SIMON, 1989; PIZZUTO, 1994). Narrowing in sinuous channels occurs when the rate of alternate or point bar

growth exceeds the rate of retreat of the cut bank opposite (Nanson and Hickin, 1983; Pizzuto, 1994). Croachment of riparian vegetation into the channel is often satisfied as contributing to the growth, stability, and initiation of berm or bench features (Hadley, 1961; Schumm and Lichty, 1963; Harvey and Watson, 1986; Simon, 1989). In braided channels, narrowing may result when a marginal anabranch in the braided system is abandoned (Schumm and Lichty, 1963). Sediment is deposited in the abandoned channel until it merges into the floodplain. Also, braid bars or islands may become attached to the floodplain, especially following a reduction in the formative discharge. Island tops are already at about floodplain elevation and attached bars are built up to floodplain elevation by sediment deposition on the surface of the bar, often in association with establishment of vegetation. Attached islands and bars may, in time, become part of the floodplain bordering a much narrower, sometimes single-threaded channel (Williams, 1978; Nadler and Schumm, 1981).

If the flow regime and sediment supply are quasi-steady over periods of decades, the morphology of the river adjusts to create a metastable, equilibrium form (Schumm and Lichty, 1965). Such rivers are described as being graded or in regime (Mackin, 1948; Leopold and Maddock, 1953; Wolman, 1955; Leopold et al. 1964; Ackers and Charlton, 1970a). Although the width of an equilibrium stream may change due to the impact of a large flood or some other extreme event, the stable width is eventually recovered following such perturbations (Costa, 1974; Gupta and Fox, 1974; Wolman and Gerson, 1978). Unfortunately, predicting the time-averaged morphology of equilibrium channels remains, despite years of effort, a difficult problem (Ackers, 1992; Ferguson, 1986; Bettess and White, 1987).

Many rivers, however, cannot be considered to have equilibrium channels even as an engineering approximation. These rivers display significant morphological changes.

Under the assumption that the only information available on a drainage basin is its mean elevation, the connection between entropy and potential energy is explored to analyze drainage basins morphological characteristics. Nearly, 30 years ago, Leopold and Langbein (1962) applied for the first time the concepts of physical entropy to study the behavior of streams. Their application was based on the analogy between heat energy and temperature in a thermodynamic system and potential energy and elevation, respectively, in a stream system. Two thermodynamic principles were applied. The first principle is that the most probable state of a system is the one of maximum entropy. The second is the principle of minimum entropy production rate.

Using these principles, Yang (1971) derived for a stream system the law of average stream fall, and the law of the least rate of energy expenditure. Yang (1971) and others have since applied the latter law to a range of problems in hydraulics. The connection between entropy and potential energy, which these workers so successfully exploited to investigate river engineering, sediment transport, and other problems, was not exploited in hydrology. In this work we pursue this connection to derive relations between entropy and mean elevation for a drainage basin network and to derive relations for the river profiles.

Much of the work employing the entropy concepts in hydrology has been with the application of informational entropy. The beginnings of such a work can be traced to LIENHARD (1964), who used a statistical mechanical approach to derive a dimensionless unit hydrograph of a drainage basin.

It may be visualized that the study of the landscape is the study of constraints imposed by geologic structure, lithology, and history. The way in which some constraints affect the river profile can be evaluated if one considers the profile to approximate its maximum probable condition under a given set of constraints. The most important observations are summarized as below:

a) The absence of all constraints leads to no solution.
b) The longitudinal profile of a stream system subject only to the constraint of base level is exponential with respect to elevations above base level.
c) The profile of a stream subject only to the constraint of length is exponential with respect to stream length which is a logarithmic function with respect to elevation.
d) Introduction of the constraint of a partial base level above that of the sea adds a measure of convexity in the profile.

PRINCIPLE OF MAXIMUM DISCRETE ENTROPY

For a discrete variable X, Shannon (1948) defines quantitatively the entropy in terms of probability as:

$$H(X) = -\sum_{i=1}^{n} P(X_i) LnP(X_i) \qquad (1)$$

where $P(X_i)$ is the probability of a system being in state X_i which is a member of $\{X_i, i = 1, 2, \ldots\}$, and $\sum_{i=1}^{n} P(X_i) = 1$. It has been proved that H(X) defined by Equation 1 is the only function to satisfy the following three conditions:

a) H(X) is the continuous function of $P(X_i)$.
b) If and only if all $P(X_i)$ are equal, H (X) attains its maximum value. This conclusion is known as the principle of maximum discrete entropy.
c) If the states X and Y are mutually independent, then H(XY) = H(X)+H(Y).

JAYNES (1957) have proved that an equilibrium system under steady constraints tends to maximize its entropy. Based on this statement, the entropy of a river system, having reached its dynamic equilibrium, should approach its maximum value, also the principle of maximum entropy should be valid too for the case of regime rivers.

Stream Power

Although many formulas for sediment transport have been devised, most can be expressed in terms of stream power as suggested by BAGNOLD (1960). Power is an important factor in the formulation of the hydraulic geometry of river channels. As explained by Bagnold, the stream power at flows sufficiently great to be effective in shaping the river channel is directly related to the transport of sediment, whose movement is responsible for the channel morphology. LAURSEN (1958) gives several typical equations for the transport of sediment, based on flume experiments and the average relation shows sediment transport

in excess of the point of incipient motion to vary about as $(vDS)^{1.5}$ where vDS is the stream power per unit area. In terms of sediment per unit discharge, that is the concentration, C, the several equations average out as $C \propto n\,(vD)^{0.5}\,S^{1.5}$, a result that is consistent with the conclusion reached by BAGNOLD (1960). There is in addition to be considered the effect of sediment size. Examination of several equations indicates that sediment transport varies inversely as about the 0.8 power of the particle size. There have been several attempts to relate particle size to the friction factor n and by using the Strickler relation that the value of n varies as the 1/6 power of the particle size. It is realized full well that both the sediment transport and the friction factor are influenced by many other factors such as bed form and the cohesiveness, sorting, and texture of the material. These are the kinds of influences, themselves effects of the river, that prevent a straightforward solution of river morphology. In order to limit the number of variables only the effect of particle size on transport will be considered, as this factor varies systematically along a river from headwater to mouth. Thus, sediment transport concentration is given as $C \propto (vD)^{0.5}\,S^{1.5}\,/\,n^4$. The sediment transport per unit discharge in the river system will be recognized as a hydrologic factor that is independent of the hydraulic geometry of a river in dynamic equilibrium. Consequently sediment concentration may be considered constant.

Thus, there are three equations: continuity, hydraulic friction, and sediment transport. There are five unknowns. The two remaining equations will be derived from a consideration of the most probable distribution of energy and total energy in the river system.

The probability of a given distribution of energy is the product of the exponential functions of the ratio of the given units to the total as

$$p \propto e^{-\frac{E_{n1}}{E}}\, e^{-\frac{E_{n2}}{E}}\, e^{-\frac{E_{n3}}{E}} \ldots etc. \qquad (1a)$$

The ratios of the units of energy E_1, E_2, etc., representing the energy in successive reaches along the river sufficiently long to be statistically independent, to the total energy E in the whole length, are E_1/E ; E_2/E; …… E_n/E. The product of the exponentials of these is the probability of the particular distribution of energy. As previously, the most probable condition is when this joint probability, p, is a maximum and this exists when $E_1 = E_2 = E_3 \ldots = E_n$. Thus energy tends to be equal in each unit length of channel (LEOPOLD AND LANGBEIN, 1962).

Equable distribution of energy corresponds to a tendency toward uniformity of the hydraulic properties along a river system. Considering the internal energy distribution, uniform distribution of internal energy per unit mass is reached as the velocity and depth tend toward uniformity in the river system. Since the energy is largely expended at the bed equable distribution of energy also requires that stream power per unit of bed area tend toward uniformity. An opposite condition is indicated by PRIGOGINE'S (1955) rule of minimization of entropy production which leads to the tendency that the total rate of work, $\sum QS\Delta Q$ in the system as a whole be a minimum. Because $S \propto Q^z$, then $\sum Q^{1+z}\,\Delta Q \rightarrow$ a minimum. For a given drainage basin this condition is met as z takes on increasingly large negative values. However, there is a physical limit on the value of z,

because for any drainage basin the average slope $\sum S\Delta Q/\sum \Delta Q$ must remain finite. This condition is met only for values of z greater than –1, and therefore z must approach –1 or 1 + z approaches zero. The condition of minimum total work tends to make the profile concave; whereas the condition of uniform distribution of internal energy tends to straighten the profile. Hence, we seek the most probable state.

The most probable combination is the one in which the product of the probabilities of deviations from expected values is a maximum. It is unnecessary to evaluate the probability function, provided one can assume normality, as we can then state directly that the product of the separate probabilities is a maximum when their variances are equal.

$$\left(\frac{F_1}{\sigma_{F_1}}\right)^2 = \left(\frac{F_2}{\sigma_{F_2}}\right)^2 = \left(\frac{F_3}{\sigma_{F_3}}\right)^2 = etc. \qquad (2)$$

where F_1, F_2, F_3 represent the several functions. The standard deviations σ_m, σ_f, σ_z, and σ_y represent the variability of the several factors as may occur along a river system. Since these values are not known initially, the problem must be solved by iteration (LEOPOLD AND LANGBEIN, 1962). Fortunately, the solution is not sensitive to the values of the several standard deviations, so the solution converges rapidly. Therefore,

$$\left(\frac{F_1}{\sigma_{F_1}} + \frac{F_2}{\sigma_{F_2}}\right)\left(\frac{F_1}{\sigma_{F_1}} - \frac{F_2}{\sigma_{F_2}}\right) = 0 \qquad (3)$$

for which there are two possible solutions:

$$\left(\frac{F_1}{\sigma_{F_1}} + \frac{F_2}{\sigma_{F_2}}\right) = 0 \qquad (4)$$

or

$$\left(\frac{F_1}{\sigma_{F_1}} - \frac{F_2}{\sigma_{F_2}}\right) = 0 \qquad (5)$$

To summarize, we have introduced three statements on the energy distribution:

$$\frac{1}{2}z - y \to 0$$
$$m + f + z \to 0$$
$$(1+z) \to 0 \qquad (6), (7), (8)$$

The absolute values of the standard deviations need not be known, as we can infer their relative values. For example, letting $F_1 = (1/2)z - y$, the standard deviation of F_1 is

$$\sqrt{(\sigma_{z/2})^2 + \sigma_y^2} \qquad (9)$$

and $F_2 = m + f + z$; $\sigma_{F_2} = \sqrt{\sigma_m^2 + \sigma_f^2 + \sigma_z^2}$; $F_3=(1+z)$; $\sigma_{F3} = \sigma_z$

$F_2=m+f+z$ (10)

Leopold and Maddock (1953) describe and evaluate from field data the hydraulic geometry of river channels by a set of relations as follows:

$v \propto Q^m$ (11)

$D \propto Q^f$ (12)

$w \propto Q^b$ (13)

$S \propto Q^z$ (14)

$n \propto Q^y$ (15)

where v is the mean velocity, D is the mean depth, w is the surface width, and S is the energy slope, and n is the friction factor at a cross section along a river channel where the mean discharge is Q. It is desired to evaluate the exponents in a downstream direction as discharge of uniform frequency increases. Some of the principles that have been described can provide estimates of the magnitude of the exponents of the above relationships. The exponents m, f, b, z, and y describe the variability in velocity, depth, width, slope, and friction along a river channel, but do not uniquely determine the magnitudes of these properties. The first condition is that specified by the equation of continuity Q=vDw, which requires that

$m + f + b = 1.0$ (16)

The solution of their values is not available for the first trial solution so all values are considered equal. Thus:

$$\left(\frac{m+f+z}{\sqrt{3}}\right)^2 = \left(\frac{\frac{1}{2}z - y}{\sqrt{1.5}}\right)^2 \quad (17)$$

$$\left(\frac{\frac{1}{2}z - y}{\sqrt{1.5}}\right)^2 = \left(\frac{1+z}{1}\right)^2 \quad (18)$$

$$\left(\frac{m+f+z}{\sqrt{3}}\right)^2 = \left(\frac{1+z}{1}\right)^2 \quad (19)$$

The results of the first solution are then used to derive first estimates of the standard deviations, and a second computation carried forward. A third calculation is made to confirm the results of the second trial solution. These three equalities lead to two independent equations

$y = - ½ (m + f)$ (20)

$z = - 0.53 + 0.93 y$ (21)

which, together with the three hydraulic conditions

$m + f + b = 1.0$ (22)

$m = (2/3)m + (1/2)z – y$ (23)

$(1/2)m = (1/2)f + 1.5 z – 4y = 0$ (24)

lead to a solution for m, f, b, z, and y. The final values, derived without reference to field data, are compared below with others obtained previously from analysis of field data on actual rivers.

Table 1. Values of exponents of the hydraulic geometry in downstream direction (LEOPOLD AND MADDOCK, 1953)

Theoretical values	Average values from data on rivers
Velocity, m = 0.09	m = 0.10
Depth, f = 0.36	f = 0.40
Width, b = 0.55	b = 0.50
Slope, z = - 0.74	z = - 0.49
Friction, y = - 0.22	

Velocity is such a large factor in energy expenditure, the value of m, the exponent of velocity, is close to zero, making this characteristic the most conservative. The value of z which is the measure of the variability in slope is least satisfactorily defined from field data, as it is affected by variation in the friction factor. Thus, the value of z as reported above is – 0.53 + 0.93 y. Hence the value of z is – 0.53 where grain size is constant. The value of z was found by Leopold (1953) to be – 0.49 for midwestern rivers. Henderson (1961) shows that for a stable channel of uniform grain size the slope varies as the – 0.49 power of the discharge (Table 1). However, when a large variety of river data were averaged, including data on ephemeral channels, Leopold and Miller (1956) obtained a value of z averaging near z = - 0.95. Values of z in excess of 0.50 may be attributed to the common tendency for the friction factor to decrease downstream by increasing discharge as particle size decreases. In canals, for example, where y is positive, the value of z is less than 0.50 (LEOPOLD AND LANGBEIN, 1962). The study of hydraulic geometry develops a method of solution through introduction of probability statements. The results which are obtained by this theoretical derivation of exponents in the hydraulic geometry agree quite well with field data , but we are far from satisfied physical relationships. For example, there is uncertainty whether the transport equations represent physical relationships or are in fact formulas for sediment transport under regime conditions. Several alternative assumptions were tried and the resulting exponents also agreed quite well with field data.

Drainage Network

In the longitudinal profile, the probability that a random walk will fall in certain positions within the given constraints can be ascertained. There is also a mean or most probable position for a random walk within those constraints. This statement suggests the possibility that a particular set of constraints might be specified that would describe the physical situation in which drainage channels would develop and meet. If the precipitation falls on a uniformly sloping plain which develops an incipient set of rills near the watershed, the rills deepen with time and crossgrading begins owing to overflow of the shallow incipient rills. The direction that the crossgrading takes place is a matter of chance until the rills deepen sufficiently to become master rills. The randomness in the first stages of crossgrading might be approximated in the conceptual model which is amenable to mathematical description. Considering a series of initial points on a line and equidistant from one another at spacing a and assuming random walks originating at each of these points.

Experimental setup

A movable laboratory channel with varying slope was installed for investigating the meander evolution, measuring the erosion rate, and studying the sediment-water interaction in the meandering channel. On the bottom of the channel that is filled with the cohesionless sand, a straight initial channel that was to follow a meandering path during flow was carved. Discharge, slope of the main channel, and sediment transport rate were observed during the meandering plan-formation.

The main channel was 10 m long, 1.60 m wide, and 0.42 m deep. The original channel was filled through a feedback system with a uniform sand of 1.35 mm of median diameter up to a depth of 0.30 m. A movable carriage was mounted on the 8.80 m long side rails for measuring the channel and sediment-flow characteristics. Water coming from the head tank was passed through a water tranquilizer, which was 1.60 m wide, 0.26 m long, and 0.65 m deep. The sediment supplier for the feedback system was laid at the entrance, but after the tranquilizer. The downstream reservoir for outflow with the end gate (0.15 m wide and 0.15 m high) was 1.10 m long, 1.60 m wide, and 0.65 m deep. The sand collector (0.42 m x 1.60m x 0.65m) was placed at the end of the channel. Into the uniform sand (of 1.35 mm of median diameter) of the 8.80 m long flume channel, a trapezoidal cross-section was carved, with a bottom width = 0.10 m, water width = 0.20 m, and flow depth = 0.10 m.

The movable carriage on the side rails was used for setting the profile indicator instrument and the velocity measurement instrument for obtaining the geomorphological and physical characteristics of the meandering channel. In experimentation, it was possible to change the slope, discharge, and other hydraulic parameters. For exact measurements of the sediment transport rate, a Sartorius weight measuring instrument was placed at the end of the channel. The sediment washed down from the flume was collected with a sieve in the downstream reservoir. It was dried and weighed with the Sartorius weight measuring instrument for computing the total sediment transport rate.

Experimental observations

The experimental model in the present study consists of a very simple straight channel, which, after some time, converts to meander planforms on the sandy bottom of the main channel. Thus, the experimental setup seems to mimic a natural meandering river, for it reflects the development of a meandering channel on the cohesionless bottom boundary layer, exhibiting every phase from the beginning to the end of the erosion event at the bank and the bottom boundary layer. However, one of the limitations of the experimental setup was its inability to observe braiding planforms. It was seen that there was no sediment transport after meandering and the stability of the flume was observed with the development of the meandering planform. Since flow exerts shear stresses that can remove particles from the banks and the near-bank flow pattern is determined by discharge, the influence of only discharge was taken into account in the experimental investigation.

Observations for the transported bed material weight in time were taken for Q = 0.1536 l/s and S = 0.08 %, and these

are presented in this study. However, the main channel slope could be varied between 0.04–0.5 % and the main channel discharge between 0.07–0.73 l/s. Measurements could not be made for experimental limitations beyond this range. For example, the flow in the flume of sandy bottom changed from subcritical to supercritical regime as the slope increased beyond the given range. Furthermore, more versatile equations for bed load transport and for meandering bend planform are required to deal with supercritical flows. In the case of high flows, the zone of maximum bedload transport shifted outward through the bend. Over 80% of the bed load in transport traveled to the right (closer to the inside bank) of the centerline in the upstream part of the bend. In the downstream portion of the bend, over 50% traveled to the left (closer to the outside bank) of the centerline.

The temporal variation of the total dry mass of the collected sediment amount is depicted. Dividing the total dry weight of the collected sediment amount by the sediment-collection time yields the average sediment transport rate in mass per unit time. Sand transport varied from 21–200 gm per hour during 320 hours of the experiment. The sand-water mixture introduced into the initial straight channel caused it to transform to the meandering form after 320 hours, the time after which an equilibrium condition was reached. Here, the equilibrium condition infers no sediment transport condition. In the developing meandering channel, bed profiles and velocities were measured by the profile indicator and velocity-measurement instruments.

It was observed that the slope of the channel increased as it developed from the straight form through a shoaled condition to the meandering pattern, and that this channel pattern was associated with significantly higher sediment transport rates than the straight form. To prevent the channel from overflowing due to the increasing bed slope at the head of the system, a constant small freeboard was maintained during experimentation.

Analysis of Experimental Measurements

Modeling of Sediment Transport Rates

Utilizing the laboratory observations, two equations were developed: one for bed load transport and the other for meander planform. This involves (1) an investigation of sediment transport in the laboratory flume, considering the prototype, and (2) development of an experimental meander bend equation. Sediment–transport processes lead to meandering planforms at the flume-bank erosion and consequently, to flume widening. Using the sediment transport measurements, the correlation between the sediment transport change and meandering planform was analyzed. To that end, an attempt was made to begin the experimental procedure with first 'measuring the sediment transport' and then 'measuring the meander bend formation'.

For the above Q- and S-values, the measurements of the sediment transport rates for the whole period of 320 hrs are depicted. It is apparent from this figure that there exists a specific value of the sediment rate at time equal to zero. It is for the reason that the sediment load was supplied through the feed-

back system just before the time of the start of experimentation. Soon afterwards, the rate increases sharply and then decreases in a fluctuating manner, but generally decays with time. The sudden kinks here and there in the graph are the result of sudden erosion of the bed and banks of the channel and its washing away to the end of the channel, where it is finally collected for measurements. The sudden washing away of the sediment particles is also attributed to the generation of secondary currents that augment the flow velocity because of the variation in the effective discharge due to the supplying of sediment load through feed-back system. After the occurrence of such a phenomenon, a reverse trend of decreasing sediment rate is visible. It occurs because of the negative role of secondary velocities, leading to the reduction of the effective downstream flow velocity. Ignoring these effects, the overall result is that the sediment rate decays almost exponentially with time and reaches almost a constant or equilibrium value after approximately 320 hrs.

The decaying trend of the depicted sediment transport rates can be modeled by the following empirical relation:

$$Q_b = 1.5227\ e^{-0.0091\ t} \qquad (25)$$

with the correlation coefficient (R^2) equal to 0.8993, indicating a reasonably good fit. In Equation 25, Q_b is the total bed load in the experimental channel in kg/hr, t is the time in hour (after the beginning of meandering). It is noted that this equation is fitted to the observed data points excluding the points showing sudden kink at 115 and 225 hrs. It exhibits an intercept of 1.5227 kg/hr at time equal to 0 and sediment transport rate approaches zero when time approaches infinity. Physically, the intercept indicates approximately the sediment transport rate supplied through the feed-back system at time t = 0. The disadvantage of the fitted model, however, is that the equilibrium condition reaches at t approaching infinity. On the other hand, this condition was practically observed between 250 and 320 hrs since the beginning of meandering. Thus, many more sets of observations will be required before finally recommending an equation of the kind of Horton (1945) infiltration model, which incorporates a static infiltration component analogous to the equilibrium condition of sediment transport rate achieved after a certain time. However, taking the value of this equilibrium condition equal to 0.165 kg/hr, Equation 25 is modified as:

$$Q_b = 0.1650+1.3577\ e^{-0.0091\ t} \qquad (26)$$

where the decay factor is equal to 0.0091 per hr. The development of such an equation is of significance for reason that the bed load molds the geometry of rivers. Since the short-duration (for example, 5 minutes or shorter) sand transport rates were not measured, Equations 25 and 26 may not be valid for the short-duration measurements and require a detailed investigation for the development of a comprehensive sand transport curve.

Modeling of Channel Meander Planforms

In channel meandering, flume erodibility is not the only limiting factor for cross-section widening. When a cross-section becomes very wide and shallow, its cross-sectional shape may become unstable and develop into a number of separate, narrower chan-

nels, thus transforming into a braided or an anabranching river. In the present experimentation, limited runs were taken only for achieving the meandering planforms and for braiding or anabranching river cross-sections, the experiment was not continued.

The formation of the meandering channel at different times and in a specific channel reach of 250 cm is shown in Figure 1, in which x is the space coordinate in the flow direction, and y is the space coordinate in the normal direction. Since longitudinal planform changes were insignificant, only lateral planform changes were considered. It is apparent from Figure 1 that at time t increases the departure of the meandering channel (measured from the center of the initially straight channel) increases with time and at time t = 160 hrs, a fully developed meandering planform was observed. It is also apparent from this figure that the radius of curvature of the meander increases from 0 to 125 cm, where it is maximum, and then, continually decreases up to 250 cm. The apparent kinks in the meander planforms are the result of local changes in secondary currents of the flume. These planform changes can be modeled by a quadratic equation of the form:

$$y = a\,x^2 + b\,x + c \qquad (27)$$

where y is the lateral departure of the meandering channel from the initially straight channel in the longitudinal direction x, and a through c are the parameters. The computed parameter values for time-varying planform changes are given in Table 1. It is seen from this table that the values of the coefficient of correlation range from 0.8405 to 0.9847 suggesting satisfactory fits to the planform changes.

In an attempt to investigate the variation of the parameters of Equation 27 with the changing meandering planforms, these were correlated with time for making the planform model (Equation 27) fully predictive.

Table 2. Changes of parameter values of Equation 27 With Time.

Time (hr)	Parameter			Coefficient of determination, R^2
	'a'	'b'	'c'	
0	0	0	0	-
40	0.0003	-0.0628	7.284	0.8405
80	0.0008	-0.1937	18.185	0.9573
120	0.0011	-0.2643	26.082	0.9798
160	0.0016	-0.4011	34.962	0.9847

Table 3. Fitting Values of Parameters M and C1 Of Equation 28

Parameter	M	c_1	Coefficient of determination, R^2
'a'	1.0×10^{-5}	-4×10^{-5}	0.9926
'b'	-0.0025	0.0164	0.9855
'c'	0.2218	-0.4418	0.9971

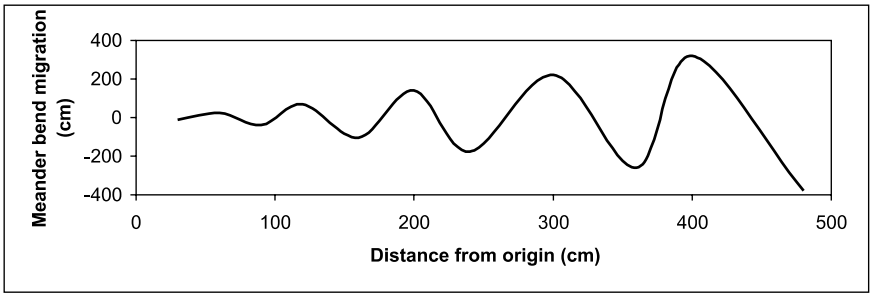

Q = 0.08 l/s ; S_o= 0.08 %

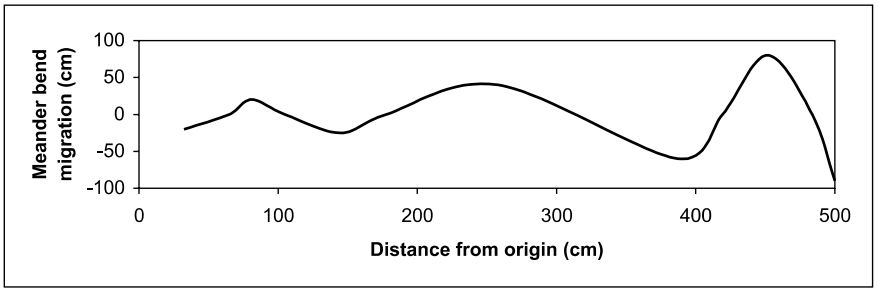

Q = 0.20 l/s ; S_o=0.10%

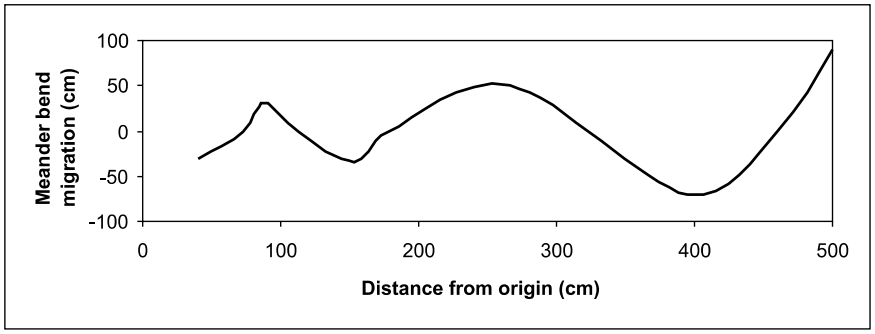

Q = 0.40 l/s ; S_o = 0.20 %

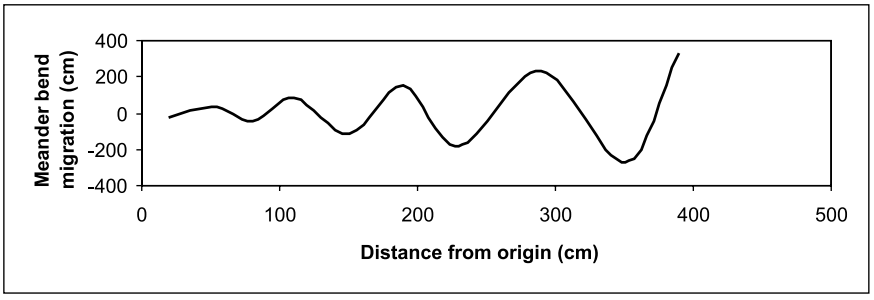

Q = 0.50 l /s ; S_o= 0.35 %

Figure 1. Fully developed meandering channel patterns for various of discharge (Q) and bed slopes (S_o) of the channel after 72 hours

In Table 3, the fitted relations for the parameters of Equation 28 with time exhibit the straight-line relationship:

$$y_1 = m\, x_1 + c_1 \qquad (28)$$

where y_1 represents the parameter a, b, or c of Equation 27; x_1 is the time (hr); and m and c_1 represent the slope and intercept of the straight line, respectively. The computed values of the parameters of Equation 28 for the parameters a, b, and c of Equation 28 are summarized in Table 3. Apparently the computed values of R^2 range from 0.9855-0.9971, exhibiting excellent fits. It is apparent from Table 2 that parameter 'a' grows linearly with time, and so does the parameter 'c'. Parameter 'b', however, decreases with time. The consistent regular relationship of each parameter with time exhibits a sound predictability of the above meander planform model (Equation 27). It is interesting to note that all parameters exhibit a linear variation with time. However, the meandering phenomenon is a non-linear process, for the parameters change with time although linearly. The workability of the developed meandering model (Equation 27) and the parametric relations (Equation 28) is demonstrated by comparing the observed meander departures from the initially straight channel with the computed ones in Figure 1. In this figure, the line of perfect fit (LPF) indicates a perfect match between the observed and computed values. The values above and below the LPF indicate over- and under-prediction by the model (Equation 27). It is seen that all the data points hover around the LPF, indicating a satisfactory prediction. The NASH AND SUTCLIFFE'S (1970) efficiency is computed as equal to 97.2187, which shows an excellent model prediction.

DISCUSSION AND GEOMORPHIC RESULTS

The investigation shows that several geomorphic forms appear to be explained in a general way as conditions of most probable distribution of energy, the basic concept in the term "entropy". The word entropy has been used in the development of systems other than thermodynamic ones, specifically, in geomorphological theory. Stream channels show in many ways the effects of previous climates, and of structural or stratigraphic relations that existed in the past. In some instances the present streams reflect the effects of sequences of beds which have been eradicated by erosion during the geologic past. However, these conditions that presently control or have controlled in the past the development of geomorphic features now observed need not be viewed as preventing the application of a concept of maximum probability. Rather, the importance of these controls strengthens the usefulness and generality of the entropy concept. In a sense, much of geomorphology has been the study of the same constraints that have been attempted to express in a mathematical model. The geomorphic results show that the present model should not be considered to deal with random walks. It is concerned with the distribution of energy in real landscape problems. The experimental model also give the proofs to this consideration.

References

Ackers, P., and Charlton, F. G., 1970a, Meander geometry arising from varying flows, Journal of Hydrology, Vol. 11, No.3, pp. 230-252.

Bagnold, R. A., 1960, Sediment discharge and stream power – a preliminary announcement: U. S. Geol. Survey Circ. 421, 23 p.

Best, J. L. and Bristow, C. S., 1993, A cellular model of braided rivers, Geological Society, London. p.113

Bettess, R., and White, W. R., 1987, Flood Mitigation Strategy for Medium-sized Streams, Canadian Water Resources, Vol. 11, pp. 132 – 141.

Burkham, D. E., 1972, Channel changes of the Gila River in Safford Valley, Arizona 1846 – 1970, U.S. Geological Survey Professional Paper 655 –6.

Da Costa, Newton C. A., 1974, On the theory of Inconsistent Formal Systems, NDJFL, Vol. 15, pp. 497 – 510.

Einstein, H. A., 1950, The bed-load function for sediment transportation in open channel flows : Tech. Bull., U.S.D.A., Soil Conservation Service, No. 1026.

Everitt, B. L., 1968, Use of the cottonwood in an investigation of the recent history of a floodplain, American Journal of Science, Vol. 266, pp. 417 – 439.

Ferguson, R. I., 1986, Hydraulics and hydraulic geometry, Progress in Physical Geography, Vol. 10, pp. 1 – 31.

Gupta, A, and Fox, H., 1974, Effects of High Magnitude Floods on Channel Form: A Case Study in the Maryland Piedmont, Water Resources Research, Vol: 10, pp. 499 – 509.

Hadley, R. F., 1961, Progress in the application of landform analysis in studies of semiarid erosion, U. S. Geological Survey Circular, 437.

Harvey, M. D., and Watson, C. C., 1986, Fluvial processes and morphologic thresholds in stream channel restoration, Water Resources Bulletin, Vol. 22, no:3, pp. 359 – 368.

Henderson, F. M., 1961, Sediment Transport, Open Channel Flow, Chapter 10, MacMillan, New York.

Hereford, R., 1984, Climate and ephemeral stream processes: Twentieth –Century geomorphology and alluvial stratigraphy of the Little Colorado River, Arizona: Geological Society of Amerika Bulletin, Vol. 95, pp. 654 – 668.

Horton, R. E., 1945, Erosional development of streams and their drainage basins; hydrophysical approach to quantitative morphology: Geol. Soc. America Bull., v. 56, p. 275-370.

Jaynes, E. T., 1957, Information theory and Statistical mechanics, I, Physics Review, Vol. 106, pp. 620-630.

Laursen, E. M., 1958, Sediment-transport mechanics in stable channel design: Am. Soc. Civil Engrs. Trans. V. 123, p. 195-206.

Leopold, L. B., 1953, Downstream change of velocity in rivers: Am. Jour. Sci., v. 251, p. 606-624.

Leopold, L. and T., Maddock, 1953, The hydraulic geometry of stream channels and some physiographic implications, U.S. Geological Survey Professional Papers, United States Government Printing Office, Washington.

Leopold, L. B., and Maddock, T., Jr., 1953, The hydraulic geometry of stream channels and some physiographic implications: U. S. Geol. Survey Prof. Paper 252, 56 p.

Leopold, L. B., and Miller, J. P., 1956, Ephemeral streams – Hydraulic factors and their relation to the drainage net: U. S. Geol. Survey Prof. Paper 282-A, p. 1 – 36.

Leopold, L. B., and Wolman, M. G., 1957, River channel patterns; Braided, meandering and straight, USGS Professional Paper 282-B, pp. 45-62.

Leopold, L. B. and LangbeinW. B., 1962, The concept of entropy in landscape evolution, Geological Survey Professional Paper, 500-A.

Leopold, L. B., Wolman, M. G., and Miller, J. P., 1964, Fluvial processes in geomorphology, W. H. Freeman and Co., San Francisco, Calif., p. 522.

Lienhard, J. H., 1964, A statistical mechanical prediction of the dimensionless unit hydrograph, Journal of Geophysical Research, Vol. 69, No: 24, pp. 5231.

Little, A. D. and Curren, C. E., 1982, Archaeological Investigations in the Buttahatchee River Valley, Journal of Alabama Archaeological Society.

Nadler, C. T. and S. A. Schumm, 1981, Metamorphosis of South Platte and Arkansas Rivers, Eastern Colorado, Physical Geography, Vol. 2, pp. 95 – 115.

Nanson, G. C. and Hickin, E . J., 1983, Channel migration and incision on the Beatton River, ASCE, Journal of Hydraulic Engineering, Vol. 109, pp. 327 –337.

NASH, J. E. AND J. V. SUTCLIFFE, 1970, River flow forecasting through conceptual models part 1, A discussion of principles, Journal of Hydrology, Vol. 10, No. 3.

PIZZUTO, J. E., 1992, The morphology of graded gravel rivers: a network perspective, Geomorphology, Vol. 5, pp. 457 – 474.

PRIGOGINE, I., 1955, Introduction to thermodynamics of irreversible processes: C. C. Thomas, Springfield, III., 115 p.

SCHUMM, S. A., AND LICHTY, R. W., 1963, Channel widening and flood – plain construction along Cimarron River in Southwestern Kansas, U. S. Geological Survey Proof.

SCHUMM, S. A., AND LICHTY, R. W., 1965, Time, space and causality in geomorphology, American Journal of Science, Vol. 263, pp. 110 – 119.

SHANNON, C. E., 1948, A mathematical theory of communication, Bell System Technical Journal, Vol. 27, Part I, July, pp. 379-423; Part II, Oct., pp. 623 –656.

SIMON, A., 1989, Energy, time, and channel evolution in catastrophically disturbed fluvial systems, Geomorphology, Vol. 5, pp. 345 – 372.

SIMON, A. AND THORNE, C. R., 1996, Channel adjustment of an unstable coarse – grained stream: opposing trends of boundary and critical shear stress and the applicability of extremal hypotheses: Earth Surface Processes and Landforms, Vol: 28, pp. 1271 – 1287.

THORNE, C. R., RUSSELL, A. P. G., AND ALAM, M. K., 1993, Planform pattern and channel evolution of the Brahmaputra River, Bangladesh, in Best, J. L. and Bristow, C.S. (Eds.), Braided Rivers, Geological Society Special Publications 75, pp. 257 –276.

WILLIAMS, G. P., 1978, Planetary circulations: 1. Barotropic representation of Jovian and terrestrial turbulence, J. Atmos. Sci., Vol. 35, pp. 1399 – 1426.

WOLMAN, M. G., 1955, The natural channel of Brandywine Creek, Pennsylvania, U. S. Geological Survey Professional Paper, 271.

WOLMAN, M. G. AND GERSON, R., 1978, Relative scales of time and effectiveness of climate in watershed geomorphology, Earth Surface Processes and Landforms, Vol: 3, pp. 189 – 208.

WOODYER, K. D., 1968, Bankfull frequency discharge in rivers , J. Hydrology , Vol. 6, pp. 114 – 142.

YANG, C. S., 1971, On river meandering. J. Hydraul. Engrg, ASCE, Vol. 13, pp. 231-253.

Structural maps of seismic horizons in the Krško basin

Strukturne karte seizmičnih horizontov v Krški kotlini

Andrej Gosar[1,2], Bojana Božiček[2]

[1]Environmental Agency of the Republic of Slovenia, Dunajska 47, SI-1000 Ljubljana, Slovenia,
E-mail: andrej.gosar@gov.si
[2]University of Ljubljana, Faculty of Natural Sciences and Engineering,
Aškerčeva 12, SI-1000 Ljubljana, Slovenia

Received: November 02, 2006 **Accepted**: November 14, 2006

Abstract: Structural maps of the pre-Tertiary basin and of five horizons inside the sequence of Neogene sediments were prepared based on the interpretation of seismic reflection profiles recorded in three surveys performed in the Krško basin so far. Interpolation of the Mesozoic basement between seismic profiles was supported by gravity data. The structural maps clearly shows rather regular synclinal shape of the Krško basin which is composed of two depressions. The larger Globoko depression in the eastern part is 2050 m deep and the smaller Raka depression in the western part is 1600 m deep. The thicknesses of some Neogene sequences in-between seismic horizons varies considerably. Most prominent is thickening of the Ottnangian and Lower Badenian layers between horizons C and B from 300 m in the Globoko depression to up to 1000 m in the Raka depression. On the other hand the thickness of the Upper Pontian sand, gravel and clay increases from 100 m in the western part to up to 500 m in the Globoko depression. There are several indications of synsedimentary folding of the area but also some indications of postsedimentary activity. The structural models of seismic horizons allow additional geophysical and structural-geological interpretations of the area. Together with seismic velocity models they served also as input data for the construction of two-dimensional cross-sections in arbitrary directions for numerical modelling of seismic ground motion in the frame of seismic hazard assessment

Izvleček: Na podlagi interpretacije refleksijskih seizmičnih profilov izmerjenih v okviru treh raziskav opravljenih do sedaj v Krški kotlini so bile izdelane strukturne karte predterciarne podlage in petih horizontov znotraj neogenskih sedimentov. Interpolacija mezozojske podlage je bila podprta z gravimetričnimi podatki. Strukturne karte jasno kažejo dokaj pravilno sinklinalno obliko Krške kotline, ki jo sestavljata dve depresiji. Večja je Globoška depresija v vzhodnem delu kotline, ki je globoka 2050 m, manjša pa Raška depresija v zahodnem delu, ki je globoka 1600 m. Debelina nekaterih neogenskih sekvenc med seizmičnimi horizonti se znatno spreminja. Najbolj izrazita je odebelitev ottnangijskih in spodnjebadenijskih plasti med horizontoma C in B od 300 m v Globoški depresiji do skoraj 1000 m v Raški depresiji. Po drugi strani pa se debelina zgornjepontijskih peskov, prodov in gline poveča iz 100 m v zahodnem delu na do 500 m v Globoški depresiji. Podatkih kažejo precej indikacij na sinsedimentarno gubanje območja, pa tudi nekatere indikacije za postsedimentarno aktivnost. Strukturni modeli omogočajo dodatne geofizikalne in strukturnogeološke analize raziskanega območja. Skupaj s seizmičnimi hitrostnimi modeli so služili tudi za izdelavo dvodimenzionalnih prerezov v poljubnih smereh za numerično modeliranje potresnega nihanja tal v okviru ocenjevanja potresne nevarnosti.

Key words: seismic reflection, seismic horizon, gravity data, structural map, Krško basin, pre-Tertiary basement
Ključne besede: seizmična refleksija, seizmični horizont, gravimetrični podatki, stukturna karta, Krška kotlina, predtercirana podlaga

Scientific paper

INTRODUCTION

Several geological and geophysical investigations have been performed in the Krško basin starting about fifty years ago for a wide range of objectives: for oil and gas prospecting, for exploitation of geothermal energy, for underground gas storage in aquifers and for assessment of earthquake hazard at the location of the Krško nuclear power plant (NPP). Although the goals of these investigations were different, it was realised that a thorough understanding of the regional structural-tectonic setting of the basin is essential for most of these objectives. According to the prevailing hypothesis the Krško basin was considered as a tectonic graben structure (PLENIČAR & PREMRU, 1977; ŠIKIĆ ET AL., 1979; POLJAK & ŽIVČIĆ, 1995), although that no proofs were available for supposed normal border faults at the northern and southern margin of the basin. Since most of geophysical investigations were limited to the flat central part of the basin, it was not possible to confirm this hypothesis, before multi-fold seismic reflection profiling was completed (GOSAR, 1998; PERSOGLIA ET AL., 2000). Based on these data the Krško basin is considered now as a folded syncline with no border faults at least in the eastern part of the basin (GOSAR, 1998; VERBIČ ET AL., 2000; POLJAK & GOSAR, 2001).

Three seismic reflection surveys were performed in the Krško basin so far. From two to six seismic horizons were interpreted on these profiles depending on the quality of the seismic data recorded in time span from 1959 to 2000. The deepest horizon correspond to pre-Tertiary bedrock composed of Mesozoic carbonates. Another one to five horizons were interpreted inside the sequence of Neogene sediments. The aim of this paper is to present structural geological maps of all six seismic horizons for the Krško basin which is composed of two depressions. The western Raka depression is up to 1600 m deep and the eastern Globoko depression is up to 2050 m deep. The structural model of the Krško basin will allow additional geophysical and geological interpretations of the area based on the variation of unit thicknesses. It served also as input data for the construction of two-dimensional cross-sections in arbitrary directions for numerical modelling of seismic ground motion in seismic hazard assessment.

SEISMIC REFLECTION INVESTIGATIONS

Single-fold analogue reflection profiling in 1959

The first seismic reflection investigations were performed in 1959 by *Geofizika* Zagreb for oil and gas prospecting. Four profiles with analogue recording and single fold coverage were measured in length totalling 36.5 km (Figure 1), three in transverse (P-83/59, P-84/59 and P-85/59) and one in longitudinal direction (P-86/59) with respect to the axis of the syncline. 24-channel seismograph with 3 geophones per point and 20 m group spacing were used and explosive as a source. The original report of these measurements and their interpretation is not preserved.

The analogue seismic data were later digitized and reprocessed (KALOPER, 1984). In comparison with modern digital profiles the quality of these sections is rather poor. In general deeper part of the basin is better imaged, whereas the noise is dominating in

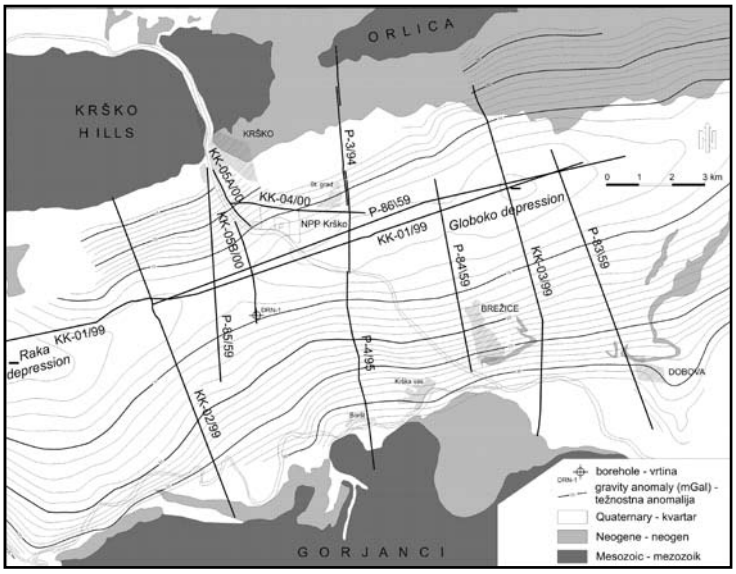

Figure 1. Simplified geological map of the Krško basin (after Pleničar & Premru 1977; Šikić et al., 1979) with Bouguer anomaly map (after Urh, 1955) and location of seismic reflection profiles

Slika 1. Poenostavljena geološka karta Krške kotline (po Pleničarju & Premruju 1977; Šikiću et al., 1979) s karto Bouguerjevih anomalij (po Urhu, 1955) in položajem refleksijskih seizmičnih profilov

the shallow part. The profiles were reinterpreted using new structural and velocity data obtained from the multi-fold data recorded in 1994/95. In general it was possible to interpret two horizons (Table 1), the top of Badenian limestone (horizon B) and the pre-Tertiary basement (horizon C) (Gosar, 1996). These seismic lines do allow interpretation of the main Krško syncline axis. The southern limb of the syncline is also secondarly folded in segments as is seen in the P-85/59 profile. Among faults, visible on these profiles is the most important south verging steep reverse Artiče fault (P-84/59) that crosscut the whole Tertiary sedimentary sequence.

Multi-fold reflection profiling in 1994/95

To improve the structural model, high-resolution seismic reflection methods were used in the first phase of the re-evaluation study of the Krško NPP site. Profiling in two depth ranges was performed in the frame of national research project entitled *Neotectonic investigations in the vicinity of the Krško NPP* (Poljak et al., 1996). The goal of the near-regional profile of intermediate depth penetration was to collect structural data down to the pre-Tertiary basement (Gosar, 1996; 1998). A 13-km-long profile (P-3 and P-4/95) was recorded 2 km east of NPP (Figure 1) by using 15 m group spacing, arrays of 12 geophones and 12-fold coverage. Acquisition parameters and processing parameters were optimised to improve the resolution.

The most prominent reflections were obtained from the top of the Badenian limestone (horizon B), whereas the Mesozoic (horizon C) basement was less pronounced (Table 1). In the upper section, a clear image of the boundary between Pontian sandy marl and Pannonian marl (horizon A) was obtained. A folded structure is clearly visible from the profile. The maximum depth to the Badenian limestone is 1200 m, whereas the depth to the pre-Tertiary basement reaches 1500 m. The northern limb of the syncline is steeper than the southern one, where more steps are visible in the basement.

The reflections in the northern part of the syncline, down to the horizon B, are predominantly parallel and could be an indication of postdepositional folding, although this observation is made over a limited distance of 1 km. On the other hand, surface geological observations indicate a condensed thinned Neogene section near the north margin of the basin that is an argument in favour of synsedimentary folding (GOSAR, 1998).

Reflection profiling in the frame of the EC-PHARE project

Reflection seismic profiling continued with an international project entitled *Geophysical Research in the Surroundings of the Krško NPP* financed by the European Commission - program PHARE. This was so far the largest geophysical project in the Krško area (PERSOGLIA ET AL., 2000). The main project goals were: obtaining good subsurface information about geological and tectonic features, locating possible faults cutting through the bedrock and sediments, and defining the position of faults at or near the surface as accurately as possible.

The geophysical program (Figure 1) was composed of:

1) three near-regional reflection lines totalling 42 km length,
2) three near-regional lines totalling 9.5 km recorded close to NPP and
3) four high-resolution profiles in length totalling 4 km to resolve the shallow features at selected locations.

Regional profiles were measured with explosive source fired in 5-10 m deep boreholes. By placing the source below the water table, the signal strength was significantly improved and the level of source generated coherent noise reduced. For data acquisition 120 active channels were used with arrays of 12 geophones. The group spacing was 15 m, the shot interval 15 m and the nominal coverage 18-fold (ACCAINO ET AL., 2003).

Good penetration of the seismic signals was obtained for the near-regional profiles (KK-01/99, KK-02/99, KK-03/99), within the basin down to the Mesozoic rocks (horizon C) at depths greater than 2 km. The explosive charge placed beneath the weathered zone, produced seismic signals having a wide frequency band, well suited for the required resolution and characterization of the different geological layers and for revealing the structural elements. In the shallow section, frequencies were around 80 to 90 Hz; at the base of the basin the signal frequencies were still between 40 and 60 Hz, giving a resolution of around 5 m in the shallower parts and 25 m near the base of the basin.

Further extension of the program was proposed to close the loop of seismic lines around the NPP location. The extended program (lines KK-04/00, KK-05A/00 and KK-05B/00) was completed using a mobile

accelerated weight drop (Hydrapulse) source. This choice was required by the proximity of houses, factories and other constructions. The acquired data offer good images of the terminations of the Tertiary and Quaternary sedimentary units at the northern flank of the basin (the anticline of the Libna). The line KK-05B/00 permits a tie of seismic data with the Drn-1/89 well and the stratigraphic correlation of seismic horizons with the markers encountered by the well.

In next paragraphs main three near-regional seismic lines are presented. All depths are referred to the elevation of the datum plane at 150 m above sea level.

KK-01/99 profile follows the longitudinal axis of the Krško syncline close to its deepest part. Two large sub-basins as also identified by the Bouguer anomalies (Figure 1) are clearly visible in this profile. The depth to the pre-Tertiary basement reaches more than 2000 m in the eastern sub-basin (Globoko depression) and about 1600 m in the western one (Raka depression), rising to around 1100 m depth at the saddle, interpreted as the top of Dinaric thrust. They are differentiated by the thick Lower and Middle Miocene sequences in the western part and by thicker Pliocene and Quaternary deposits in the eastern one.

KK-02/99 profile (Figure 2) crosses the basin in NNW-SSE direction between Krško hills and Gorjanci in a transition zone between structural height and the Raka depression. Some thrusts moving the Mesozoic bedrock were observed in this profile and the folding of the whole Neogene sequence. The fault system in the northern part of the profile possibly corresponds to Orlica fault.

KK-03/99 profile (Figure 3) crosses the basin in N-S direction between Orlica and Čatež. It clearly represents the almost symmetric cross-shape of the syncline in the deepest part of the Globoko depression. The Artiče fault is an important tectonic feature confirmed in the northern limb of the depression with this profile (Accaino et al., 2003). It displaces the Mesozoic bedrock as well as most of the Neogene horizons. Towards the surface the throw between different units becomes smaller. The fault can be traced to very shallow depth, but no indications of deformation were found in recent sediments.

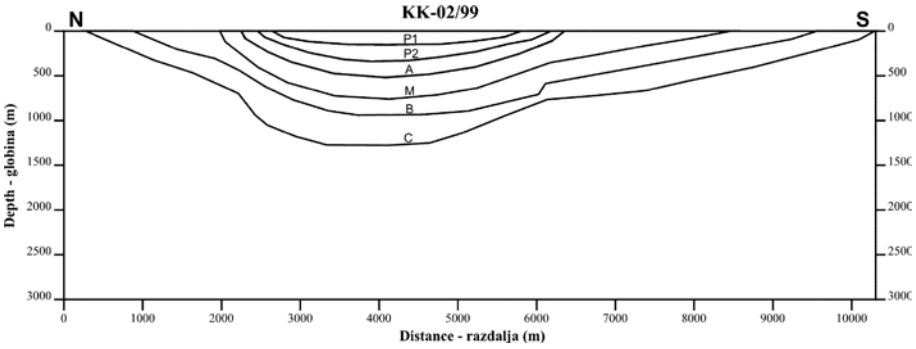

Figure 2. Interpretation of seismic reflection profile KK-02/99. Marked seismic horizons are described in Table 1.
Slika 2. Interpretacija refleksijskega seizmičnega profila KK-02/99. Označeni seizmični horizonti so opisani v tabeli 1.

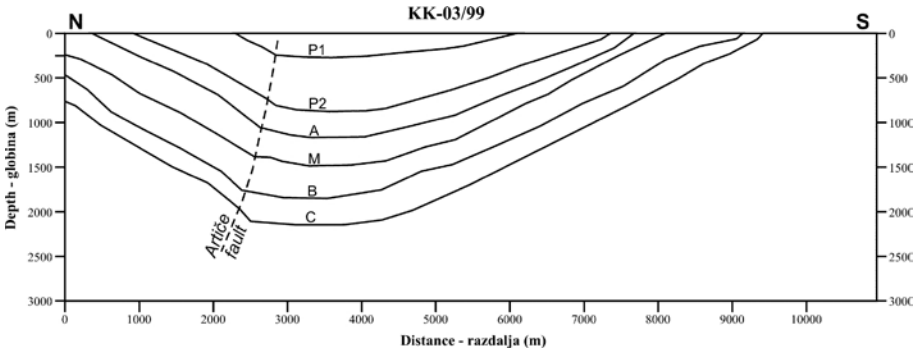

Figure 3. Interpretation of seismic reflection profile KK-03/99. Marked seismic horizons are described in Table 1
Slika 3. Interpretacija refleksijskega seizmičnega profila KK-03/99. Označeni seizmični horizonti so opisani v tabeli 1

Gravity data

The Krško basin area was investigated so far with gravity method in two detailed surveys, first for hydrocarbons exploration (URH, 1955) and the second one for underground gas storage in aquifers (STARČEVIĆ ET AL., 1989). Both maps showed good correspondence. Since the first survey comprises larger area, we used this map for contouring the maps of seismic horizons.

The gravity study performed in 1955 (URH, 1955) enclosed an area of 258 km^2 (Figure 1). Altogether 751 points were measured giving an average density of 3 points/km^2. Bouguer anomalies were computed using a density of 2.0 g/cm^3, derived from laboratory measurements and with Nettleton method. In the Bouguer anomaly map (Figure 1) the shape of the syncline is clearly reflected. Its axis is in WSW-ENE direction. At Drnovo there is a saddle which separates Raka and Globoko depressions. Bouguer anomalies range between +11 and +32 mGal. The minimum values in both depressions are +11 mGal.

Two-dimensional gravity modelling was performed along six transversal seismic reflection profiles (GOSAR, 2001) acquired in various projects across the Krško basin (Figure 1) including profiles KK-02/99 (Figure 2) and KK-03/99 (Figure 3). Modelled gravity anomalies were compared with observed anomaly profiles extracted from detailed gravity survey (URH, 1955; STARČEVIĆ ET AL., 1989) available in this area. The modelling was proved useful for the interpolation of the shape of the pre-Tertiary bedrock of the basin between seismic profiles. However the possibility to extrapolate the structures interpreted on seismic data to the area outside the grid of reflection seismic profiles is restricted due to the limited extent of the area covered by gravity surveys.

Contouring the maps of seismic horizons

In reflection profiles recorded in the frame of PHARE project six horizons were identified (Table 1). They include the Mesozoic basement (horizon C) of the Krško basin and five horizons within the Neogene sequence

Table 1. Seismic horizons interpreted on profiles recorded in the Krško basin with generalized unit thicknesses (Poljak et al., 1996) and horizon depths drilled in Drn-1/89 borehole (Kranjc et al., 1990; Gosar, 1998)
Tabela 1. Seizmični horizonti interpretirani na profilih posnetih v Krški kotlini z generaliziranimi debelinami posameznih enot (Poljak et al., 1996) in globinami horizontov navrtanimi v vrtini Drn-1/89 (Kranjc et al., 1990; Gosar, 1998)

Horizon horizont	Stage stopnja		Thickness debelina (m)	Depth in Drn-1 globina v Drn-1 (m)	Lithology litologija
P1	Pontian pontij	Pl_1^2, Q	200	48	sand, gravel, clay pesek, prod, glina
P2		Pl_1^1	600-700		sandy marl peščen lapor
A	Pannonian panonij	M_3^2	150-300		marl lapor
M	Sarmatian sarmatij	M_3^1	100	647	sandy marl, marly limestone peščen lapor, laporni apnenec
B	Badenian badenij	M_2^2	350		limestone, sandy marl apnenec, peščen lapor
	Ottnangian ottnangij	M_2^1	300		sand, gravel, conglomerate pesek, prod, konglomerat
C		$K_{1,2}$ or T_3		969	marly limestone or dolomite laporni apnenec ali dolomit

to capture its internal structure. The most prominent reflection was obtained from near the top of Badenian limestone (horizon B).

For contouring the structural maps of seismic horizons we did some trials with computer contouring algorithms (Hamilton & Jones, 1992). These gave quite satisfactory results in case of pre-Tertiary basement (horizon C) (Gosar et al., 2005) which was imaged in all considered profiles, but not so good results in all other horizons inside Neogene sequence (Božiček, 2006). By using computer methods it was also not possible to support interpolation by the use of gravity data. Therefore we decided for manual contouring of maps (Tearpock & Bischke, 2003). We didn't consider the faults in contouring, because the vertical displacements of individual horizons are mostly very small.

Time to depth conversion of seismic reflection profiles was based on velocity analyses data. The seismic velocities range from very low values in some parts of the near surface deposits to more than 2500 m/s for the Neogene sequences and 3000 m/s or larger for the Mesozoic. Lateral variations inside individual units are in general small and smooth (Božiček, 2006). For time to depth conversion of old single-fold profiles we used therefore an average velocity function derived from multi-fold reflection profiles. The depth control was available in five boreholes that reached the pre-Tertiary basement (Gosar et al., 2005). The most important is Drn-1 borehole (Kranjc et al., 1990) located near Drnovo in the central part of the basin close to the saddle which separates Raka and Globoko depression.

The depths in all structural maps are shown from the elevation 0 m a.s.l., but in the text the depths are considered from the average elevation of the surface which is in the Krško basin 150 m a.s.l..

Seismic horizons

The lithostratigraphic description of interpreted seismic horizons (Table 1) is summarized after PERSOGLIA ET AL. (2000), POLJAK ET AL. (2002), GOSAR ET AL. (2005) AND POLJAK (2006, personal communication).

The deepest horizon mapped was the top of Cretaceous flysch or of Triassic dolomite (horizon C). The lowermost Neogene sequence between horizon C and B represents the Ottnangian sediments transgressively deposited over the Mesozoic basement. These have relatively weak and diffuse seismic signals which is probably caused by their heterogeneous lithological content that consists of gravel, sand, sandy clay and conglomerate. They show several distinct angular discordances with visible onlaping structures that suggests a synsedimentary activity of the depression.

In Badenian *Lithothamnion* limestone (horizon B) was transgressively deposited over Ottnangian sequence. Upwards it transits into sandy and marly limestone, and sandy marl of Badenian to Sarmatian age. They could be distinguished as a separate unit between horizons B and M. This sequence has relative uniform thickness of 200 m, except in the eastern part of the Krško basin (Globoko depression), where it shows a slight increase. This thickness increase is well expressed by overlapping of seismic horizon that corresponds to sandy marl.

The next sequence is the Pannonian marl that corresponds to the unit between horizons M and A. Its almost uniform thickness (about 100 m) is slightly increased only in the Glo-

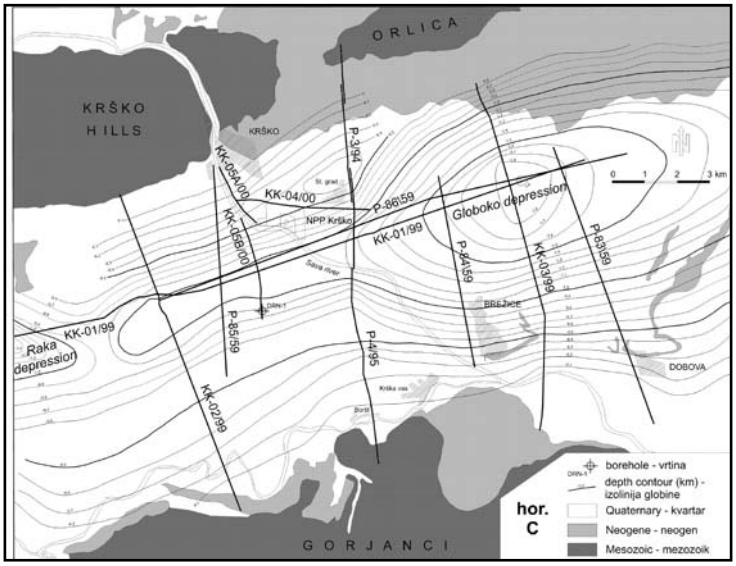

Figure 4. Structural map of seismic horizon C (pre-Tertiary basement)
Slika 4. Strukturna karta seizmičnega horizonta C (predterciarna podlaga)

boko depression. Upwards, this marl transits into sandy marl of Lower Pontian age, which could be distinguished as a separate sequence between horizons A and P2.

The Upper Pontian is represented by sand with rare lenses of gravel, except in the Globoko area, where a lateral equivalent consisting of gravel, sand and clay with coal is developed. The beginning of this sequence is recognized as the P2 seismic horizon. The main characteristics of this unit is variable thickness, from 100 m in the western part to up to 500 m in the Globoko depression in the east. The uppermost horizon P1 is related to no clear lithological change within Upper Pontian.

Seismic horizon C (pre-Tertiary basement) (Figure 4)

The structural map of the pre-Tertiary basement clearly shows the shape of the basin which is elongated in WSW-ENE direction. In the cross direction is the syncline rather symmetric. The average dip of the basement towards the central part is 20^0. This dip is similar to the average dip of Neogene sediments (Poljak et al., 1996) what is an indication of postsedimentary folding. The eastern Globoko depression has very regular elongated shape and reaches the maximum depth of 2050 m (from the surface) close to the intersection of KK-01/99 and KK-03/99 profiles south of Globoko. The western Raka depression is only partly seen in this map, which is limited to the extent of gravity data. This depression is smaller than the Globoko depression and reaches the maximum depth of 1600 m. Both depressions are separated by a wide saddle at a depth of 1150 m.

Seismic horizon B (Badenian-Sarmatian boundary) (Figure 5)

This prominent seismic horizon related to *Lithothamnion* limestone of Badenian age clearly shows a closed syncline in the

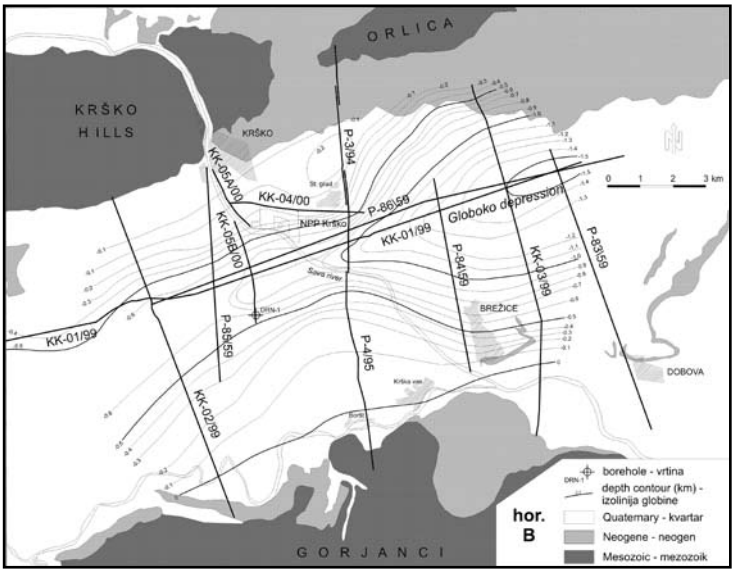

Figure 5. Structural map of seismic horizon B (inside Badenian)
Slika 5. Strukturna karta seizmičnega horizonta B (znotraj badenija)

Globoko depression where it reaches the depth of 1650 m. On the other hand in the Raka depression there is no syncline visible at this horizon and the maximum depth is only 650 m. The average thickness of Ottnangian and Lower Badenian sediments (between horizons C and B) varies therefore considerably in the Krško basin. In the Globoko depression it is about 300 m, but in the western Raka depression these sediments reach thickness of up to 1000 m. Such a great thickness is anomalous even for the entire Sava folds (Placer, 1998). Thus, the presence of older Tertiary units should not be excluded. Onlaping structures visible in seismic profiles suggests a synsedimentary activity of the depression.

Seismic horizon M (Sarmatian-Pannonian boundary) (Figure 6)

The seismic horizon M has very similar shape as horizon B. The sequence of sediments in-between has therefore relative uniform thickness of 200 m, except in the Globoko depression, where it shows a slight increase. This thickness increase is well expressed by overlapping of seismic horizon that corresponds to sandy marl that lies over the *Lithothamnion* limestone.

Seismic horizon A (Pannonian-Pontian boundary) (Figure 7)

The prominent seismic horizon related to the boundary between Upper Miocene and Lower Pliocene shows again a closed syncline in the Globoko depression with the maximum depth of 950 m. At the saddle between both depressions is its minimum depth 450 m. The thickness of the Pannonian marls is from 200 m in the shallow western part to 400 m in the Globoko depression.

Seismic horizon P2 (Lower Pontian-Upper Pontian) (Figure 8)

The depth of the P2 horizon which separates Lower Pontian sandy marl from Upper Pon-

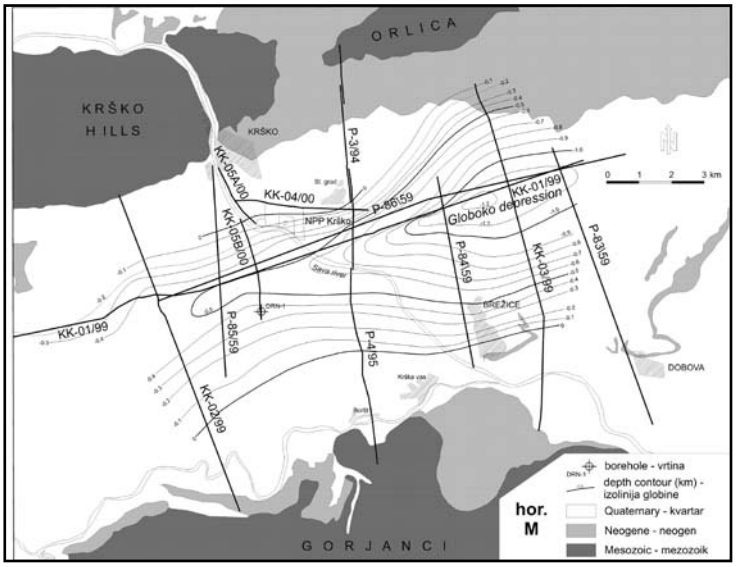

Figure 6. Structural map of seismic horizon M (Sarmatian-Pannonian boundary)
Slika 6. Strukturna karta seizmičnega horizonta M (meja sarmatij-panonij)

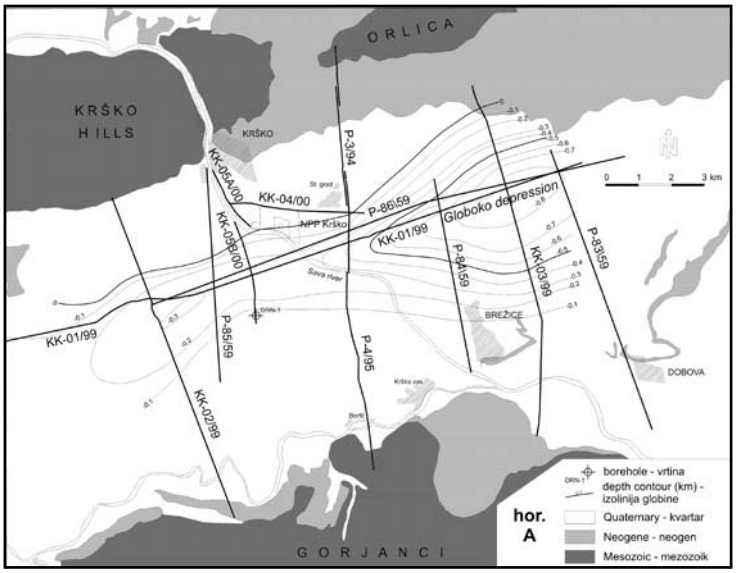

Figure 7. Structural map of seismic horizon A (Pannonian-Pontian boundary)
Slika 7. Strukturna karta seizmičnega horizonta A (meja panonij-pontij)

tian sand, gravel and clay varies considerably from 250 m in the western part to 650 m in the Globoko depression. The thickness of the Lower Pontian sandy marl is from 200 m in the west to 300 m in Globoko depression.

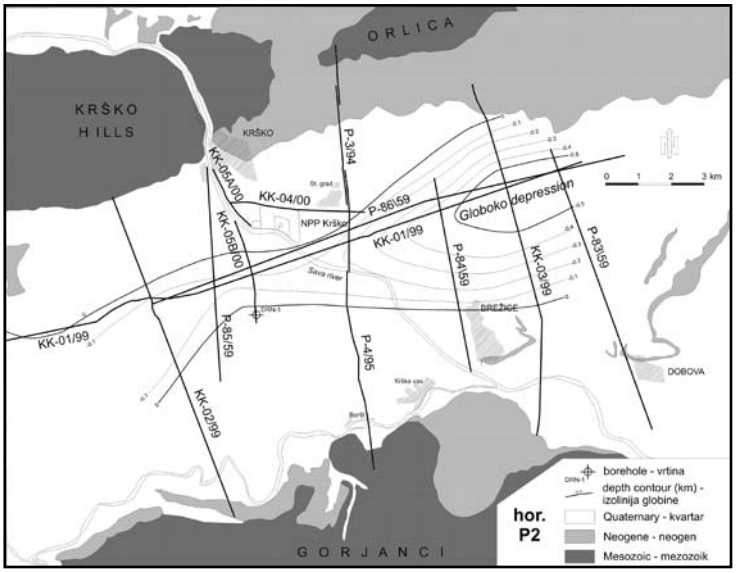

Figure 8. Structural map of seismic horizon P2 (Lower Pontian-Upper Pontian boundary)
Slika 8. Strukturna karta seizmičnega horizonta P2 (meja spodnji pontij-zgornji pontij)

Figure 9. Structural map of seismic horizon P1 (inside Upper Pontian)
Slika 9. Strukturna karta seizmičnega horizonta P1 (znotraj zgornjega pontija)

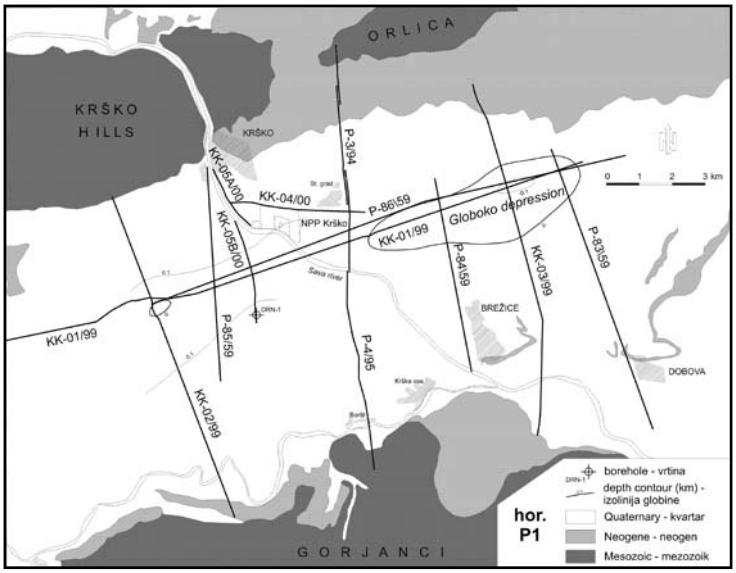

Seismic horizon P1 (inside Upper Pontian) (Figure 9)

The uppermost horizon P1 was imaged only along the axis of the syncline at shallow depths from 150 m at the crossing of KK-01/99 and KK-02/99 profiles to 250 m in the Globoko depression. The thickness of the Upper Pontian sand, gravel and clay between horizons P2 and P1 is highly variable, from 100 m in the western part to up to 500 m in the Globoko depression.

CONCLUSIONS

Structural maps of the pre-Tertiary basin and of five horizons inside the sequence of Neogene sediments were prepared based on the interpretation of eleven seismic reflection profiles recorded in three surveys performed in the Krško basin so far. Interpolation of Mesozoic basement between seismic profiles was supported by gravity data. The maps clearly shows rather regular synclinal shape of the Krško basin which is composed of two depressions. The larger Globoko depression in the eastern part is up to 2050 m deep and the smaller Raka depression in the western part is up to 1600 m deep (Figure 4). The thicknesses of some Neogene sequences in-between seismic horizons varies considerably. Most prominent is thickening of the Ottnangian and Lower Badenian sequence between horizons C and B from 300 m in the Globoko depression to up to 1000 m in the Raka depression. On the other hand the thickness of the Upper Pontian sand, gravel and clay increases from 100 m in the western part to up to 500 m in the Globoko depression. There are several indications of synsedimentary folding of the basin, but also some indications of postsedimentary activity.

The structural models of seismic horizons will allow additional geophysical and structural-geological interpretations of the area. Together with seismic velocity models they served also as input data for the construction of two-dimensional cross-sections in arbitrary directions for numerical modelling of seismic ground motion in seismic hazard assessment for the location of Krško NPP (Čarman, 2006).

Acknowledgments

Slovenian administration for nuclear safety is acknowledged for the permission to use seismic reflection data. The authors is grateful to collaborators of the project *Geophysical research in the surroundings of the Krško NPP* for most recent seismic data. Thanks go to Karl Millahn, Rinaldo Nicolich and Marijan Poljak for many valuable discussions during data interpretation. Thanks go also to Martina Čarman and Goran Vižintin for their help in preparation of maps.

References

Accaino, F., Gosar, A., Millahn, K., Nicolich, R., Poljak, M., Rossi, G., Zgur, F. (2003): Regional and high-resolution seismic reflection investigations in the Krško Basin (SE Slovenia). *Ann. Univ. Sci. Bp. Rolando Eötvös Nomin., Sect. geol.*, 35, 116-117.

Božiček, B. (2006): Izdelava hitrostnega in strukturnega modela Krške kotline na podlagi refleksijskih seizmičnih podatkov. Diplomsko delo, NTF, 54 pp.

Čarman, M. (2006): Amplification of ground motion at the area of Krško NPP due to local site effects. *Ph.D. thesis*, University of Nova Gorica, 153 pp.

Gosar, A. (1996): Seismic reflection method in structural investigations for assessment of earthquake hazard in the Krško basin. *Ph.D. thesis*, Univ of Ljubljana, 288 pp.

Gosar, A. (1998): Seismic-reflection surveys of the Krško basin structure: Implications for earthquake hazard at the Krško nuclear power plant, SE Slovenia. *J. of Appl. Geoph*., 39, 131-153.

Gosar, A. (2001): Two-dimensional gravity modeling along seismic reflection profiles in the Krško basin. *RMZ-Materials and Geoenvironment*, 48/3, 473-497.

Gosar, A., Komac, M., Poljak, M. (2005): Structural model of the pre-Tertiary basement in the Krško basin. *Geologija*, 48/1, 23-32. (in Slovenian).

Hamilton, D. E., Jones, T. A. (1992): Computer modeling of geological surfaces and volumes. AAPG, 297 pp.

Kaloper, D. (1984): Krško polje-Brežice, analogna obrada. IGGG, 9 pp. (unpublished report)

Kranjc, S., Božović, M., Matoz, T. (1990): Končno poročilo o geoloških raziskavah na Krškem polju za potrebe podzemnega skladiščenja plina, vrtina Drn-1/89. IGGG, 19 pp. (unpublished report).

Persoglia, S., Gosar, A., Millahn, K., Nicolich, R., Nieto, D., Poljak, M., Vesnaver, A., Wardell, N. (2000): Geophysical research in the surroundings of the Krško NPP. Final report. European Commission – PHARE, 68 pp. (unpublished report).

Placer, L. (1998): Structural meaning of Sava folds. *Geologija*, 41, 191-221.

Pleničar, M., Premru, U. (1977): Osnovna geološka karta SFRJ 1:100 000, Tolmač za list Novo mesto. Zvezni geološki zavod, 61 pp. (in Slovenian).

Poljak, M., Živčić, M. (1995): Tectonics and seismicity of the Krško basin. *1. hrv. geol. kongr.,* Opatija, 475-479.

Poljak, M., Verbič, T., Gosar, A., Živčić, M., Ribičič, M. (1996): Neotektonske raziskave na območju JE Krško. IGGG, 70 pp. (unpublished report).

Poljak, M., Gosar, A. (2001): Strukturna zgradba Krške kotline po podatkih geofizikalnih raziskav v letih 1994-2000. *Geološki zbornik*, 16, 79-82. (in Slovenian).

Poljak, M., Rižnar, I., Verbič, T. (2002): Geološka zgradba Krške kotline. *1. slov. geol. kongr.*, Črna na Koroškem, 73-74.

STARČEVIĆ, M., STOPAR, R., RIHTAR, B. (1989): Poročilo o gravimetričnih raziskavah na področju Krškega polja v letu 1989. IGGG, 8 pp. (unpublished report).

ŠIKIĆ, K., BASCH, O., ŠIMUNIĆ, A. (1979): Osnovna geološka karta SFRJ 1:100 000, Tumač za list Zagreb. Zvezni geološki zavod, 81 pp. (in Slovenian).

TEARPOCK, D. J., BISCHKE, R. E. (2003): Applied subsurface geological mapping with structural methods. Prentice Hall, 822 pp.

URH, I. (1955): Poročilo o detajlni gravimetrični izmeri na Krškem polju, 1953-1954. Geološki zavod Ljubljana, 7 pp. (unpublished report).

VERBIČ, T., RIŽNAR, I., POLJAK, M. TOMAN, M., DEMŠAR, M. (2000): Quaternary Sediments of the Krško Basin. *2. hrv. geol. kongr., Zbor. rad., Cavtat*. 451-457.

Uporaba petrofizikalnih preiskav pri oceni obstojnosti in stopnji preperevanja naravnega kamna

Use of petrophysical analysis for durability assessment and weathering degree of natural stone

Sabina Kramar[1], Breda Mirtič[2]

[1]Zavod za varstvo kulturne dediščine Slovenije, Restavratorski center, Poljanska 40, 1000 Ljubljana, Slovenija; E-mail: sabina.kramar@rescen.si
[2]Univerza v Ljubljani, Naravoslovnotehniška fakulteta, Oddelek za geologijo, Aškerčeva 12, 1000 Ljubljana, Slovenija; E-mail: breda.mirtic@guest.arnes.si

Received: November 02, 2006 **Accepted**: November 14, 2006

Izvleček: Poznavanje količine, oblike, velikosti in porazdelitve por v kamnini je ključnega pomena pri študiju propadanja kamnin na objektih oziroma določanja obstojnosti kamnine, ki bo uporabljena za vgradnjo. V pričujočem članku so predstavljene nekatere petrofizikalne metode, s pomočjo katerih lahko ocenimo lastnosti naravnega kamna. Določena je bila celotna in odprta poroznost, koeficient nasičenja, kapilarni dvig, dilatacija zaradi vpijanja vode ter porazdelitev velikosti por kamnine iz kamnoloma Sedovec. Pridobljeni rezultati so pokazali določene razlike v lastnostih obeh litoloških členov, ki sestavljajo kamnino v kamnolomu. Kremenov peščenjak ima večjo poroznost in večji Hirschwaldov koeficient nasičenja ter temu ustrezno nižjo volumsko gostoto kot drugi člen - peščen biosparit. Prav tako so vidne razlike tudi v vrednostih poroznosti med svežo in preperelo kamnino, ki so za slednjo višje. Meritve poroznosti s Hg-porozimetrom so pokazale, da se s stopnjo preperelosti peščenjaka poveča volumen por od 0,052 cm^3/g na 0,080 cm^3/g. Hirschwaldov koeficient ali koeficient nasičenja obeh členov je manj kot 0,8, zato naj bi bila kamnina malo dovzetna za poškodbe zaradi zmrzali.

Abstract: Learning about quantity, shape, size and distribution of pores within the stone is a major significance when studying weathering phenomena or assessing durability of natural building stone. Article deals with petrophysical methods in order to estimate natural stone properties. Bulk and open porosity, saturation coefficient, capillarity, hydric dilatation and pore size distribution of stone from Sedovec quarry has been determined. Results show some differences in properties of both lithological sequences present in the quarry. Siliceous sandstone shows higher values of porosity and Hirschwald coefficient but lower bulk density than sandy biosparite. It is possible to observe the variety in porosity between fresh and deteriorated stone as well. Hg-porosity measurements show an increase of pore volume with augmentation of weathering degree of stone from value of 0.052 cm^3/g to 0.080 cm^3/g. Value of Hirchwald coefficient or saturation coefficient is less than 0.8 which tells us about low susceptility of studied stone to froze damages.

Ključne besede: petrofizikalne preiskave, peščenjak, propadanje, poroznost, kapilarnost, dilatacija
Key words: petrophysical analysis, sandstone, degradation, porosity, capillarity, hydric dilatation

Scientific paper

UVOD

Poznavanje količine, oblike, velikosti in porazdelitve por v kamnini je ključnega pomena pri študiju propadanja kamnin na objektih oziroma določanja obstojnosti kamnine, ki bo uporabljena za vgradnjo. Obstojnost kamnine lahko ocenjujemo s petrofizikalnimi preiskavami. V Sloveniji posamezne petrofizikalne lastnosti kamnine, kot so prostorninska masa, koeficient gostote, poroznost, vpijanje vode, merimo po SIST EN 1925, SIST EN 1936 in po SIST EN 13755 standardih. Z vsemi naštetimi lastnostmi bolj ali manj posredno vrednotimo parametre, ki so povezani s porami v kamnini.

Obseg propadanja je močno odvisen od poroznosti, zato je pri ugotavljanju vzrokov poškodb na kamnini in ocenjevanju obstojnosti kamnine pomembno, da poznamo lastnosti pornega sistema. Na podlagi teh lastnosti lahko namreč ocenimo vsebnost in gibanje vode in soli v kamnini, ki spadata med pomembnejše povzročitelje njenega propadanja. Večina lastnosti materiala je odvisna od poroznosti, še posebno način transporta in čas zadrževanja vode v kamnini. Vsaka kamnina vpija, zadržuje in eventualno prepušča določeno količino vode. Količina vode predstavlja vezano, kapilarno in gravitacijsko vodo, ki jo kamnina vpije in zadrži v porah. Voda namreč igra pomembno vlogo pri propadanju kamnin (WINKLER, 1997) bodisi z neposrednim delovanjem, npr. pri procesih raztapljanja in precipitacije mineralov, ali pa voda prispeva k ustvarjanju pogojev, kjer nastopajo drugi procesi preperevanja, kot npr. kristalizacija soli, rast mikroorganizmov, slabšanje mehanske trdnosti kamnine (LAURENT, 2006).

Poroznost materiala je definirana kot razmerje med porami materiala in celotnim volumnom poroznega materiala. Strukturo porne mreže določajo poroznost, ki nam podaja volumen por v kamnini ter porazdelitev velikosti por, ki nam podaja način porazdelitve pornega prostora v kamnini v smislu, ali je večje število manjših por ali manjše število večjih por. Slednje močno vpliva na obstojnostne lastnosti kamnine pri učinkih zmrzovanja in kristalizaciji soli (KNÖFEL ET AL., 1987, v BOS, 1990). Ločimo mikropore (< 0,01 μm), mezopore (0,01 - 0,1 μm) in makropore (0,1-100 μm) (Amoroso&Fassina, 1983). Pore s premerom, večjim od 1 mm, imenujemo tudi superkapilare, kjer se voda pretaka gravitacijsko (ne zadržujejo vode). Pri kapilarah (0,2 μm - 1 mm) je gibanje vode pod vplivom kapilarnih sil (tu se voda zaradi kapilarnih sil tudi zadrži) pri subkapilarah ($r < 0,2$ μm) pa je voda vezana na površino mineralnih delcev z molekulskimi in elektrostatičnimi silami. Pore z radijem $r > 0,03$ μm ostanejo, z izjemo v izjemnih okoliščinah, nezapolnjene z vodo, zato ne povečujejo nevarnosti nastanka poškodb zaradi zmrzovanja. Zaradi mehanskih pritiskov novih mineralov na njihove stene se večje pore ožijo, manjše pa širijo (BRATLEY, 1998, v GOLEŽ, 1999). Kapilare tako v največji meri prispevajo k preperevanju kamnine. Mikroporoznost/makroporoznost je pri Hg-porozimetriji definirana za pore, ki so manjše/večje od 7,5 μm (GONI ET AL., 1968, v GAL, 2004). Kapilarnost je lastnost materiala, da absorbira tekočine v porah s kapilarnim dvigom. Pogojujeta jo poroznost in porazdelitev velikosti por (MAMILLAN, 1985 v BOS, 1990). Dilatacija zaradi vpijanja vode je funkcija strukture in mineralne sestave kamnine. Temu fenomenu sta vzrok dva neodvisna faktorja, in sicer nabrekanje

glinenih mineralov in kapilarne sile med mineralnimi zrni.

Petrofizikalne preiskave so bile opravljene na peščenjaku srednjemiocenske starosti iz kamnoloma Sedovec, iz katerega je bila uporabljena kamnina za gradnjo pomembnih baročnih spomenikov (Golež, 1999, Vesel&Senegačnik, 2002, Golež et al., 2005). Kamnolom je bil nedavno ponovno odprt zaradi potreb pri restavratorskih posegih na kompleksu cerkve sv. Roka v okolici Šmarja pri Jelšah. Mineraloške spremembe tega peščenjaka, ki so nastale kot posledica preperevanja, so bile že predstavljene (Golež, 1999, Golež et al., 2005, Kramar et al., 2006). V pričujočem članku pa smo določili nekatere petrofizikalne lastnosti omenjenega peščenjaka, na podlagi katerih smo skušali oceniti vpliv mikrostrukture na obstojnost oziroma na propadanje peščenjaka.

Eksperimentalni del

Izbira vzorcev

Preiskovan material je srednjemiocenski peščenjak iz področja Zahodnih Haloz, ki so ga v preteklosti uporabili pri gradnji različnih objektov. V kamnolomu se menjavajo plasti kremenovega peščenjaka s kalcitnim vezivom s plastmi peščenega biosparita. Kamnino od terigenih zrn v glavnem sestavljajo zrna kremena, medtem ko so glinenci, litična zrna in muskovit podrejeni. Med alokemičnimi komponentami močno prevladujejo fosili (predvsem ploščice ehinodermov, foraminifere, preseki iglic iglokožcev, briozoji), nekaj odstotkov pa je glavkonita.Vezivo je v glavnem kalcitni cement. Piritni cement je prisoten v sledovih, ki pa je povečini že limonitiziran. Ponekod se kot medzrnski in znotrajzrnski cement pojavlja tudi glavkonit. Nekaj je še mikritne in glinene osnove (Golež, 1999, Vesel&Senegačnik, 2002, Golež et al., 2005, Kramar et al., 2006).

Odvzeta sta bila dva vzorca sveže kamnine obeh litoloških členov, sivozelen peščen biosparit (P1) in rjav kremenov peščenjak (P2). Nekatere preiskave so bile opravljene tudi na vzorcu preperele kamnine, da bi lahko opazovali spremembe v vgrajeni kamnini. Slednji je bil odvzet iz dekorativne krogle pete kapele kompleksa cerkve sv. Roka, in sicer na površini (KZ) in v notranjosti (KN) krogle.

Uporabljene metode

Meritve poroznosti ter kapilarno vpijanje vode so bile merjene po priporočilih RILEM-a (RILEM recomendations - Réunion Internationale des Laboratoires et Experts des Matériaux, Systèmes de Constructions et Ouvrages) (RILEM, 1980). Vzorci sveže

Tabela 1. Mineralna sestava vzorcev, določena z optično mikroskopijo v presevni svetlobi (Kramar et al., 2006)
Table 1. Mineral composition of used samples, determined by optical microscopy in transmitted light (Kramar et al., 2006)

	P1	P2	KN in KZ
kalcitno vezivo, mas.%	35	30	30
nekarb. zrna, mas.% (kremen, litična zrna, muskovit)	25	40	40
kalcitni drobci fosilov	40	30	30

kamnine P1 in P2 so bili oblikovani v kocke 4x4x4 cm, meritve so se izvajale pravokotno na plastnatost.

Vrednost celotne poroznosti, ki je dostopna vodi v vakuumu (RILEM I.1) dobimo na podlagi treh meritev. Najprej izmerimo maso suhega vzorca - W_s, ki smo ga sušili v sušilnici na 65±5 °C do konstantne mase. Vzorec nato postavimo v eksikator, iz katerega izčrpamo zrak. Po pretečenem času v eksikator natočimo vodo, iz katere smo predhodno prav tako izčrpali zrak. Po namakanju vzorcev (24 ur) najprej izmerimo maso vzorcev pod vodo - hidrostatična masa W_1. Sledi meritev mase vzorcev, prepojenih z vodo na zraku - masa W_2. Razlika mas W_2-W_s predstavlja volumen por, ki je zapolnjen z vodo - Vv. Iz izmerjene hidrostatične mase - W_1 dobimo celotni volumen - V_t vzorcev po formuli: $V_t = W_2$-W_1.

Celotno poroznost izračunamo po naslednji formuli:

$$N_t = \frac{W_2 - W_s}{W_2 - W_1} \times 100 \quad [\%] \qquad (1)$$

Poroznost po 48 urah - N_{48} (odprta ali efektivna poroznost) (RILEM II.1) omogoči določiti odprto poroznost, ki je dostopna za vodo v naravnih pogojih (ne v vakuumu) pri atmosferskem tlaku. Gre za sposobnost vpijanja vode. Po sušenju vzorcev do konstantne mase - Ws_{48}, so vzorci podvrženi kapilarnemu vpijanju vode za 24 ur, nato pa popolnemu potapljanju v vodo za naslednjih 24 ur. Ko izmerimo maso suhega vzorca - W_s pred namakanjem in maso po namakanju - W_{48}, določimo poroznost kamnine po 48 urah:

$$N_{48} = \frac{W_{48} - W_s}{W_2 - W_1} \times 100 \quad [\%] \qquad (2)$$

N_{48} je vedno manjša ali enaka N_t, ker vedno del mreže por ostane zapolnjen z zrakom. Ta vrednost je primerljiva s prosto poroznostjo oz. z volumnom por, ki jih lahko zapolni voda s kapilarnim dvigom. Razlika N_t-N_{48} omogoči, da ocenimo zaprto poroznost, ki predstavlja porni volumen, ki ostane zapolnjen z zrakom pri kapilarnem vpijanju vode pri atmosferskem tlaku.

Na podlagi teh dveh meritev lahko izračunamo Hirschwaldov koeficient (S_{48}) ali koeficient nasičenja z vodo po 48 urah iz razmerja N_{48}/N_t. Hirschwaldov koeficient predstavlja največjo sposobnost vpijanja vode neke kamnine v naravnih pogojih. Podaja razmerje med praznimi in zapolnjenimi porami, s katerim je definirana odpornost kamnine na zmrzal. Kamnine s koeficientom, ki je večji od 0,8, naj bi bile dovzetne za poškodbe, nastale kot posledica zmrzali, tiste z manjšim koeficientom pa ne (AMOROSO&FASSINA, 1983, BOURGÈS, 2006).

Na podlagi izmerjenih parametrov je nadalje mogoče izračunati tako volumsko kot skeletno gostoto kamnine (RILEM I.2). Volumska gostota (ang. bulk ali apparent density) predstavlja razmerje med maso in celotnim volumnom vzorca

(enačba 3). Skeletna gostota (angl. real density) odgovarja volumnu mase brez por. Je razmerje med maso in volumnom brez por vzorca (enačba 4) in je vedno večja od volumske gostote.

$$\rho_{vol} = \frac{W_s}{W_2 - W_1} \times 1000 \quad [kg/m^3] \quad (3)$$

$$\rho_{vol} = \frac{W_s}{W_s - W_1} \times 1000 \quad [kg/m^3] \quad (4)$$

Kapilarno vpijanje vode (RILEM II.6) omogoči določiti kinetiko absorpcije vode v kamnini v atmosferskih razmerah, ki je pomemben faktor pri ocenjevanju navlaževanja kamnine z vodo. Določeni so bili koeficienti kapilarnega dviga. Vsak vzorec je bil po predhodnem osuševanju do konstante mase (W_s) postavljen pravokotno na plastnatost na blazinico, prepojeno z destilirano vodo, ki je omogočila kapilarno vpijanje vode s spodnje površine. Nato merimo maso vode, ki jo vzorec vpije in višino kapilarnega dviga v odvisnosti od časa, dokler se vpijanje ne stabilizira. Metoda temelji na absorpciji vode skozi osnovno ploskev (ploskev, na kateri stoji vzorec) vzorca kamnine zaradi kapilarnih sil. V principu gre za zamenjavo manj močljivega fluida (zraka) z bolj močljivim fluidom (voda). Možno je definirati dva parametra kapilarnih lastnosti kamnine:

- koeficient A, ki nam podaja spremembo količine absorbirane vode, izražen v $gcm^{-2}h^{-1/2}$,
- koeficient B, ki nam podaja linearno hitrost kapilarnega dviga, podana v $cmh^{-1/2}$.

Dilatacija predstavlja spremembo volumna materiala, ki nastane zaradi ogrevanja in ohlajanja kamnine ali močenja z vodo. V obravnavanem primeru smo merili linearno dilatacijo, ki je odvisna od hidričnih pritiskov, ki nastanejo pri absorpciji vode v vzorcu v odvisnosti od časa in temperature. Dilatacija zaradi vpijanja vode (RILEM II.7) je bila merjena z dilatometrom tipa Capteur LVDT (Low Voltage Transducer) Channel 122 v Laboratoire de Recherche des Monuments Historiques v Franciji. Vzorca, predhodno osušena do konstantne mase, sta bila vstavljena v dilatometer, kjer se je vzorec s kapilarnim dvigom postopoma močil do nasičenosti z vodo. Meritev se je avtomatično izvajala vsaki 2 minuti 48 ur pri stalni temperaturi 25 °C do stabilizacije. Z metodo lahko določimo koeficient linearne dilatacije α (mm/m) = $\Delta L/L_0$, pri čemer je ΔL sprememba dolžine vzorca med meritvijo, L_0 pa začetna dolžina vzorca.

Velikost in porazdelitev velikosti por v vzorcih P1 in P2 ter v vzorcih iz krogle KN in KZ smo določili s pomočjo Hg – porozimetra na Kemijskem inštitutu v Ljubljani. Uporabljen je bil inštrument PoreSizer 9310 (Micromeritic Instrument Co., U.S.A.). Metoda temelji na neomočljivosti živega srebra na stene por kamnine. Ob povečanju pritiska vtiskovanja živega srebra v pore, se radij por, ki je lahko zapolnjen z njim, zmanjša in posledično se celotna količina vtisnjenega Hg poveča. Za izračun rezultatov so bile uporabljene standardne vrednosti parametrov: omočitveni kot med Hg in površino vzorca, $\theta = 130°$ in površinska napetost Hg, $\gamma = 0{,}485$ N/m. Gostota Hg pri temperaturi meritve, $\rho = 13.527{,}6$ kg kg/m^3. Meritve so bile opravljene na sveže odlomljenih kosih kamnin, približne velikosti 0,5 cm^3.

REZULTATI IN RAZPRAVA

Za ocenjevanje mikrostrukture kamnine smo izmerili celotno poroznost - N_t in poroznost po 48 urah – N_{48} (odprta ali efektivna poroznost) ter kapilarno vpijanje vode. Porazdelitev velikosti por je bila na nekaterih vzorcih določena s Hg-porozimetrom. Prav tako smo testirali dilatacijo kamnine zaradi vpijanja vode. Na ta način smo poskusili oceniti vpliv mikrostrukture na propadanje peščenjaka.

Meritev celotne poroznosti, ki je dostopna vodi v vakuumu, je pokazala, da ima peščen biosparit (P1) celotno poroznost $N_t = 9,85$ %, kremenov peščenjak (P2) pa ima $N_t = 13,71$ %. Če primerjamo rezultate s kremenovimi peščenjaki iz serije Bundsandstein, ki dosegajo vrednosti med 16,6 % in 24 % (GAL, 2004), vidimo, da ima preiskovan peščenjak dokaj nizke vrednosti.

Poroznost N_{48} peščenega biosparita (P1) je 6,10 %, rjavega pa 10,58 %. Opazimo, da N_{48} predstavlja približno 2/3 N_t. Pri vzorcu P1 ostane 3,75 % pornega volumna zapolnjenega z zrakom, pri vzorcu P2 pa 3,13 %. Razlike lahko iščemo v znotrajzrnski poroznosti biosparita, saj le ta vsebuje nekatere fosile, ki so vir zaprte poroznosti (briozoji, foraminifere).

Hirschwaldov koeficient ali koeficient nasičenja (S_{48}) obeh členov je sicer manj kot 0,8, zato naj bi bila kamnina malo dovzetna za poškodbe zaradi zmrzali. Vendar pa vidimo, da je vrednost vzorca P2 na kritični meji. Dejansko lahko opazujemo, da slednji člen v naravi intenzivneje prepereva. Pri procesu zmrzovanja vode in taljenja ledu v primeru popolnega nasičenja kaže struktura kamnine raztezanje, nastalo zaradi povečanja volumna pri zmrzovanju vode, ki pa po odtajanju ni reverzibilno. V primeru delnega nasičenja pa zmrzovanje kaže krčenje porozne strukture. Pojav lahko razložimo tako, da se zmrzovanje začne v večjih porah, kjer s tem rast ledu odvzame vodo iz manjših por, kar povzroči krčenje (Everet, 1961 v Snethlage et al., 1996, Stochausen, 1981 v Snethlage et al., 1996). Čeprav je proces pri eksperimentih v laboratorijih reverzibilen, pa lahko domnevamo, da v naravnem okolju po nekaj ciklih ostanejo ireverzibilni premiki, ki povzročajo utrujenost materiala.

Rezultati meritev poroznosti s Hg-porozimetrom na svežih vzorcih kamnine (tabela 2) potrjujejo rezultate meritev, podanih v tabeli 1. Peščeni biosparit (P1) ima manjšo poroznost od kremenovega peščenjaka (P2). V obeh kamninah je površina por enaka, čeprav povprečni premer por kaže, da ima kremenov peščenjak več večjih por. Volum-

Tabela 2. Poroznost svežih vzorcev kamnine, peščenega biosparita (P1) in peščenjaka (P2)
Table 2. Results of porosity of samples of fresh stone, sandy biosparite (P1) and sandstone (P2)

Oznaka vzorca	Celotna poroznost N_t (%)	Odprta poroznost N_{48} (%)	Zaprta poroznost $N_t - N_{48}$ (%)	Hirchwaldov koeficient nasičenja (S_{48})	Volumska gostota (g/cm^3)	Skeletna gostota (g/cm^3)
P1	9,85	6,10	3,75	0,62	2,38	2,63
P2	13,71	10, 58	3,13	0,77	2,28	2,64

Tabela 3. Vrednosti preiskave vzorcev z živosrebrno porozimetrijo
Table 3. Results of Hg-porosimetry

Oznaka vzorca	Volumen por (cm^3/g)	Površina por (m^2/g)	Povprečni premer po r (μm)	Volumska gostota (g/cm^3)	Skeletna gostota (g/cm^3)
P1	0,052	2,8	0,074	2,36	2,69
P2	0,065	2,8	0,093	2,27	2,66
KN (1. meritev)	0,075	3,3	0,092	2,21	2,65
KN (2. meritev)	0,077	2,4	0,127	2,20	2,65
KZ	0,080	2,7	0,120	2,19	2,66

*Specifične površine so izračunane iz izmerjenih premerov por in njihove porazdelitve ob predpostavki cilindrične oblike por.

ska in skeletna gostota sta v obratnem sorazmerju s poroznostjo (volumnom por).

Največjo poroznost ima vzorec kamnine, odvzet na površini krogle, ki je bil tudi najbolj izpostavljen dejavnikom preperevanja po vgradnji. Površina por se v vzorcih iz krogle ni veliko spremenila, pač pa se je znatno povečal povprečni premer por, kar dokazuje, da se v vgrajeni kamnini s časom večajo razpoke in da se slabo vezan material z vodo izpira iz kamnine. Zmanjšanje količine materiala na volumsko enoto se odraža tudi v znižanju volumske gostote. Skeletna gostota se ni značilno spremenila.

Rezultati Hg – porozimetra kažejo, da je porazdelitev por v vzorcu P1 bolj nehomogena kot v vzorcu P2, pri vzorcu KN ter KZ pa močno nehomogena.

Količina velikih por (R>5 μm) je v primeru vzorcev sveže kamnine več kot trikrat manjša od tiste v vzorcih preperele kamine. Proces preperevanja peščenjaka spremlja povečanje poroznosti na račun večje količine velikih por. Povečano poroznost praviloma spremlja zmanjšanje mehanske trdnosti kamnine.

Krivulji kapilarnega dviga kažeta, da je struktura porozne mreže pri vzorcu P1 malo manj homogena kot v primeru vzorca P2 (slika 1). V začetku je hitrost kapilarnega dviga večja, nato pa vedno manjša. Posebno pri vzorcu P2 opazujemo da je hitrost kapilarnega dviga velika, potem pa se zmanjšuje oziroma se prične stabilizirati. Pri vzorcu P1 lahko opazujemo, da je v prvih petih urah hitrost kapilarnega dviga velika, potem se zelo zmanjša, šele po sedmih dneh se prične stabilizirati.

Tabela 4. Porazdelitev velikosti por (%)
Table 4. Pore size distribution (%)

	P1	P2	KN (1., 2. meritev)	KZ
R>5μm	7	10	30, 33	34
0,5 μm <R< 5 μm	49	50	38, 39	39
R<0,5 μm	45	40	32, 28	27

Iz grafa je možno izračunati vrednosti obeh koeficientov kapilarnega dviga. Vrednost koeficienta A (podaja spremembo količine absorbirane vode) pri vzorcu P1 je 0,043 $gcm^{-2}h^{-1/2}$ pri P2 pa 0,072 $gcm^{-2}h^{-1/2}$. Vrednost koeficienta A vzorca P1 je skoraj za polovico manjša od vzorca P2. Vrednosti koeficienta A so v primerjavi z vrednostmi, ki so jih dobili tuji raziskovalci za kremenove peščenjake, npr. Bundsandstein (0,12 - 0,39 $gcm^{-2}h^{-1/2}$), od 2 do 9 krat manjše (GAL, 2004). Peščenjak iz Sedovca vpija vodo veliko počasneje in manj od njih. Vrednosti koeficienta B (podaja linearno hitrost kapilarnega dviga) je 0,46 $cmh^{-1/2}$ za vzorec P1, za vzorec P2 pa 0,65 $cmh^{-1/2}$. Tudi te vrednosti so za peščenjake nizke, saj peščenjaki sicer dosegajo vrednosti med 1,1 in 4,2 $cmh^{-1/2}$ (GAL, 2004). V povprečju se obravnavani peščenjak napoji s hitrostjo 0,2 - 0,3 cm/uro, kar je malo v primerjavi s prej omenjenimi, kjer znaša hitrost vpijanja tudi do 2 cm/uro. Izmerjene vrednosti se pravzaprav bolj približujejo vrednostim za apnenec, kjer se vrednosti koeficienta A gibljejo okoli 0,08 $gcm^{-2}h^{-1/2}$ in koeficienta B okoli 0,79 $cmh^{-1/2}$ (GOSSELIN, 2005).

Kapilarni dvig poteka samo po kapilarnih porah, ki so večje od 0,01 µm. V ultrakapilarnih porah (d<0,01 µm) kapilarnega dviga ne opažamo, saj je celotna pora zapolnjena z vodo. S kapilarnim dvigom potujejo po kamnini tudi raztopine soli, ki po kristalizaciji v medzrnskih prostornih povzročajo hitro preperevanje (AZZONI ET AL., 1992 v GOLEŽ, 1999). Kamnina, ki ima več manjših por, bo vpila vodo hitreje kot kamnina z isto poroznostjo, toda večjimi porami. Vzorca sveže kamnine P1 in P2 vsebujeta 97 % večjih por (R > 0,01 um), vzorca iz krogle, KN in KZ pa 98 % por z R > 0,01um. Razlika je premajhna, da bi lahko iz nje sklepali na hitrost kapilarnega dviga. Glede na povprečni premer por lahko sklepamo, da ima vzorec P2 večje pore, zaradi česar bi morala biti tudi hitrost kapilarnega dviga manjša (manjša vrednost koeficienta B), česar pa meritve

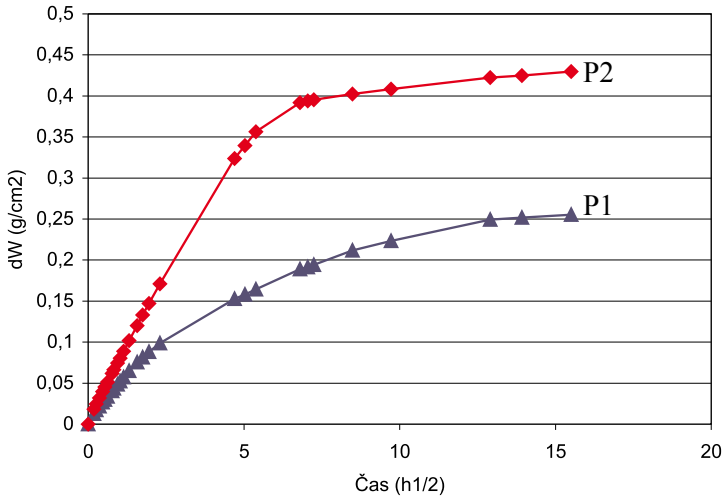

Slika 1. Kapilarno vpijanje vode vzorcev sveže kamnine. P1: peščeni biosparit, P2: kremenov peščenjak
Figure 1. Curves of capillary imbibition. P1: sandy biosparite, P2: siliceous sandstone

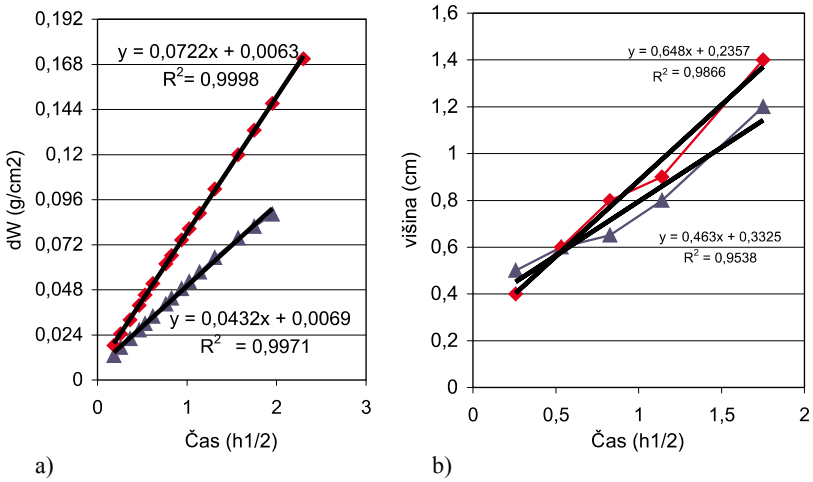

Slika 2. Določitev kinetičnih parametrov kapilarnega vpijanja vode. a) Koeficient A in b) koeficient B
Figure 2. Water absorption coeficients. a) Coefficient A and b) Coefficient B

niso potrdile Povprečni premer por očitno ni zadosten dokaz o vrsti in količini posameznih por, ki vplivajo na hitrost kapilarnega dviga. Najvišji nivo kapilarnega dviga, ki ga lahko vidimo v vgrajeni kamnini po nekaj letih, je velikokrat zaznamovan z eflorescenco ali temnim robom, ki zadržuje vlago dalj časa zaradi koncentracije soli na tem nivoju (Bilbija, 1984). Med sušenjem se na meji med conama največje in najmanjše vsebnosti vode razvijejo notranji pritiski. Te napetosti so lahko vzrok za nastanek razpok in oslabitev strukture v coni največjega gradienta vsebnosti vode (Gal, 2004).

Raziskava je pokazala, da z uporabljenimi metodami lahko ugotavljamo vrsto in jakost propadanja kamnin, ki so bile uporabljene v kompleksu Sv.Roka. Prav tako lahko z uporabljenimi petrofizikalnimi preiskavami primerjamo obstojnost apnenca in/ali peščenjaka po njuni vgradnji.

Dilatacija zaradi vpijanja vode naj bi bil odločujoč parameter pri razumevanju načina obnašanja peščenjaka. Dilatacija je funkcija tako strukture kot mineralne sestave kamnine. Temu fenomenu sta vzrok dva neodvisna faktorja, in sicer nabrekanje mineralov glin in kapilarne sile med mineralnimi zrni. Učinek kapilarnih sil je odvisen od stopnje nasičenja kamnine z vodo. V kamnini, ki je malo nasičena, so meniski omejeni na medzrnske kontakte, njihove kapilarne sile pa delujejo tako, da se kamnina močno skrči. Ko se stopnja nasičenja poveča, se kapilarne sile zmanjšajo, hkrati pa se poviša višina meniska, zato pride do dilatacije. Časa, ki sta potrebna, da dosežemo maksimalno hidrično dilatacijo in kapilarno vpijanje vode, sta ekvivalentna. Dilatacija je torej sorazmerna s stopnjo nasičenja v kamnini. Velja tudi, da je vpijanje vode hitro, kjer je hitrost evaporacije majhna (Gal, 2004). Rezultati so pokazali, da je koeficient dilatacije peščenega biosparita (vzorec P1) 0,098 mm/m ter kremenovega

peščenjaka (vzorec P2) 0,589 mm/m. Kremenov peščenjak se razteza kar 6 krat bolj. Iz dobljenih dilatometričnih krivulj vidimo, da dilatacija pri sivozelenemu členu poteka zelo počasi, medtem ko je pri rjavem členu silovita in hitra. Vzroke temu lahko iščemo v naravi zrn (glineni minerali) in poroznosti posameznih členov. Ob intruziji vode pride na začetku vedno do krčenja materiala, kar je razvidno tudi z grafa (slika 3). Vrednosti lahko primerjamo z rezultati, dobljenimi pri drugih raziskovalcih za kremenov peščenjak (Bundsandstein), ki se razteza v intervalu 0,14 - 0,18 mm/m, preperel različek pa 0,46 mm/m (GAL, 2004). Vrednost peščenega biosparita v primerjavi z omenjenim kremenovim peščenjakom je dokaj majhna, medtem ko se dilatacija kremenovega peščenjaka približuje vrednostim preperelega kremenovega peščenjaka (Bundsandstein) oziroma se razteza celo bolj. Dilatacija mehansko bolj odpornega peščenjaka (P1) je zelo majhna (0,1 mm/m), medtem ko se vrednost mehansko slabše odpornega (P2) (0,6 mm/m) približuje vrednostim, navedenim v literaturi (SNETHLAGE&WENDLER, 1996). Glede na to, da se že sveža kamnina zelo razteza, lahko pričakujemo od preperele kamnine še večji faktor.

Znano je, da porozni sistemi odražajo higrično in hidrično raztezanje in krčenje zaradi spreminjajoče se vlažnosti (in vode) kamnine. Z izrazom higrično definiramo omakanje zaradi vlage v plinasti fazi (v intervalu med 0 in 95 % RH), izraz hidrično (namakanje v vodi) pa definira omakanje zaradi vode. Po literaturi je vrednost hidrične dilatacije za peščenjake okoli 0,5 mm/m, lahko pa tudi 5 mm/m v primerih peščenjakov, ki vsebujejo veliko glinene komponente (SNETHLAGE&WENDLER,1996). Prisotnost sadre ali drugih manj topnih produktov preperevanja poveča dilatacijo iz 0,5 na 2 mm/m (WENDLER, 1996). Čeprav je dilatacija reverzibilen

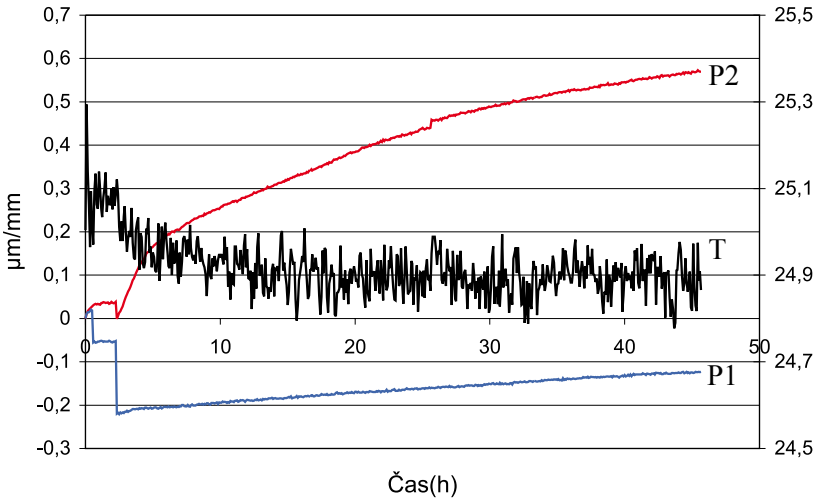

Slika 3: Dilatacija zaradi vpijanja vode vzorcev sveže kamnine. P1: peščeni biosparit, P2 : kremenov peščenjak, T: temperatura
Figure 3: Hydric dilatation of stone. P1: sandy biosparite, P2: siliceous sandstone, T: temperature

proces, je treba upoštevati, da lahko pride do utrujenosti materiala zaradi ponavljajočih se ciklusov sušenja in močenja. Utrujenost materiala je na področju proučevanja materiala dobro poznan fenomen, ki nastane zaradi neelastičnega obnašanja kamnine. Pogosto lahko vodi do resnih nepričakovanih poškodb, ki pa jih lahko predvidimo le skozi dolgotrajne preiskave.

Preiskave kamnitih objektov, na katerih naj bi potekali restavratorski posegi, so zaradi varovanja objekta vedno narejene na minimalni količini in številu vzorcev. Zato ponovljivost meritev posameznih merjenih parametrov praviloma ni znana. Poleg tega kamnina ni material, ki bi bil vedno homogen čez celoten volumen objekta. Tako smo šele s primerjavo rezultatov vseh izvedenih preiskav lahko ugotavljali obstojnost litoloških členov kamnin, ki jih najdemo v kamnolomu Sedovec.

Sklepi

Preiskave so pokazale razlike med lastnostmi obeh litoloških členov, in sicer ima rjav laminiran kremenov peščenjak nekoliko slabše obstojnostne lastnosti, saj ima večjo poroznost, vpijanje vode in dilatacijo zaradi vpijanja vode ter je bolj podvržen poškodbam zaradi zmrzovanja. Oba litološka člena po vgradnji tvorita sistem, v katerem se vsak člen razteza drugače, kar lahko privede do nenenakomernih pritiskov na meji med plastmi. Ob absorpciji vode se vsak člen kamnine obnaša drugače, saj je tudi pretok vode v vsakem členu drugačen. Predpostavljamo, da v kremenovem peščenjaku (dilatacija je 6x večja kot v peščenem biosparitu) verjetno prihaja do zastajanja vode na stiku v peščen biosparit, saj je evaporacija obratnosorazmerna hitrosti vpijanja vode. Takšna struktura kamnine je namreč ugodna za retencijo vode, ki lahko privede do „mehčanja“ strukture ter tudi povečanja nevarnosti razpadanja kamnine pri procesih zmrzovanja. Nasprotno pa je vpijanje vode pri peščenem biosparitu manjše in s tem evaporacija hitrejša. Kamnina ne zadržuje dolgo vlage, kar omejuje prevajanje vode med fazama močenje-sušenje, ki določajo „termo-hidrične“ pritiske, ki delujejo na kamnino, vgrajeno na objektu. Oba mehanizma, sušenje in močenje ter zmrzovanje in taljenje ledu, očitno povzročata razmike med zrni in prispevajo k izgubi kohezije kamnine. Rezultati tudi kažejo, da se poroznost kamnine, ki je izpostavljena delovanju okoljskim dejavnikom, poveča.

Glede na to, da je voda glavni dejavnik propadanja, je poznavanje pornega sistema, ki ga lahko ocenimo s petrofizikalnimi preiskavami, ključnega pomena pri študiju obstojnostih lastnosti in procesov propadanja kamnin. Pri tem je pomembno tudi natančna določitev parametrov vpijanja vode, ki nam osvetli razumevanje načina gibanja vode v določeni kamnini, saj na podlagi tega lahko sklepamo na posledice vpijanja vode in kristalizacije soli v njih. Vse te zgoraj uporabljene metode v kombinaciji s petrografskimi oz. mineraloškimi preiskavami so tako nujne pri proučevanju procesov propadanja naravnega kamna.

SUMMARY

Use of petrophysical analysis for durability assessment and weathering degree of natural stone

Learning about quantity, shape, size and distribution of pores within the stone is a major significance when studying weathering phenomena or assessing durability of natural building stone. Article deals with petrophysical methods in order to estimate natural stone properties. The bulk and open porosity, saturation coefficient, capillarity, hydric dilatation and pore size distribution of stone from Sedovec quarry has been determined.

Studied stone is medium coarse siliceous calcium sandstone with transition to sandy biosparite. Sandstone consists mainly of quartz, on the contrary feldspars, lithic grains and muscovite are in minor proportions. Glauconite grains and fragments of different fossils (echinoderma, foraminifera, bivalvia, lithotamnia, briozoi) represent allochemical components of sandstone. Cements consist mainly of calcite, while pyrite and glauconite is present in trace.

In attend to estimate stone microstructure the total porosity, porosity of 48 h, capillarity and hydric dilatation were measured. Results show some differences in properties of both lithological sequences present in the quarry. It is possible to observe the variety in porosity between fresh and deteriorated stone as well. Values of total porosity comprised between 9.85 % (sandstone) to 13,71 % (sandy biosparite). Values of porosity 48 h raised from 6.10 % /(sandstone) to 10.58 % (sandy biosparite). These two parameters allow us to determine the Hirchwald coefficient or saturation coefficient which value is in our case less than 0.8 what tells us about low susceptibility of studied stone to froze damages. Pore size distribution was given by Hg-porosimetry, which was carried out on fresh and weathered samples of stone. The main difference of both lithological sequences lies in quantity of large pores, which is higher in sandstone. Regarding fresh and weathered samples, it is obvious that bigger pores contain the sample, which was the most exposed to weathering phenomena. From capillary curves it is possible to obtain the A and B coefficients. Values of A coefficient are 0.043 $gcm^{-2}h^{-1/2}$ for sandy biosparite and 0.072 $gcm^{-2}h^{-1/2}$ for sandstone. Values of B coefficient are 0.46 $cmh^{-1/2}$ for sandy biosparite and 0.65 $cmh^{-1/2}$ for sandstone. Values of hydric dilatation are 0.46 mm/m in case of sandy biosparite and 0.6 mm/m in case of sandstone.

Comparing both litological sequences, sandy biosparite in first of all because of its low porosity show quite better properties regarding susceptibility to weathering. Additionally it has lower velocity of capillarity and hydric dilatation as well and lower susceptibility to froze weathering. Anyway, both – the sandstone and sandy biosparite - form a system, within which each behaves differently. It is to believe that on the sandstone – sandy biosparite are because of different dilatation produced different forces; also they represent a barrier in capillary transfer.

As water is considered to be one of the main factors of weathering, studying of pore system with petrophysical analysis means major significance in weathering phenomena of natural stone.

Zahvale

Avtorici se zahvaljujeva LRMH v Franciji, kjer so nam omogočili opravljanje nekaterih petrofizikalnih preiskav. Posebna zahvala gre tudi prof.dr. Venčeslavu Kavčiču iz kemijskega inštituta za opravljeno Hg-porozimetrijo.

Viri

Amoroso, G.G. & Fassina, V., Stone decay and conservation, Atmospheric pollution, cleaning, consolidation and protection. Materials science Monographs.Vol.11. Amsterdam: Elsevier, 1983. 453 str.

Bilbija, Nenad. Tehnička petrografija. Svojstva i primene kamene: Univerzitetski udžbenik. Beograd: IRO » Naučna Knjiga«, 1984. 239 str.

Bilbija, Nenad in GRIMŠIČAR, Anton. Obstojnost arhitektonskega naravnega kamna iz Slovenije, *Geološki zbornik*, 1987, št. 8, str.151-160.

Bos, K., *Weathering and conservation of ferruginous sandstones used as building material in Northern Belgium:The degree of master.* Brussel: Faculty of Medecine and Pharmacy of the Vrije Universiteit Brussel, 1990. 220 str.

Bourges, A., *Holistic Correlation of Physical and Mechanical Properties of Selected Natural Stones for Assessing Durability and Weathering in the Natural Environment*, Dissertation der Fakultät für Geowissenschaften der Lunwigs-Maximilians- Universität Műnchen, 2006, 201p.

Gal, G., *Influence de la microstructure de différents grès en oevre et de carrière sur leur résistance à l´altération.* Aplication aux *grès à meules de la cathédrale Notre-Dame de Strasbourg.* Travail de diplôme. Ecole polytéchnique fédérale de Lausanne. 2004. 52 str.

Golež, M., *Geološko vrednotenje kamnitih izdelkov iz miocenskih peščenjakov vzhodne Slovenije: magistrsko delo*. Ljubljana: Naravoslovnotehniška fakulteta, Oddelek za geologijo,1999. 122 str.

Golež, M., Mirtič, B. & Mladenovič, A., Študij procesov propadanja sljudnato-kremenovega peščenjaka iz Jelšingrada. *Materiali in Tehnologije*, 2004, let.38, št.1-2, str. 67-70.

Golež, M., Mirtič, B., Mladenovič, A. & Kramar, S., Reopening of an abandoned quarry of calcareus sandstone for the restoration of two cultural monuments in Slovenia. *10th Euroseminar on microscopy Applied to Building Materials*. Paisley, 2005.

Gosselin, C. *Le ciment romain. Une source potentielle de sulfates dans la dégradation des pierres de la Cathédrale de Bourges: Travail du Master.* Paris: Université Paris 7 et Laboratoire de Recherche des Monuments Historiques, 2005. 81 str.

Kramar, S., Mirtič, B., Gunde-Cimerman, N., Zalar, P.&Golež, M., Vpliv mineralne sestave in mikroorganizmov na propadanje peščenjaka iz kamnoloma Sedovec. Influence of mineral composition and microorganisms on sandstone degradation from Sedovec quarry. *RMZ-Materials and Geoenvironment*. 2006, v tisku

Laurent, J.-P., Capillary Water Transfert in Stone Materials: Theoretical and Experimental Aspects. Dostopno na svetovnem spletu: http://www.lthe.hmg.inpg.fr/~laurent/PDFs/Communications/98EASCParis.PDF

RILEM 25 – PEM, Recommended tests to measure the deterioration of stone and to asses the effectivenes of treatment methods, Bordas-Dunod.1980

SIST EN 13755:2002 - Preskušanje naravnega kamna – Ugotavljanje vpijanja vode pri atmosferskem tlaku - Natural stone test methods - Determination of water absorption at atmospheric pressure.

SIST EN 1925:2000 - Preskušanje naravnega kamna - Ugotavljanje vpijanja vode zaradi kapilarnega dviga - Natural stone test methods - Determination of water absorption coefficient by capillarity.

SIST EN 1936:2000 - Preskušanje naravnega kamna - Ugotavljanje prostorninske mase brez por in votlin in prostorninske mase s porami in votlinami ter skupne in odprte poroznosti - Natural stone test method - Determination of real density and apparent density, and of total and open porosity.

SNETHLAGE, R. IN WENDLER, E. Moisture Cycles and Sandstone degradation. V *Saving Our Architectural Heritage. The Conservation of Historic Stone Structures. Dahlem Workshop Report.* Edited by Baer, N.S. in Snethlage, R. Berlin: Freie Universität Berlin, 1996. str.7-24.

VESEL, J. & SENEGAČNIK, A., *Poročilo o rezultatih predhodnega raziskovanja naravnega kamna - peščenjaka na območju opuščenega kamnoloma Sedovec pri Šmarju pri Jelšah.* Ljubljana: Geološki zavod Slovenije, 2002. 10 str., 5 pril.

WENDLER, E. New materials and approaches for the Conservation of Stone. V *Saving Our Architectural Heritage. The Conservation of Historic Stone Structures.Dahlem Workshop Report*. Edited by Baer, N.S. in Snethlage, R. Berlin: Freie Universität Berlin, 1996. str.181-198.

WINKLER, E.M., *Stone: Properties, Durability in Man's Environment*. Verlag, Berlin Heidelberg New York: Springer, 1997. 313 str.

Ladinijske plasti na območju Oble Gorice, osrednja Slovenija

Ladinian Beds in the Obla Gorica Area, Central Slovenia

Stevo Dozet

Geološki zavod Slovenije, Dimičeva 14, 1000 Slovenija;
E-mail: stevo.dozet@geo-zs.si

Received: September 25, 2006 **Accepted**: November 14, 2006

Izvleček: Oblo Gorico in njeno okolico grade skitske, anizijske, ladinijske in cordevolske kamnine. Med njimi so najbolj pestro razvite okoli 225 m debele ladinijske plasti, sestavljene iz različnih sedimentnih in vulkanoklastičnih kamnin. Vulkanoklastične kamine in karbonatni sedimenti z roženci ter ladinijskimi fosili leže diskordantno na anizijskem dolomitu, krovnino ladinijskega zaporedja pa predstavlja masivni cordevolski dolomit z ostanki dazikladacej *Diplopora annulata* Schafhäutl. Ladinijske plasti Oble Gorice so razčlenjene v sedem litostratigrafskih enot. Starost obravnavanega zaporedja je določena z makrofavno.

Abstract: Obla Gorica and its surroundings is composed of various Scythian, Anisian, Ladinian and Cordevolian rocks. Among them are most heterogeneously developed about 225 m thick Ladinian beds, composed of different sedimentary and volcaniclastic rocks. Volcaniclastic rocks as well as carbonate sediments with cherts and Ladinian fossils lie discordantly over the Anisian dolomite, while teh hanging wall of the Ladinian rock succession is represented by the massive Cordevolian Dolomite with remains of the Dasicladacea *Diplopora annulata* Schafhäutl. The Ladinian beds of Obla Gorica are subdivided in seven lithostratigraphic units. The age of the considered stratigraphic sequence is proved by macrofauna.

Ključne besede: litostratigrafska razčlenitev, opis enot, fosili in starost, okolje nastanka, ladinij, Posavske gube, osrednja Slovenija
Key-words: lithostratigraphic subdivision, description of units, fossils and age, environment, Ladinian, Sava Folds, Central Slovenia.

Uvod

Na mejnem ozemlju med Posavskimi gubami in Dolenjskim krasom je zaradi dostopnosti terena, odkritosti kamin in neprekinjenega zaporedja plasti za študij ladinijske sedimentacije in geoloških dogodkov izbran profil na območju Oble Gorice (slika 1), ki se začne v Obli Gorici, poteka po zahodnem in vzhodnem pobočju Vinjega vrha in se vleče naprej ob makadamski cesti vse do kontakta s cordevolskim dolomitom pod Starim gradom.

Prvi detajlnejši opis ladinijskih plasti na območju med Posavskimi gubami in Dolenjskim krasom je podal Germovšek (1955). K ladinijskim plastem je prištel klastične sedimente, temen apnenec, svetle apnence in breče ter dolomit.

Scientific paper

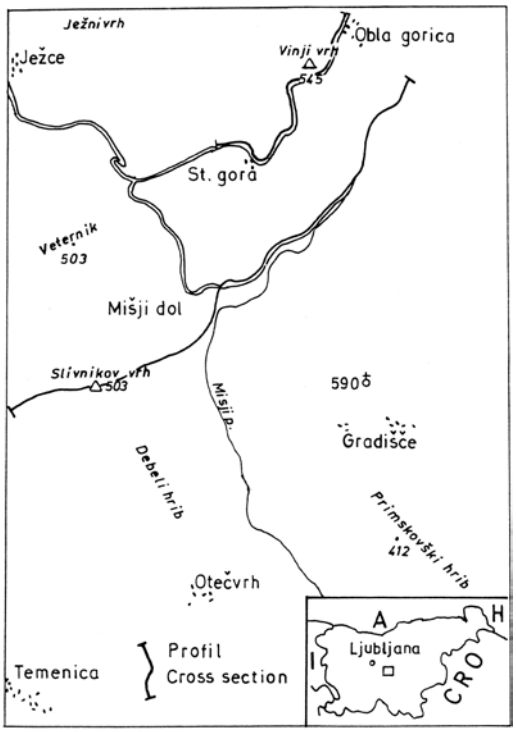

Slika 1. Lega raziskanih profilov
Figure 1. Location map of the investigated cross-sections

Triasni vulkanizem na Dolenjskem je opisal RAKOVEC (1946). Prišel je do zaključka, da so tufske kamnine v Posavskih gubah produkt istega vulkanizma kot tiste z Bohorja, Orlice in Rudnice.

BUSER (1976) je detajlno raziskal in opisal profil ladinijskih plasti ob cesti Mišji Dol-Primskovo.

Mejno ozemlje med Posavskimi gubami in Dolenjskim krasom je doslej skartirano dvakrat. Prvič je bilo kartirano v merilu 1:10 000 v okviru raziskav Dolenjske (GERMOVŠEK, 1955), drugič v merilu 1:25 000 v okviru izdelave Osnovne geološke karte SFRJ list Ribnica 1:100 000 (BUSER, 1969, 1974).

Glavni namen naših detajlnih stratigrafskih raziskav je bil, da v okviru kartiranja za Geološko karto Slovenije 1:50 000 te plasti nadrobno stratimetrijsko raziščemo, kar je omogočilo detajlno litostratigrafsko razčlenitev ladinijske skladovnice v tem delu Slovenije.

Geološka zgradba ozemlja

Geološka zgradba obravnavanega ozemlja je najbolj razvidna iz stratimetrijskega profila Preska (Obla Gorica)-Mišji Dol-Slivnikov vrh, ki na dolžini več kilometrov preseka grödenske, spodnjetraisne (skitske), anizijske, ladinijske in cordevolske plasti s skupno debelino okoli 2000 metrov (slika 1).

Od grödenskih plasti seka profil le njihov 100 m debel zgornji del, ki je sestavljen iz sivkastordečega, svetlordečega in zmerno rdečega srednjezrnatega do zrnatega, pogosto konglomeratičnega in redkeje drobnozrnatega močno sljudnatega kremenovega peščenjaka. V kompleksu rdečih grödenskih klastitov ni nikjer sledov plastnatosti, zato sklepamo, da gre za masivne kopenske sedimente v katerih se pogosto, zlasti pa na površini razpok opaža tirkiznomodra in modrikastosiva oksidna prevleka. Rdeči grödenski sedimenti prehajajo ponekod v bočni in navpični smeri v zelenkastosive klastite s podobno mineralno sestavo.

Nedaleč od tod je na Ježnem vrhu ohranjena celotna skladovnica grödenskih klastitov, ki je debela okoli 400 m, med rdečimi drobnozrnatimi klastiti pa se pojavljajo tudi vložki kompaktnega, plastnatega, debelozrnatega kremenovega peščenjaka in konglomerata.

Nad grödenskimi plastmi ni v profilu niti temnih zgornjepermskih karbonatnih kamnin niti sedimentov dveh bazalnih skitskih členov, zato smatramo, da je v zgornjem permu in najspodnjejšem skitu obstajalo v tem delu Slovenije kopno, na katerem pa ni bilo akumulacije kopenskih sedimentov. Gre za občutno stratigrafsko vrzel in odsotnost sedimentacije, saj se skitske plasti pričenjajo šele s klastiti seiskega člena, ki sestoji iz zaporedja sivkastordečega lističastega in tankoploščastega sljudnatega peščenjaka sivkastorumenega in sivkastooranžnega peščenega (sljudnatega) laporovca. Srednjemu skitu bi lahko prišteli pisane sljudnate klastite z okoli 4 m debelim vložkom ploščastega in plastnatega (3-40 cm), drobno in srednjezrnatega, sivkastordečega oosparitnega apnenca s preseki gastropodov /*Holopella gracilior* Schauroth/ ter 2,5 m debelih vložkov sivkastorumenega, kompaktnega, ploščastega in plastnatega (3 cm do 30 cm), močno peščenega apnenčevega laporovca. Zgornji (campilski) del skitskega zaporedja sedimentov sestoji iz treh členov. Spodaj je okoli 50 m debel klastični člen, ki sestoji iz tankoploščastih pisanih peščenjakov, peščenih laporovcev in skrilavih glinavcev, navzgor sledi okoli 125 m debel člen rumenkastosivega, ploščastega in plastnatega peščenega (sljudnega) dolomita z interkalacijami peščenega dolomitnega laporovca. Na vrhu skitskega zaporedja je okoli 50 m debel člen črnega plastnatega apnenca, ki je deloma gomoljast in vsebuje krinoidne ostanke. Nepopolna skitska skladovnica (manjkata najspodnjejša člena) je debela okoli 300 m.

Konkordantno na črnem plastnatem gomoljastem skitskem apnencu leži plastnat, zelo svetlosiv, drobno do srednjezrnat anizijski dolomit. Skladovnica anizijskega dolomita je debela okoli 75 m. Tudi v tem profilu je meja med anizijskim dolomitom in ladinijskimi plastmi precej pokrita.

Kontakt grödenskih in skitskih plasti je razkrit tudi ob cesti severozahodno od Oble Gorice. Diskordantno na opekastordečem, lističastem in zelo tankoploščastem (1-2 cm) rdečem skrilavem glinavcu z vložki zelenkasto in modrikastosivega ter rjavkastordečega, ploščastega (2-10 cm), drobnozrnatega peščenjaka leži okoli 45 m debelo zaporedje pretežno ploščastega (2-5 cm), tu in tam plastnatega (10-29 cm), izredno močno peščenega (sljudnatega), sivega, olivnosivega, temnoolivnosivega, oranžnorumenega, sivkastorumenega, opekastordečega, mestoma rdečega, tirkiznomodrega in zelenosivega dolomita, peščenega laporovca in peščenjaka. Na lezikah plasti opazujemo močno nakopičenje sljude. Nad opisanim klastično-karbonatnim zaporedjem leži okoli 15 m debela skladovnica rumenkastosivega do oranžno rumenega, močno peščenega (sljudnatega) dolomita. Po litološki sestavi pripada opisano zaporedje pisanih sedimentov nad kontaktom z grödenskimi plastmi seiskemu členu werfen-a v Dolomitih.

Nad opisanimi seiskimi platmi leži okoli 65 m debelo zaporedje izredno pisanih klastičnih in dolomitnih plasti, ki sestoji iz dveh približno enako debelih delov. V spodnjem delu prevladujejo izredno pisane klastične kamnine nad peščenim dolomitom, v zgornjem delu pa prevladujejo manj pisani ploščasti in tankoplastnati peščeni dolomiti. Te plasti lahko primerjamo s horizontom Andraz I v Tirolskih Dolomitih.

Nad horizontom Andraz I je pri Kuhlju (Obla Gorica) in severno od tod razvit tudi gastropodni oolitni člen, ki je debel okoli 50 m. V njem prevladujejo pisani skitski klastiti, kjer razlikujemo dva dela. V spodnjem delu so v pisanih klastitih plasti in leče srednje temnosivega do temnosivega, ploščastega in plastnatega (30-50 cm), mikritnega in drobno zrnatega apnenca z redkimi ooidi, v opekasto in sivkastordečem, tankoploščastem (1-5 cm) kremenovem peščenjaku in skrilavem glinavcu pa so dokaj pogostne plasti in leče sivkastordečega oolitnega dolomita z Fe ooidi. Zgornji del skitskih sedimentov je odsekan s prelomom, tako da mejijo tukaj spodnjeskitske plasti z anizijskim dolomitom prelomno.

Na svetlosivem do srednje temnosivem, plastnatem (15-40 cm), drobnozrnatem anizijskem dolomitu ležita v profilu Obla Gorica-Mišji Dol rumenkasto olivnozelen pelitni tuf in temno olivnozelen ter olivnosiv zelo drobnozrnat do srednjezrnat tuf z vložki črnega mikritnega apnenca in debelozrnatega kalkarenita. Navzgor sledi 11 m debel apnenčev člen, ki v spodnjem delu sestoji iz sivkastočrnega in črnega, plastnatega (15-30 cm), mikritnega in drobnozrnatega apnenca, v zgornjem delu pa iz sivkastočrnega in rumenkastosivega apnenčevega laporovca s prehodi v laporni apnenec. V vrhnjem delu vsebuje apnenec roženec in tanjše vložke tufov. Nad apnenci s tufi leži okoli 100 m debela skladovnica srednje sivega, ploščastega (2-10 cm) in plastnatega drobnozrnatega dolomita z gomolji in tankimi vmesnimi plastmi črnega roženca. Nato se v debelini 65 m menjavajo črni laporni apnenec, apnenčev laporovec in redkeje kalkarenit z več tankimi vložki tufa in tufskega peščenjaka. Preostali del ladinijske skladovnice izpolnjuje bledorumenkastosiv, ploščast (5-15 cm) drobnozrnat dolomit z gomolji roženca. Izmerjena debelina ladinijskega litološkega zaporedja znaša 400 m. Konkordantno na ladinijskih plasteh leži precej debela skladovnica srednjesivega in svetlosivega do belega, masivnega, debelozrnatega, luknjičastega cordevolskega dolomita, tu in tam z ostanki in preseki diplopor.

V tektonskem pogledu leži obravnavano ozemlje v mejnem prostoru med severno ležečimi Posavskimi gubami in južno ležečimi mezozojskimi grudami. Med njimi doslej ni ugotovljena izrazitejša tektonska meja. Da je stik Posavskih gub in Dolenjskega krasa bolj ali manj normalen so menili KOSSMAT (1913), GERMOVŠEK (1955), RAKOVEC (1956) in BUSER (1974), tektonske elemente tega stika pa so ugotovili SEDLAR ET AL. (1948), BUSER (1965) in DOZET (1966, 1985). V tektonskem pogledu prevladujejo na obravnavanem ozemlju strukture s smerjo severozahod-jugovzhod.

MATERIAL IN METODE

Podatki, uporabljeni v tem članku, so pridobljeni pri regionalnem geološkem kartiranju za izdelavo Geološke karte Slovenije 1:50 000, kjer je prevladovala metoda profiliranja. Najnovejši, predvsem sedimentološki podatki so dobljeni pri stratimetrijskem profiliranju. Istočasno s stratimetrijskim profiliranjem je potekalo vzorčevanje kamnin za različne laboratorijske preiskave. Karbonatne kamnine so določene po FOLKOVI (1959) in DUNHAM-ovi (1962), klastične pa po PETTIJOHN-ovi klasifikaciji.

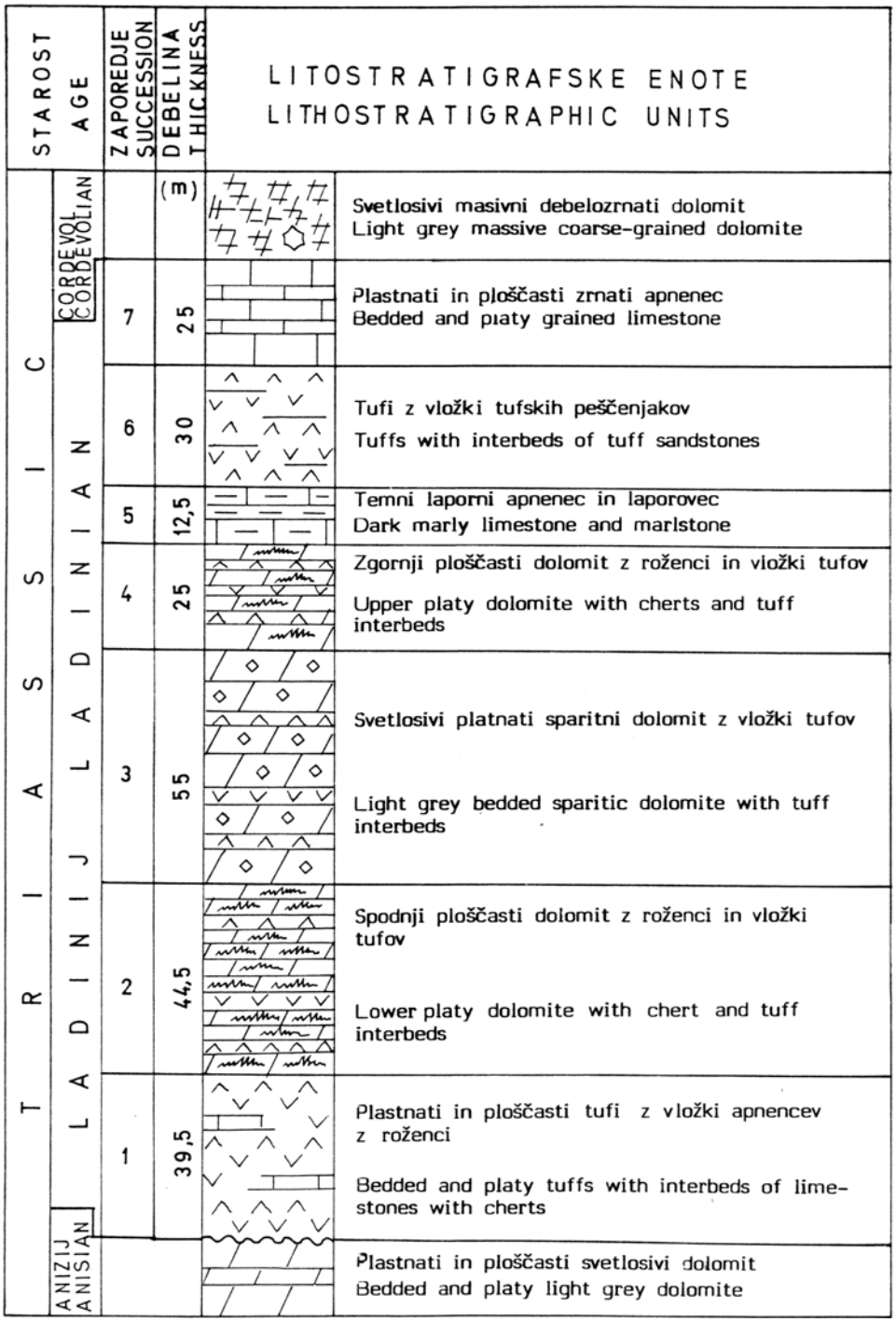

Slika 2. Litostratigrafska razčlenitev ladinijskih (langobardskih) plasti na območju Oble Gorice
Figure 2. Lithostratigraphic subdivision of the Ladinian (Langobardian) beds in the Obla Gorica area

STRATIGRAFIJA

Ladinij

Ladinijske plasti so nadrobno raziskane in detajlno litostratigrafsko razčlenjene v profilu med Vinjim vrhom in Starim gradom na območju Oble Gorice.

PROFIL OBLA GORICA

Ladinijske plasti se na obravnavanem ozemlju pojavljajo v obliki več sto metrov debelega pasu, ki ga sledimo v smeri severozahod-jugovzhod med Oblo Gorico in Zaplazom. Sestavljajo jih vulkanoklastične in sedimentne kamnine. Po litološki sestavi in superpoziciji je ladinijska skladovnica obravnavanega ozemlja razdeljena na sedem litostratigrafskih enot; to so (slika 2): 1 – tufi z vložki karbonatnih kamnin z roženci, 2 – spodnji ploščasti dolomit z roženci in vložki tufov, 3 – svetlo sivi plastnati sparitni dolomit z vložki tufov, 4 – zgornji ploščasti dolomit z roženci in vložki tufov, 5 – temni laporni apnenec in skrilavi laporovec, 6 – tufi z vložki tufskih peščenjakov in 7 – plastnati in ploščasti zrnati apnenec.

Spodnja meja ladinijskih plasti

V podlagi ladinijskega litološkega zaporedja leži povsod na obravnavanem ozemlju anizijski svetlosivi, plastnati in redkeje ploščasti dolomit, ki po strukturi pripada drobno in srednjezrnatemu dolosparitu, redkeje dolomikritu. V vrhnjem delu anizijske skladovnice so ohranjene redke stromatolitne in brečaste teksture, ni pa drugih loferskih tekstur. Kamnine ob ladinijsko-anizijskem stiku (tabla 1., slika 3., slika 4.) so povsod bolj ali manj tektonizirane, vendar po vpadu anizijskega dolomita in ladinijskih plasti sklepamo, da med njimi ni večje kotne diskordance.

Tabla 1 – Plate 1

Slika 3. Tektoniziran kontakt med svetlosivim plastnatim in ploščastim anizijskim dolomitom (na sliki desno) in ladinijskimi tufi z vložki tufskih peščenjakov in temnih apnencev (na sliki levo). Pretrte so zlasti vrhnje plasti anizijskega dolomita
Figure 3. Tectonized contact between the light grey bedded and platy Anisian dolomite (in the picture to the right) and Ladinian tuffs interbedded by tuff sondstones and dark limestones (in the picture to the left). Dislocated are especially the topmost beds of the Anisian dolomite

Slika 4. Prelom, ki loči srednje svetlosivi, plastnati in ploščasti anizijski dolomit (levo od preloma) od pisanih klastično-dolomitnih skitskih sedimentov (desno od preloma) pri Vavtarju
Figure 4. The fault separating the medium light grey bedded and platy Anisian dolomite (to the left of the fault) from the variegated clastic-dolomite Scythian sediments (to the right of the fault) at Vavtar

Slika 5. Ploščasti in tankoplastnati tufi, tufski peščenjaki in temni apnenci (1. litostratigrafska enota)
Figure 5. Platy and thin-bedded tuffs, tuff sandstones and dark limestones (1th lithostratigraphic unit)

Slika 6. Črni ploščasti in tankoplastnati gomoljasti apnenec z nodulami črnih rožencev (1. litostratigrafska enota)
Figure 6. Black, platy and thin-bedded, nodular limestone with black chert nodules (1th lithostratigraphic unit)

Slika 7. Sivi in temnosivi pretežno tankoploščasti (1-5 cm) dolomit s tankimi vmesnimi plastmi črnih rožencev (2. litostratigrafska enota)
Figure 7. Grey and dark grey predominantly thin-bedded (1-5 cm) dolomite with thin intercalations of black chert (2nd litostratigraphic unit)

Slika 8. Močno nagubane plasti sivega in temnosivega ploščastega dolomita s črnimi roženci in do 1 m debelimi plastmi srednje svetlosivega dolomita (2. litostratigrafska enota)
Figure 8. Greatly folded grey and dark grey platy dolomite with black cherts and up to 1 metre thick beds of medium light grey dolomite (2nd lithostratigraphic unit).

Tabla 2 – Plate 2

Slika 9. Sivi in temnosivi ploščasti in tankoplastnati dolomit z interkalacijami in nodulami črnih rožencev (2. litostratigrafska enota)
Figure 9. Grey and dark grey platy and thin-bedded dolomite with intercalations and nodules of black cherts (2nd lithostratigraphic unit)

Slika 10. Več kot pol metra debel vložek sivkastočrnega mikritnega (mudstone) apnenca, ki se kolje v tanjše plošče, v sivem in temnosivem ploščastem dolomitu z roženci (2. litostratigrafska enota)
Figure 10. More than half a metre thick interbed of grayish black micritic (mudstone) limestone decomposing in thinner plates, in the grey and dark grey platy dolomites with cherts (2 nd lithostratigraphic unit)

Slika 11. Sivi in temnosivi ploščasti dolomit z roženci in vložki tufov (2. litostratigrafska enota)
Figure 11. Grey and dark grey platy dolomite with cherts and tuff interbeds. (2nd lithostratigraphic unit)

Slika 12. Desno od preloma so skitske plasti, ki sestoje iz sivega in temnosivega močno pretrtega plasnatega sivkastega dolomita z vložki pisanih peščenjakov in dolomitnih laporovcev
Figure 12. To the right of the fault there are the Scythian beds consisting of grey and dark grey greatly dislocated bedded dolomite with interbeds of variegated sandstones and dolomitic marls.

Zgornja meja ladinijskih plasti

Ladinijske plasti prehajajo navzgor brez sledov erozije oziroma diskordance v svetlosivi skoraj beli, masivni, luknjičavi debelozrnati cordevolski dolomit. V črnih apnencih vrhnjega dela ladinijske skladovnice so najdeni konodonti ladinijske starosti, v bazalnem cordevolskem dolomitu pa se dobe ostanki dazikladacej iz rodu *Diplopora.*

V peščenjakih okoli Primskovega in vzhodno od tod je LIPOLD (1858) našel med drugim tudi školjke *Daonella lommeli* (Wissmann).

Fosili in starost

V podlagi ladinijskih plasti, to je v anizijskem dolomitu, nismo doslej našli nobenih določljivih organskih ostankov, v krovninskem cordevolskem dolomitu pa so ponekod ohranjeni preseki diplopor, ki so podobni tistim z območja Pleš (DOZET, 1966, 1982) in pripadajo najverjetneje vrsti *Diplopora annulata* (Schafhäutl).

Pri Primskovem je GERMOVŠEK (1955) v obravnavanem litološkem zaporedju našel amonite, ki jih je Kühn določil kot *Protrachyceras mundevillae* in *Anolcites doleriticum*, BUSER (1974) pa školjke *Daonella lommeli* in majhne cefalopode. Oba amonita pripadata horizontu z amonitom *Protrachyceras archelaus*, torej zgornjewengenskim plastem (KÜHN,1954).

V apnencih in dolomitih z roženci iz spodnjega, srednjega in zgornjega dela ladinijske skladovnice smo vzeli vzorce za radiolarije, ki pa so bili vsi sterilni.

V 4,5 m debelem vložku plastnatega kalkarenita s piritnimi zrni (bazalna litološka enota) je avtor našel odtise školje *Daonella lommeli* (Wissmann), v 3 m debelem vložku laporнega in debelozrnatega apnenca z gomolji roženca (bazalna litološka enota) pa krinoide, morske lilije in ploščice ehinodermov.

Litostratigrafske enote

Kot je že omenjeno je v ladinijskem zaporedju vulkanoklastičnih kamnin in karbonatnih sedimentov izločeno sedem litostratigrafskih enot, in sicer (slika 2): 1 – tufi z vložki karbonatnih kamnin z roženci, 2 – spodnji ploščasti dolomit z roženci in vložki tufov, 3 – svetlosivi plastnati sparitni dolomit z vložki tufov, 4 – zgornji ploščasti dolomit z roženci in vložki tufov, 5 – temni laporni apnenec in skrilavi laporovec, 6 – tufi z vložki tufskih peščenjakov in 7 – temni plastnati in ploščasti zrnati apnenec.

1 – Tufi z vložki karbonatnih kamnin z roženci

Bazalno litostratigrafsko enoto (tabla 1, slika 5, slika 6) karakterizirajo piroklastične kamnine v katerih se pojavljajo do nekaj metrov debeli vložki karbonatnih kamnin. Debelina bazalnega zaporedja vulkanoklastičnih in karbonatnih sedimentnih kamnin ladinijske starosti znaša 39,5 m.

- V glavnem profilu ob makadamski cesti, ki pelje od Oble Gorice proti asfaltni cesti Kožljevec-Mišji Dol, bazalna enota ne pričenja s tufi temveč s 4,5 m debelim paketom temnosivega ploščastega apnenčevega laporovca ter ploščastega in tankoplastnatega laporнega apnenca. Kontakt s spodaj ležečimi srednje svetlosivim do srednje temnosivim, plastnatim (20-50 cm) ani-

zijskim dolomitom s stromatolitnimi in brečastimi vložki je precej dislociran.
- Navzgor sledi 17,5 m debel paket svetlo do temnozelenega, pelitnega in debelozrnatega, ploščastega in plastnatega, bolj ali manj kompaktnega ter tu in tam pasnatega tufa in tufskega peščenjaka, v katerem se pojavljajo redke tanke interkalacije sivkastočrnega in črnega mikritnega apnenca.
- Konkordantno na tufih leži 3,5 m debel vložek črnega in sivkastočrnega plastnatega (10-35 cm), debelozrnatega kalkarenita s piritnimi zrni in odtisi daonel.
- Na kalkarenit se je v debelini 5 m odložen rjavkastosiv tufski peščenjak, ki zaradi debelozrnate strukture in slabo obstojnega veziva zelo hitro prepereva v tufski pesek.
- Bazalno litostratigrafsko enoto zaključuje 5.5 m debela skladovnica črnega in sivkastočrnega, ploščastega (5-10 cm) in tankoplastnatega (10-20 cm), laporнega in debelozrnatega (kalkarenit) apnenca z nepravilnimi gomolji rožénca, krinoidi, morskimi lilijami in ploščicami ehinodermov. Roženec se pojavlja tudi razpršen v kamnini.

2 – Spodnji ploščasti dolomit z roženci in vložki tufa

V drugi ladinijski litostratigrafski enoti (tabla 1, slika 7,8, tabla 2, slika 9,10,11) močno prevladuje ploščasti dolomit z roženci in vložki tufov predvsem v zgornjem delu. Ta enota je v litološkem pregledu sestavljena pravzaprav iz petih delov.

- Prav spodaj je 1,5 m debel horizont rumenkastosivega peščenega tufa z redkimi tankimi interkalacijami dolomita z roženci.
- Navzgor sledi okoli 5,0 m debela skladovnica pretežno tankoploščastega (1-5 cm) temno sivega dolomita s tankimi vmesnimi plastmi črnih rožencev in z več tankih plasti (10-15 cm) temnosivega dolomita z roženci.
- Nad ploščastim dolomitom se v debelini 4,5 m menjavata tankoploščasti temnosivi dolomit z interkalacijami črnega rožénca in dolomitnega laporovca ter debeloplastnati (50-75 cm) rumenkastosivi do temnosivi zrnati dolosparit.
- Više v litološkem stolpcu imamo ponovno okoli 8,5 m debel paket tankoploščastega (1-5 cm) temnosivega, če je preperel pa rumenkasto ali olivnosivega dolomita z interkalacijami črnih rožencev in enim 3,5 m debelim vložkom (približno v sredini) ploščastega in plastnatega (2-20 cm) modrikastosivega tufa z interkalacijami ploščastega dolomita z roženci. Te plasti so izredno močno nagubane.
- V vrhnjem delu druge litostratigrafske enote je 25 m debela skladovnica tankoploščastega temnosivega dolomita s pogostnejšimi interkalacijami dolomitnega laporovca in tankimi plastmi črnih rožencev ter z vložki tufov.
- Debelina druge litostratigrafske enote znaša 44,5 m.

3 – Svetlosivi plastnati sparitni dolomit z vložki tufov

Tretja litostratigrafska enota ima nekoliko bolj homogeno litološko sestavo kot prvi dve enoti. V njeni sestavi močno prevladuje svetlosivi, srednje svetlosivi in srednje temnosivi, srednje do debelozrnati dolosparit, ki se pojavlja v 35 cm do 50 cm debelih plasteh z ravno površino. V sladovnici dolosparita opazujemo le redke tanke plasti tufov in

tufskih peščenjakov. Nekaj debelejših vložkov tufov in tufskih peščenjakov dobimo v bazalnem delu dolosparitne skladovnice, najdebelejši tufni vložek, ki je debel okoli 7,5 m, pa najdemo v vrhnjem delu skladovnice svetlosivega dolosparita. Skupna debelina opisanih plasti znaša okoli 55 m.

4 – Zgornji ploščasti dolomit z roženci in tufi

Gre za 25 m debelo skladovnico temnosivega tankoploščastega (1-5 cm) debelozrnatega dolomita s tankimi vmesnimi plastmi črnih rožencev in olivnosivih do temnosivih dolomitnih laporovcev.

5 – Temni laporni apnenec in skrilavi laporovec

Peto litostratigrafsko enoto sestavlja črni ploščasti laporovec, ki vsebuje redke plasti in tanjše vložke črnega in sivkastočrnega lapornega apnenca. Laporovec kaže izrazito skrilavo teksturo, ki je posledica singenetskega tektonskega delovanja. V lapornem apnencu in skrilavem laporovcu ni rožencev, njuna debelina pa znaša 12,5 m.

6 – Tufi z vložki tufskih peščenjakov

Šesta litostratigrafska enota je sestavljena iz ploščastega in lističastega močno preperelega svetlozelenega tufa z 20 cm do 25 cm debelimi vložki rumenkasto in zelenkastosivega, srednje kompaktnega, debelozrnatega peščenjaka. Debelina tufske enote znaša 30 m.

7 – Temni plastnati in ploščasti zrnati apnenec

Najmlajšo litostratigrafsko enoto ladinijskega litološkega zaporedja predstavlja 25 m debela skladovnica srednje temnosivega, zrnatega, plastnatega in ploščastega, bituminoznega apnenca. Površine ploskev so ravne. Apnenec je včasih laminiran. Laminiranost nastopa zaradi različne zrnavosti lamin, včasih tudi zavoljo povečane vsebnosti hematita ali organske snovi.

Okolje nastanka

Iz rezultatov geološkega kartiranja za osnovni geološki karti Slovenije v merilih 1:100 000 in 1:50 000, pri katerih je sodeloval tudi avtor članka, je razvidno, da so sedimenti od začetka do konca mezozoika nastajali v obravnavanem delu Dinaridov pretežno v plitvomorski sredini na obsežni stabilni karbonatni platformi, kar velja predvsem za anizijske in cordevolske karbonatne sedimente. V plitvem, toplem in čistem cordevolskem morju so na obsežnih podmorskih tratah uspevale apnenčeve alge dazikladaceje, ki so po odmrtju dale material za plastnati biostromalni apnenec, ki se je pri pozni diagenezi spremenil v slabo plastnat ali masiven debelozrnat dolomit, v katerem so le tu in tam ohranjene teksture in struktura prvotnega sedimenta.

V fassanski dobi je na obravnavanem ozemlju obstajalo najverjetneje dokaj ravno kopno, na katerem ni bilo sedimentacije.

V langobardu se je karbonatna platforma tektonsko spustila v globljo morsko sredino, v kateri so izmenično nastajali ploščasti in tankoplastnati mikritni apnenci, apnenčevi laporovci, dolomiti in kalkareniti z roženci ter drobnozrnati tufi. Dotok materiala s kopnega je bil sorazmerno majhen.

Primerjava in razprava

V podlagi obravnavanega ladinijskega litološkega zaporedja leži v vseh profilih, ki so detajlneje pregledani, anizijski dolomit. Meja med anizijem in ladinijem je največkrat tektonizirana (tabla 1, slika 3,4), vendar po vpadih enih in drugih plasti sodeč bolj ali manj konkordantna. V glavnem ni podatkov, ki bi govorili za močnejšo blokovsko tektoniko niti kotno tektonsko erozijsko diskordanco na prehodu iz anizija v ladinij v tem delu Slovenije. Na morfološko razgibano dno lagune kažejo predvsem hitre spremembe sedimentacije na zelo kratkih razdaljah (deset ali več deset metrov), kar pa je tudi posledica živahne vulkanske dejavnosti, ki se kaže v pogostnosti vložkov vulkanoklastičnih kamnin vzdolž celotnega ladinijskega litološkega stolpca. Za obstoj diskordance med ladinijskimi in anizijskimi plastmi govori predvsem odsotnost buchensteinskih plasti in hitre spremembe bazalne sedimentacije predvsem v najspodnejšem delu litološke enote, kar se opaža zlasti, če med seboj primerjamo ladinijske stolpce raziskanih profilov.

Ker ni nikjer sledov blokovske tektonike, izrazitejšega paleoreliefa in kopenskih brečastih tvorb, sklepamo, da je na obravnavanem ozemlju obstajalo v fassanski dobi dokaj ravno kopno. Na ravnem kopnem je erozija bila dokaj šibka, zato se tudi ni nikjer izoblikovala izrazitejša erozijska površina in ni nikjer sledov karstifikacije. Tudi debelina ladinijske sedimentacije je v vseh profilih precej enaka. Transgresija langobardskega morja je bila mirna in ni nikjer pustila za sabo debelozrnatih klastičnih tvorb.

Če pa primerjamo začetno ladinijsko sedimentacijo vidimo, da le-ta pričenja v profilu ob makadamski cesti Obla Gorica-Mišji Dol s 4,5 m debelim paketom temno sivega ploščastega apnenčevega laporovca z vložki ploščastega in tankoplastnatega lapornega apnenca, na zahodnem pobočju Vinjega vrha pa s 7,5 m debelim horizontom ploščastega (1-17 cm) in tankoplastnatega (10-20 cm), olivnosivega dolomita s paralelepipedsko krojitvijo. Dolomit je mestoma precej lapornat in vsebuje v vrhnjem delu redke plošče črnega zrnatega apnenca. Južno od tod na poti proti spodnjemu Vavtarju in peskolomu anizijskega dolomita, leži neposredno na anizijskem dolomitu naprej 10 cm debela plošča črnega zrnatega močno rekristaliziranega apnenca, na njej pa kompakten, ploščast (2-5 cm) zelenkastosiv do olivno siv pelitni tuf. Slednji je včasih laminiran (kovinsko rjave hematitne lamine). Debelina pelitnega tufa znaša 6 m. Navzgor sledi 5 m debelo zaporedje plastnatega zelenkastosivega pelitnega tufa in srednjezrnatega kompaktnega tufskega peščenjaka. Še više je 10 m debel litološki interval olivno in zelenkastosivega, lističastega in zelo tankoploščastega, slabo kompaktnega tufa. Na slednjem leži 10 m debelo zaporedje črnkastoolivnega, ploščastega, kompaktnega pelitnega tufa s pogostnimi od 0,25 m do 0,75 m debelimi vložki svetlozelenkastega in bledo rumenkasto-zelenkastega, zrnatega, pasnatega (limonitni pasovi) tufskega peščenjaka. Debelina bazalnega tufskega člena znaša v tem profilu 31 m.

Posebno izrazit je v tem profilu tudi 16,5 m debel apnenčev člen, sestavljen iz črnega mikritnega apnenca, apnenčevega laporovca, lapornega apnenca in kalkarenita. V spodnjem delu te skladovnice, ki je debela 12 m, opazujemo menjavanje črnega do olivnosivega in rjavosivega ploščastega in

tankoplastnatega apnenčevega laporovca in lapornega apnenca ter redke plasti kalkarenita. V opisanem zaporedju močno prevladujejo apnenčevi laporovci, zanimivo pa je tudi, da se roženec pojavlja v naštetih karbonatnih kamninah le v sledovih, ali pa ga sploh ni. V zgornjem delu obravnavanega apnenčevega člena, ki je debel 4,5 m, je ploščast in tankoplastnat sivkastočrn do črn lapornat ali drobnozrnat rahlo gomoljast apnenec z nodulami črnega roženca.

Izrazit 9 m debel apnenčev člen se pojavlja tudi v bazalni enoti ladinijskega litološkega zaporedja na zahodnem pobočju Vinjega vrha. Sestavljen je iz treh delov. V spodnji tretjini apnenčevega člena je temnosiv, sivkastočrn in črn, lapornat ali zrnat, pretežno debeloplastnat, tu in tam laminiran mikritni apnenec z rožencem. Lamine so iz črnega roženca, večji del roženca pa je nepravilno razpršen po celi kamnini. Srednji del apnenčevega člena je iz temnosivega in črnega ploščastega (3-10 cm), zrnatega apnenca s kroglasto krojitvijo in veliko vsebnostjo roženca, ki je nepravilno razpršen po kamnini. V apnencu s kroglasto krojitvijo dobimo ponekod lečaste plasti (10-25 cm) kalkarenita. V zgornji tretjini apnenčevega člena zahodnega pobočja Vinjega vrha je sivkastočrn do črn, ploščast laporni apnenec.

Če primerjamo najspodnjejše dele opisanih ladinijskih litoloških stolpcev z bližnjim ekvivalentnim litološkim stolpcem ladinijskega zaporedja v profilu Mišji Dol-Primskovo (Buser, 1976) vidimo, da pričenja ladinijska sedimentacija v slednjem profilu z vulkanoklastičnimi kamninami oziroma s tufi.

Iz primerjave štirih opisanih profilov, ki leže v raziskanem prostoru zelo blizu, je razvidno, da sedimentacija v vseh štirih profilih začenja z drugačnimi kamninami, primerjava bazalne enote vseh štirih geoloških presekov pa kaže, da so obstajale precejšnje razlike v debelini in sedimentaciji posameznih členov tega dela ladinijske skladovnice. Opisani litološki stolpci potrjujejo razgibanost morfologije okolij nastanka teh kamnin. Odsotnost buchensteinskih plasti na celotnem raziskanem ozemlju pa kaže na občutno sedimentacijsko vrzel oziroma diskordanco.

SKLEP

Ladinijsko sedimentacijo na območju Oble Gorice karakterizirajo temne karbonatne kamnine z veliko rožencev ter rumenkasto in zelenkastosive vulkanoklastične kamnine, predstavljene z različnimi tufi in tufskimi peščenjaki. Karbonatne in vulkanoklastične kamnine se med seboj menjavajo s tem, da je v ladinijski dobi prevladovala sedimentacija zdaj enih zdaj drugih.

V podlagi ladinijskega litološkega zaporedja leži sparitni, mikritni, redkeje stromatolitni in brečasti anizijski dolomit, ki je bil v neotektonski fazi skupaj z mlajšimi kamninami precej tektoniziran. Strukturne in teksturne značilnosti kažejo, da je anizijski dolomit nastajal v plitvem šelfnem morju na stabilni karbonatni platformi.

Dosedaj pridobljeni geološki podatki kažejo, da na obravnavanem območju v najspodnjejšem ladiniju (fassan) ni bilo sedimentacije. Buchensteinske plasti namreč v tem delu Slovenije doslej niso bile nikjer odkrite.

Na območju Oble Gorice so ladinijske plasti razdeljene na sedem litostratigrafskih enot, in

sicer (slika 2): 1 – tufi z vložki karbonatnih kamnin z roženci, 2 – spodnji ploščasti dolomit z roženci in vložki tufov, 3 – svetlosivi plastnati sparitni dolomit z vložki tufov, 4 – zgornji ploščasti dolomit z roženci in vložki tufov, 5 – temni laporni apnenec in skrilavi laporovec, 6 – tufi z vložki tufskih peščenjakov in 7 – temni plastnati in ploščasti zrnati apnenec.

Ladinijska starost obravnavanega zaporedja sedimentov in vulkanoklastičnih kamnin je dokazana z najdbo vodilnih školjk daonel in amonitov. V teh plasteh so najdeni tudi krinoidi, morske lilije in majhni amoniti, ki pa še niso določeni. Paleontološka analiza vzorcev karbonatnih kamnin na radiolarije ni dala pričakovanih rezultatov. Ladinijsko starost teh plasti dokazuje posredno tudi njihova stratigrafska lega med pod njimi diskordantno ležečim anizijskim dolomitom in konkordantno na njih ležečim cordevolskim dolomitom z algo *Diplopora annulata* Schafhäutl.

Temne plastnate karbonatne kamnine z roženci so nastajale v poglobljenem delu šelfa z veliko vsebnostjo kremenice. Prisotnost pirita in temna barva teh sedimentov kažeta na redukcijsko okolje.

Nastanek vulkanoklastičnih kamnin je povezan z intenzivnim vulkanskim delovanjem. Zelo drobnozrnati tufski sedimenti so se odlagali v mirnem pelagičnem okolju z občasnim terigenim vplivom. Vulkanoklastične kamnine so dokaj čiste. V njih ni opaziti večje količine primesi starejših ladinijskih kamnin ali sedimentov podlage, kar kaže na to, da na tem območju ni bilo večje tektonske aktivnosti niti posebno močne erozijske dejavnosti. Ladinijske plasti na območju Oble Gorice so torej nastajale na tektonsko slabo aktivnem področju z živahno dejavnostjo vulkanov v okolici, vendar s slabo erozijsko obdelavo podlage. Na prehodu iz anizijske v cordevolsko dobo se je dno šelfa-lagune dvignilo do te mere, da so bili ustvarjeni pogoji za nastanek nove stabilne karbonatne platforme, na kateri se je odlagal biostromalni diploporni apnenec, ki je pozneje vsled intenzivne diageneze prešel ves v debelozrnat masiven dolomit.

Zahvala

Ministrstvu za visoko šolstvo, znanost in tehnologijo Republike Slovenije in Geološkemu zavodu Slovenije se avtor tega članka zahvaljuje za financiranje sistematičnih regionalnih in detajlnih geoloških raziskav v tem delu Slovenije.

Summary

Ladinian Beds in the Obla Gorica Area, Central Slovenia

In the Obla Gorica area (Figure 1), belonging geotectonically to the boundary region between the Sava Folds and Dolenjsko Mesozoic Blocks, the Ladinian sedimentation is characterised by alternating dark carbonate rocks with a lot of cherts and volcaniclastic rocks represented by tuffs and tuff sandstones.

In the footwall of the Ladinian lithologic succession lies the sparitic, micritic, rarely stromatolitic and brecciated Anisian dolomite, which was in the neotectonic phase pretty tectonized together with younger rocks. The structural and textural characteristics of these rocks show, that the Anisian dolomite was

formed in a shallower shelf sea on the stable Dinaric Carbonate Platform.

Up to present obtained geological data indicate, that in the Obla Gorica area in the lowermost Ladinian (Fassan) there was no sedimentation. Namely, in the considered area the Buchenstein beds have not been established so far.

In the study area the Ladinian, Langobardian beds respectively, are separated in seven lithostratigraphic units, namely (Figure 2): 1 – tuffs with interbeds of carbonate rocks with cherts, 2 – lower platy dolomite with cherts and tuff interbeds, 3 – light grey bedded sparitic dolomite with tuff interbeds, 4 – upper platy dolomite with cherts and tuff interbeds, 5 – dark marly limestone and shaly marlstone, 6 – tuffs with interbeds of tuff sandstones and 7 – dark, bedded and platy, sparitic limestone.

The Ladinian age of the considered succession of carbonate sediments and volcaniclastic rocks has been proved with findings of characteristical daonellas and ammonites. In the considered beds crinoids and small cephalopodes have been found as well, but they have not been determined so far. Radiolarian analysis of several samples of carbonate rocks has not given expected results.

The Ladinian age of considered beds is proved indirectly by their stratigraphic position lying between the concordantly underlying Anisian dolomite and concordantly overlying Cordevolian Dolomite with alga *Diplopora annulata* (Schafhäutl). The dark bedded and platy carbonate rocks with cherts have been formed in a deeper shelf sea with a great contents of silica. The presence of pyrites and the dark colour of these sediments point at a reduction environment.

The formation of volcaniclastic rocks has been connected with an intensive volcanic activity. The fine-grained tuff sediments were formed in a calm pelagic environment with episodic terigenous influence.

The volcaniclastic rocks are pretty clean. They do not contain any larger amount of admixture of older Ladinian rocks or the footwall rocks, what shows, that in this area there was not neither larger tectonic nor erosional activity. Consequently, the Ladinian beds of the area in question were formed in a tectonically active area with vivacious volcanic activity, but with a rather weak erosion of the footwall rocks.

In the passage from Anisian to Cordevolian epoch the bottom of the sea elevated to the level, that the conditions for origin of a new stable carbonate platform were created. On the Cordevolian Carbonate Platform a biostromal *Diplopora* limestone was deposited, which later, due to very intensive diagenetic processes passed completely into the coarse-grained Cordevolian Dolomite.

References

Buser, S. (1965): Geološka zgradba južnega dela Ljubljanskega Barja in njegovega obrobja. *Geologija 8,* pp. 34-57, Ljubljana.

Buser, S. (1969): Osnovna geološka karta SFRJ, list Ribnica 1:100.000. *Zvezni geološki zavod,* Beograd.

Buser, S. (1974): Tolmač lista Ribnica L 33-76. Osnovna geološka karta SFRJ 1:100.000. *Zvezni geološki zavod,* 60 pp., Beograd

Buser, S. (1976): Triasne plasti na listu Ribnica. Mezozoik v Sloveniji, 1. faza, pp. 70, Ljubljana.

Buser, S. (1979): Triassic beds in Slovenia. *16th European Micropaleontological Colloquium* Zagreb-Bled, Yugoslavia,pp. 17-25, Ljubljana.

Demšar, M. & Dozet, S. (2003): Anizijske in ladinijske plasti v profilu nad Sredniško grapo pod Križno goro, osrednja Slovenija, *Geologija,* 46/1, pp. 41-48, Ljubljana.

Dozet, S. (1966): Geološke razmere ozemlja med Laniščem in Polico. Diplomsko delo. *Univerza v Ljubljani – FNT – Oddelek za geologijo,* 65 pp., Ljubljana.

Dozet, S. (1985): Geološke razmere na območju rudišča Pleše in v širši okolici. *Rud.-met. zbornik* 32/1-2, pp. 27-49, Ljubljana.

Dunham: R.J. (1962): Classification of carbonate rocks according to depositional texture. *Mem. Am. Ass. Petrol. Geol.* 1, pp. 108-121, Tulsa.

Folk, R.L. (1959): Practical classification of limestones. *Am. Ass. Petrol. Geol. Bull.* 43/1, pp. 1-38, Tulsa.

Germovšek, C. (1955): O geoloških razmerah na prehodu Posavskih gub v Dolenjski kras med Stično in Šentrupertom. *Geologija 3,* pp. 116-135, Ljubljana.

Kossmat, F. (1913): Die adratische Umrandung in der alpinen Faltenregion. *Mitteilungen d. Geol. Ges.* In Wien. Karte des alpindinarischen Grenzgebietes

Kühn, O., 1954: Triadni cefalopodi z Dolenjskega. *Razprave SAZU,* 4. razr., II, Ljubljana.

Rakovec, I. (1946): Triadni vulkanizem na Slovenskem. *Geogr. vestnik* 18/1-4, pp. 139-170, Ljubljana.

Rakovec, I. (1956): Pregled tektonske zgradbe Slovenije. *Prvi jugosl. Geol. kongres,* pp. 73-83, Ljubljana.

Sedlar, J., Petrov, I. & Čadež, N., (1948): Poročilo o geološkem kartiranju terena Orle-Pleše. *Geološki zavod Slovenije,* 61 pp., Ljubljana

Effect of the grain refinement, modification and the cooling rate on microstructure of the AlSi10Mg alloy

Vpliv udrobnevanja, modificiranja in ohlajevalne hitrosti na mikrostrukturo zlitine AlSi10Mg

Mitja Petrič, Jožef Medved and Primož Mrvar

Faculty of natural science and engineering, Department of materials and metallurgy, University of Ljubljana, Aškerčeva 12, 1000 Ljubljana, Slovenija;
E-mail: primoz.mrvar@ntf.uni-lj.si

Received: November 02, 2006 **Accepted**: November 14, 2006

Abstract: This paper describes the influence of grain refiners, modifiers and cooling rate on microstructure of AlSi10Mg alloy. Solidification of this alloy has been investigated. Investigations have been made by computer simulations on program MAGMASOFT, »in situ« thermal analysis, simultaneous thermal analysis (STA) and metallographic analysis. Investigated alloy AlSi10Mg has been grain refined and modified. By cooling curves at different cooling rates the undercooling and recalescence of primary and eutectic crystallization have been detected and related with largeness of primary crystals of α_{Al} and eutectic phase β_{Si} from eutectic ($\alpha_{Al} + \beta_{Si}$). Also the relation between largeness of microstructural constituents and cooling rate was determined.

Izvleček: Ta članek opisuje vpliv udrobnilnih in modificirnih sredstev ter ohlajevalne hitrosti na mikrostrukturo zlitine AlSi10Mg. Preiskano je bilo strjevanje te zlitine. Preiskava je potekala s pomočjo različnih metod, kot so: računalniška simulacija polnjenja in strjevanja s programom MAGMASOFT, »in situ« termična analiza, simultana termična analiza (STA) in metalografska analiza. Preiskovano zlitino smo udribnjevali in modificirali. Iz ohlajevalnih krivulj posnetih pri različnih ohlajevalnih hitrostih smo določili podhladitve in rekalescence za primarno in evtektsko strjevanje katere smo povezali z velikosttjo primarnih kristalnih zrn αAl in evtektske faze βSi iz evtektika (αAl + βSi). Prav tako je bila opredeljena povezava med velikostjo mikrostrukturnih sestavin in ohlajevalno hitrostjo.

Key words: grain refinement, modification, cooling rate and microstructure
Ključne besede: udrobnevanje, modificiranje, ohlajevalna hitrost in mikrostruktura

Introduction

AlSiX casting alloys are today commonly used because of their properties, as are good castability, mechanical properties and corrosion resistance. Microstructure, which is formed during the solidification, has a great influence on mechanical properties. That is the reasons for examination of the relations between melt and the mould.

During casting of aluminium alloys, defects on castings are common. These defects are usually micro porosity, shrinkage porosity

Scientific paper

and cracks. Reasons for these defects are usually not well-prepared melt and mistakes in the casting technology. To improve soundness of castings one can use grain-refining agents and modifying agents, which improves soundness of castings, causes better feeding and better chemical and mechanical treatment[1,2].

Thermal analysis and chemical analysis are commonly used in foundry to control the state of a melt. With thermal analysis we are monitoring the temperature during solidification. From the cooling curves of the thermal analysis we can predict solidification and microstructure. During crystallization of phases the heat is liberated what is seen on the cooling curves. From characteristic shape of the cooling curves we can identify formation of different phases and predict microstructure even before the casting. If necessary we can modify and grain refine the alloy. It is also possible to predict the level of grain refining and modification from the shape of the cooling curve, undercoolings and recalescences at primary solidification of α_{Al} and eutectic solidification ($\alpha_{Al} + \beta_{Si}$). Unmodified and modified cooling curve are shown in Figure1[3]. The first peak on cooling curve is showing that the liquidus temperature is higher and the recalescence is lower in well grain refined alloy. In a modified alloy eutectic temperature is lower and recalescence is higher[4] (second peak).

EXPERIMENTAL

In present research we used standard blocks of AlSi10Mg alloy from WAV-IMCO producer. The alloy was investigated by several methods, which were: the chemical analysis, computer simulation of cooling rates and cooling curves, simple thermal analysis and metallographic analysis.

Three samples were investigated. First sample was the basic alloy, the second sample was grain refined with B (master alloy of AlB3) and modified with Sr (master alloy of

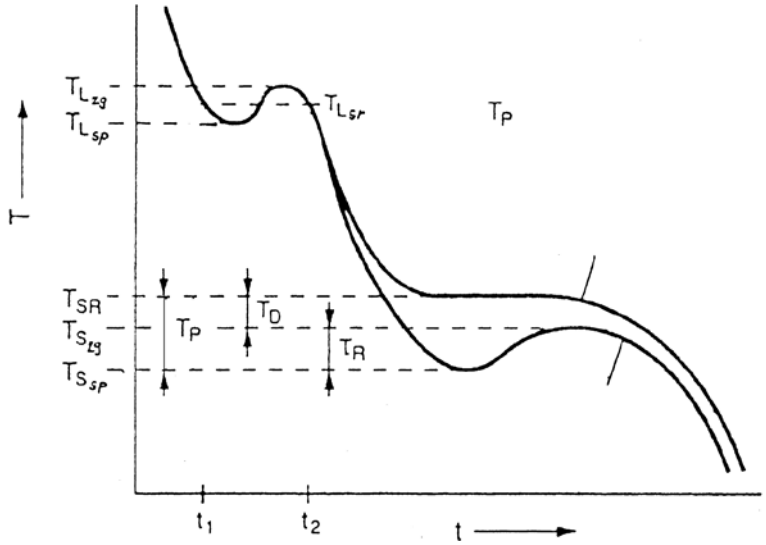

Figure1. Cooling curve of hypoeutectic Al-Si alloy[3]

Table 1. Labels of castings and additions of grain refiners and modifiers

Lable of casting	Grain refiner	Modifier
Vz1	-	-
Vz4	AlB3 – (0.05%B)	AlSr10 – (0.015%Sr)
Vz11	AlTi5B1 – (0.03%Ti)	Silutal 20 – (3%)

AlSr10) and the third one was grain refined with Ti (master alloy of AlTi5B1) and modified with Na (salt mixture of NaCl and NaF). Additions of the grain refiners and modifiers are shown in Table 1. Alloy was melted in the graphite crucibles in an induction furnace. As temperature of 700 °C was reached the grain refiners and modifiers were added and after a minute it was poured into measuring cells. At the addition of the salt mixture the temperature has reached 740 °C, after the salt was melted it was stirred into the melt and after three minutes it was poured into measuring cells.

Simple thermal analysis has been carried out in two measuring cells. The first one was made by Croning process and the second one was newly developed measuring cell called the cone probe made of the grey iron (Figure 2). This measuring cell has a continuous change of cooling rates on overall intersection. K-type thermocouples were used and placed in the center of Croning measuring cell and in the center and top of the cone probe respectively as is shown in Figure 2. Thermocouples were connected to the National Instruments DAQPad-MI0-16XE-50 measuring card and this one further to the personal computer, where the measured values were collected with LabVIEW 5.0 program. Cooling curves were plotted using the Origin 7.0 program.

The cooling curves and the cooling rates were also calculated with computer simulation program MAGMASOFT and chemical compositions were analyzed too respectively.

The specimens for metallographic analyses were cut from the castings of the measur-

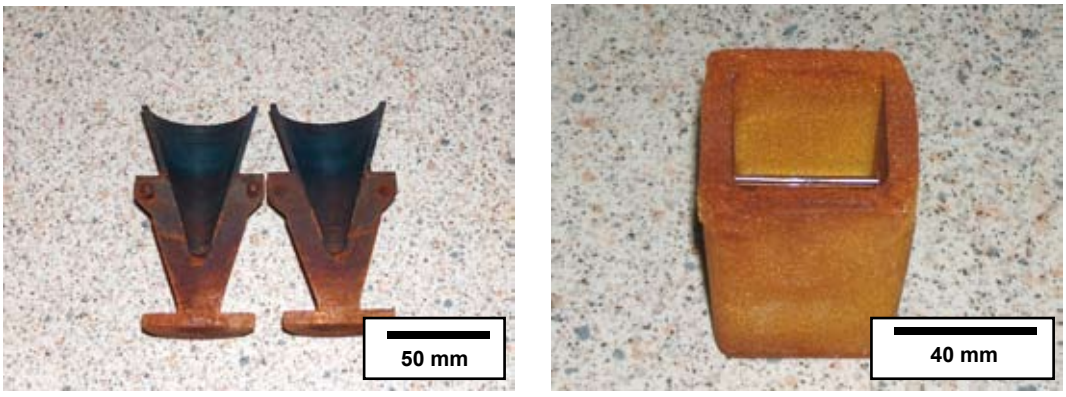

a) **b)**

Figure 2. Measuring cells: measuring cell from the grey iron (a), the standard quick cup probe made by Croning process (b)

ing cells. The samples were prepared by the standard metallographic procedure for optical microscopy and by the anodic oxidation for observation in polarized light. Anodized samples were used for determining the grain size and the others were used for determining the length of the eutectic silicon particles. Grain sizes and the grain size numbers (G) were determined by intercept counting method from ASTM standard with

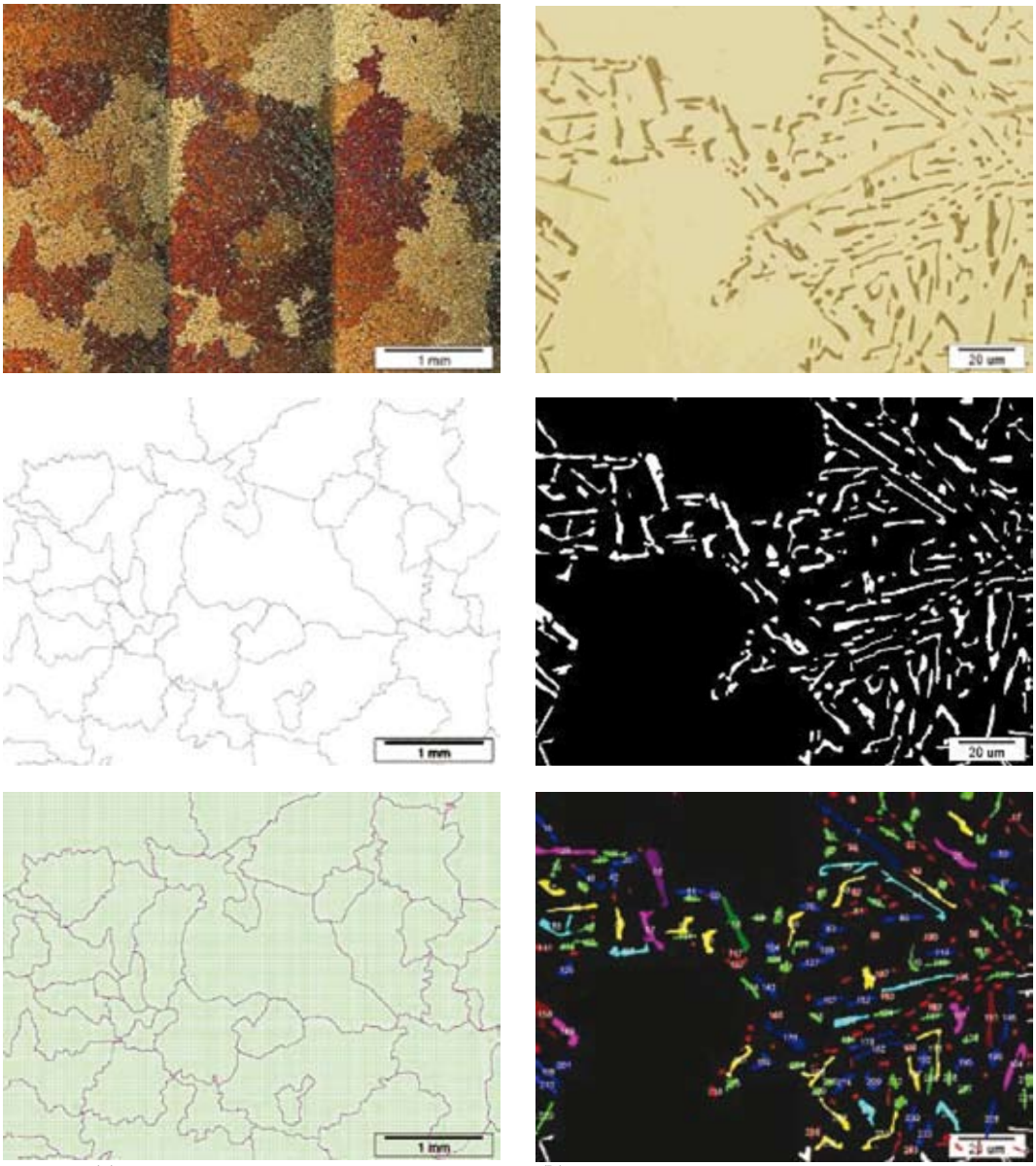

Figure 3. Presentation of the grain size determination (a) and the particle lengths (b)

analySIS 5.0 computer program. Lengths and ratios between the length and the width of the silicon particles were also determined by the analySIS 5.0 computer program. Figure 3 is showing procedures for determining grain size and particle lengths.

Results And Discussion

AlSi10Mg alloy was used at present research. This alloy contains about 10 mass % Si, 0,4 mass % Mg. Tables 2 and 3 show chemical compositions of the alloy before and after the experiment. One can see that composition is changed after the experiment, because of the addition of the grain refining and the modifying agents.

The filling, solidification, cooling rates and cooling curves for the sample in the cone probe were calculated with the computer simulation program of MAGMASOFT. Figure 4 is showing the cooling rates in overall section off the cone probe. The cooling curves were calculated in the spots shown in Figure 4 and they are similar to experimentally determined cooling curves. Figure 5 is presenting the calculated and the experimentally determined cooling curves from the cone probe for a basic alloy (Vz 1).

The calculated cooling rates are: 19 K/s on the spot A, 38 K/s on spot B and 176 K/s on spot C. Measured cooling rates are similar and in average are: 20 K/s on spot A and 43 K/s on spot B. On the spot C the measurement was impossible because the cooling rate was too high. Cooling rate in quick cup of the measuring cell was the lowest. It was 6,3K/s in average. Cooling curves of all three specimens and the derivate curve of the specimen Vz.1 are shown on Figure 6 respectively.

Microstructure of AlSi10Mg alloy is composed of the dendrite crystals of α_{Al} and of the eutectic ($\alpha_{Al} + \beta_{Si}$). It is better for mechanical properties if microstructural constituents of α_{Al} and of the eutectic ($\alpha_{Al} + \beta_{Si}$) are finer. For grain refining we used master alloys of AlTi5B1 and AlB3. With this master al-

Table 2. Chemical composition of the basic alloy

Element	Si	Fe	Mn	Mg	Zn	Ti
Mas.%	10.815	0.663	0.066	0.334	0.037	0.052
Cr	Ni	Pb	Sn	Ca	Cu	Al
0,008	0.005	0.005	0.002	0.004	0.066	87.943

Table 3. Chemical compositions of the castings after investigations

Element (Mas. %)	Si	Fe	Cu	Mn	Mg	Cr	Ni
Vz. 1	9.981	0.678	0.068	0,076	0,348	0,009	0,006
Vz. 4	9.811	0.698	0.081	0.076	0.383	0.011	0.007
Vz. 11	10.456	0.649	0.075	0.077	0.183	0.010	0.009
Element (Mas. %)	Zn	Ti	Ag	B	Na	Sr	Al
Vz 1	0.053	0.047	0.006	0.00016	<0.0001	<0.0003	Ostalo
Vz 4	0.034	0.063	0.006	0.0948	<0.0001	0.0173	Ostalo
Vz 11	0.038	0.081	0.006	0.0059	0.014	<0.0003	Ostalo

loys we introduce nuclei for heterogeneous nucleation into the melt[3,5]. At the primary crystallization the undercooling is lower and α_{Al} crystals are smaller[6].

For modification of the eutectic silicon we used master alloy of AlSr10 and the mixture of salts containing sodium. These two agents are the reason for modification of silicon from lamellar structure to fibrous structure[7] (particles become rounder). This affects on the cooling curve as depression of the eutectic temperature and the recalescence[8] (Figure 1).

The characteristic temperatures such as liquidus, eutectic and the solidus were determined from the cooling curves obtained on the quick cup measuring cell (Figure 6). The temperatures are shown in Table 4. Unmodified alloy has the liquidus temperature of 581.9 °C and the recalescence of 2.5 °C. The eutectic temperature is 570 °C and the recalescence about 0.5 °C. The specimen grain refines and modified with B and Sr has the highest liquidus temperature at 593.3 °C and there is no recalescence. The eutectic temperature is at 563.9 °C and the higher recalescence 2.5 °C respectively. Lower recalescence at the primary solidification and the higher one at the eutectic solidification is a good sign of well grain refined and well modified alloy. Similarly as for the specimen 4 is for the specimen 11 grain refined and modified with Ti and Na. Liquidus temperature is at 587.6 °C, the recalescence is 0.3 °C.

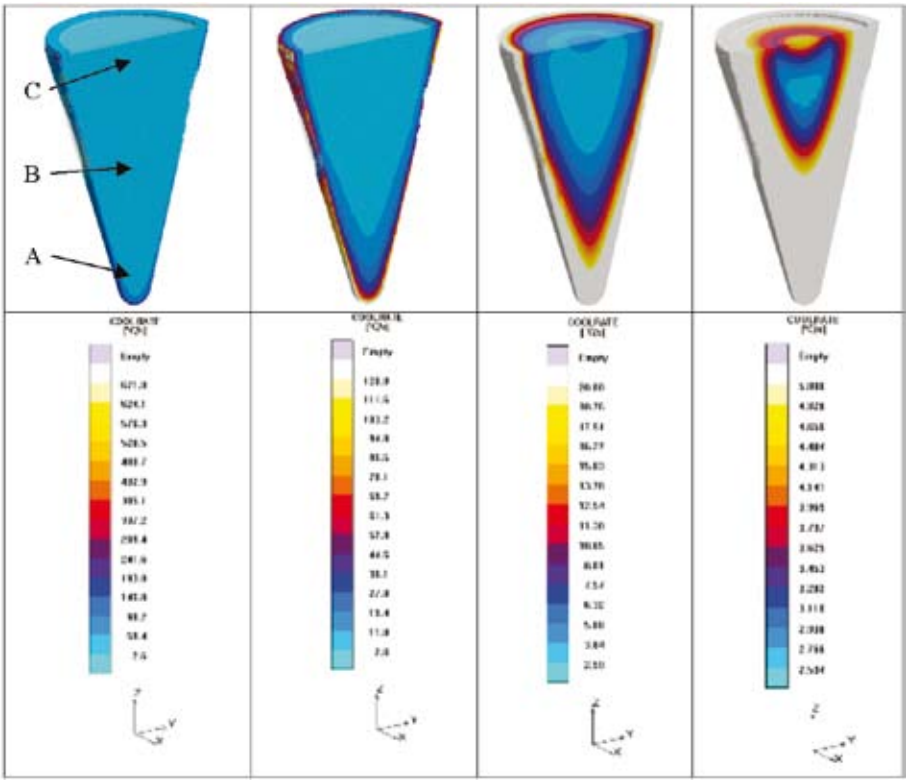

Figure 4. Cooling rates on the overall section of the cone probe

Table 4. Typical temperatures on the cooling curves

	V_{cool} [K/s]	T_{pour} [°C]	T_L^{min} [°C]	T_L^{max} [°C]	T_E^{min} [°C]	T_E^{max} [°C]	T_{E2}^{Mg2Si} [°C]	T_S [°C])	dT_L [°C]	dT_E [°C]
Vz. 1	7.2	680	582.0	584.5	570.0	570.5	549.2	527.0	2.5	0.5
Vz. 4	6.8	688	593.3	593.3	563.9	566.7	548.9	533.7	0	2.8
Vz. 11	4.7	731	587.6	587.9	562.7	564.5	550.2	537.4	0.3	1.8

At the eutectic temperature of 562.3 °C the recalescence is 1.8 °C.

We determined grain sizes and grain size numbers (G) for the all specimens. The largest crystals were in specimen of the basic alloy from quick cup measuring cell where was the lowest cooling rate. With the higher cooling rate the grain size dropped from 2079 μm to 310.8 μm. In the sample of Vz.4 the grain refined with B is the smallest grain size. At the lowest cooling rate of 6.3 K/s it is 184.9 μm and at the cooling rate of 176 K/s it is only 96.2 μm. In the sample of Vz.11 the grain size is 881.3 μm at the lowest cooling rate and 271.6 μm at highest cooling rate respectively. All the data are collected in Table 5 and the microstructures are presented in Figures 7, 8 and 9.

Table 5. Grain sizes and the grain size numbers for all specimens on the different measuring spots

Sample	Vz.1		Vz.4		Vz.11	
	G	l_{sr} [μm]	G	l_{sr} [μm]	G	l_{sr} [μm]
Quick cup	-5.4	2079	1.6	184.9	-2.9	881.3
C	-2	637.8	2.1	153.7	-1.8	595.9
B	0.1	329.9	3.3	101.5	0.5	267.5
A	0.1	310.8	3.5	96.2	0.5	271.6

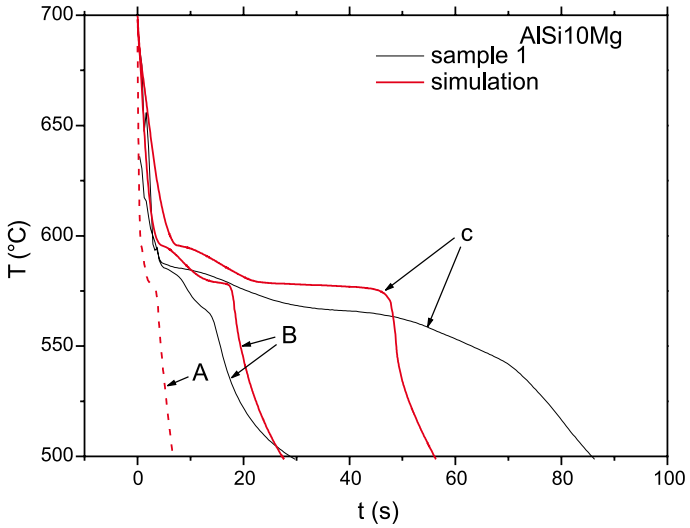

Figure 5. Calculated cooling curves and the measured cooling curves of the sample Vz.1

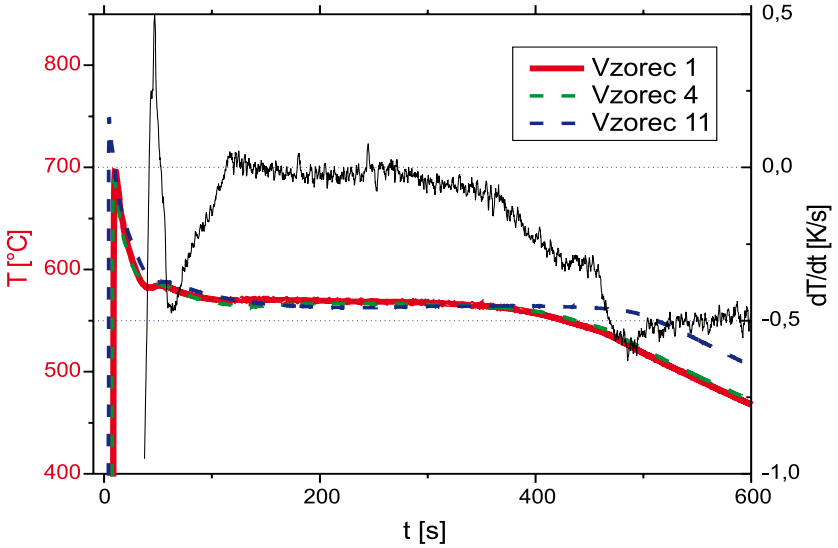

Figure 6. Cooling curve and the derivative curve of the specimen Vz.1 and the cooling curves of specimens Vz.4 and Vz.11

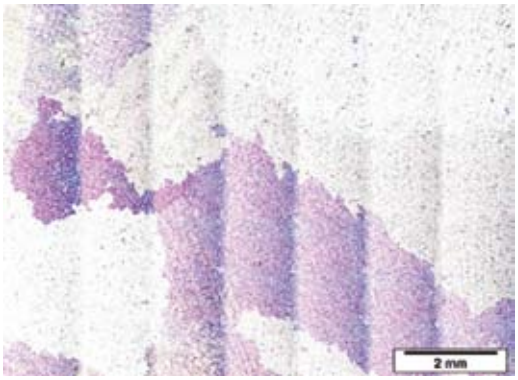

(a) Quick cup (6.3 K/s)

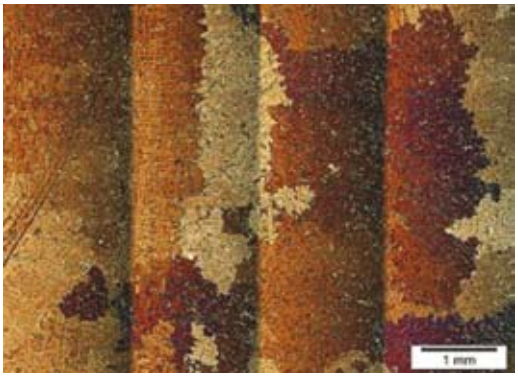

(b) Cone probe – C (19 K/s)

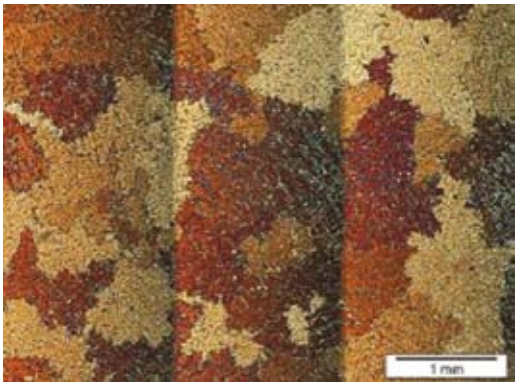

(c) Cone probe – B (38 K/s)

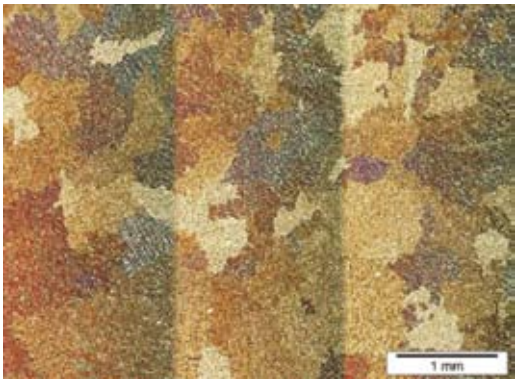

(d) Cone probe – A (176 K/s)

Figure 7. Microstructure of the sample Vz.1 (basic alloy) in the polarised light

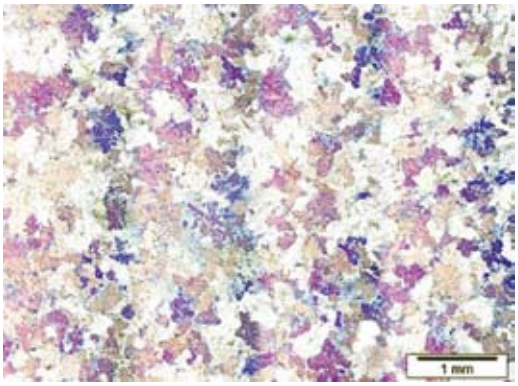

(a) Quick cup (6,3 K/s)

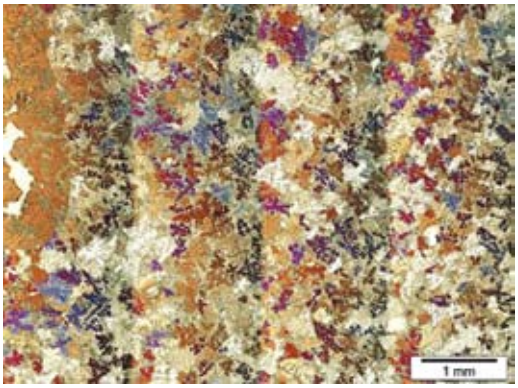

(b) Cone probe – C (19 K/s)

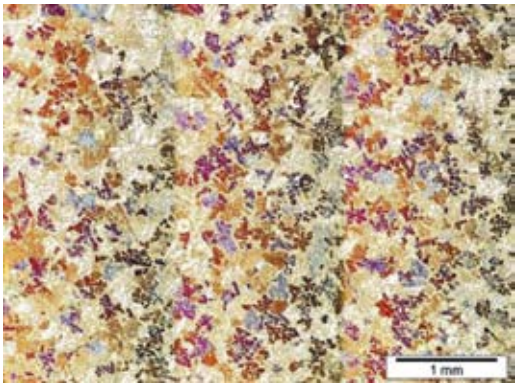

(c) Cone probe – B (38 K/s)

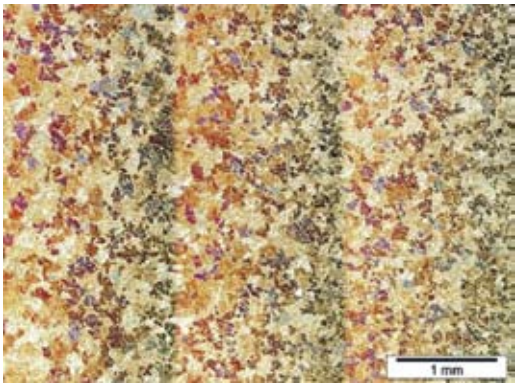

(d) Cone probe – A (176 K/s)

Figure 8. Microstructure of specimen Vz.4 (grain refined with B, modified with Sr) in the polarised light

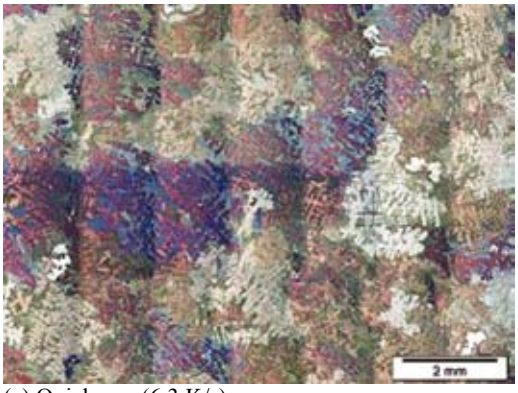

(a) Quick cup (6.3 K/s)

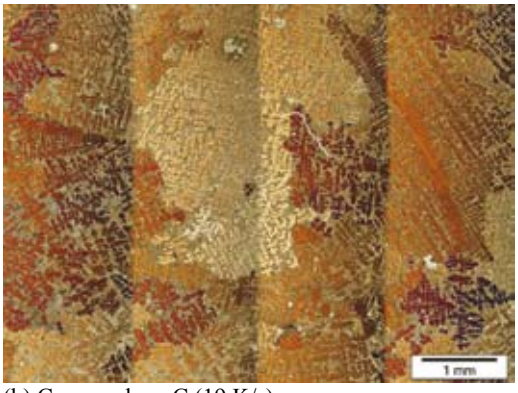

(b) Cone probe – C (19 K/s)

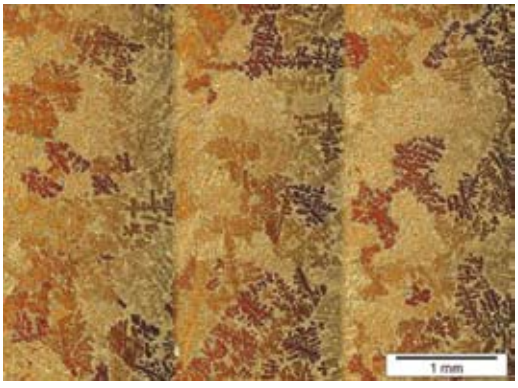

(c) Cone probe – B (38 K/s)

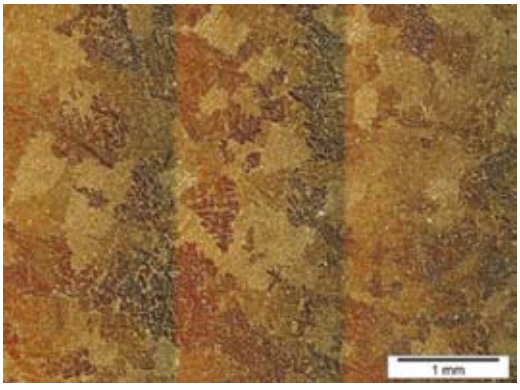

(d) Cone probe – A (176 K/s)

Figure 9. Microstructure of the specimen Vz.11 (grain refined with Ti, modified with Na) in the polarised light

The lengths of the silicon particles were determined too. The largest particles were in the unmodified alloy (sample Vz.1). At cooling rate of 6.7 K/s the average length was 15.644 μm. Particle length is also decreasing with the higher cooling rate and it reached 4.951 μm at the highest one. The length of the particles of the sample of Vz.4 modified with Sr became shorter and rounder. At the lowest cooling rate the length is 4.959 μm and at highest one it is only 0.507 μm. In the sample modified with Na the results are the best. Particles are only 1.190 μm long at the lowest cooling rate and 0.578 μm at the highest cooling rate. Table 6 is showing average lengths of the particles and ratios between length and width. Microstructures are presented in Figures 10, 11 and 12.

Table 6. The silicon particle lengths and ratios for all the specimens on the different measuring spots

Sample	Vz.1		Vz.4		Vz.11	
	l [μm]	l/d	l [μm]	l/d	l [μm]	l/d
Quick cup	15.644	3.7	4.959	3.6	1 190	1.9
C	6.354	3.3	1.619	2.0	1.120	1.9
B	6.157	3.3	0.682	2.1	0.626	1.7
A	4.951	2.4	0.507	1.8	0.578	2.3

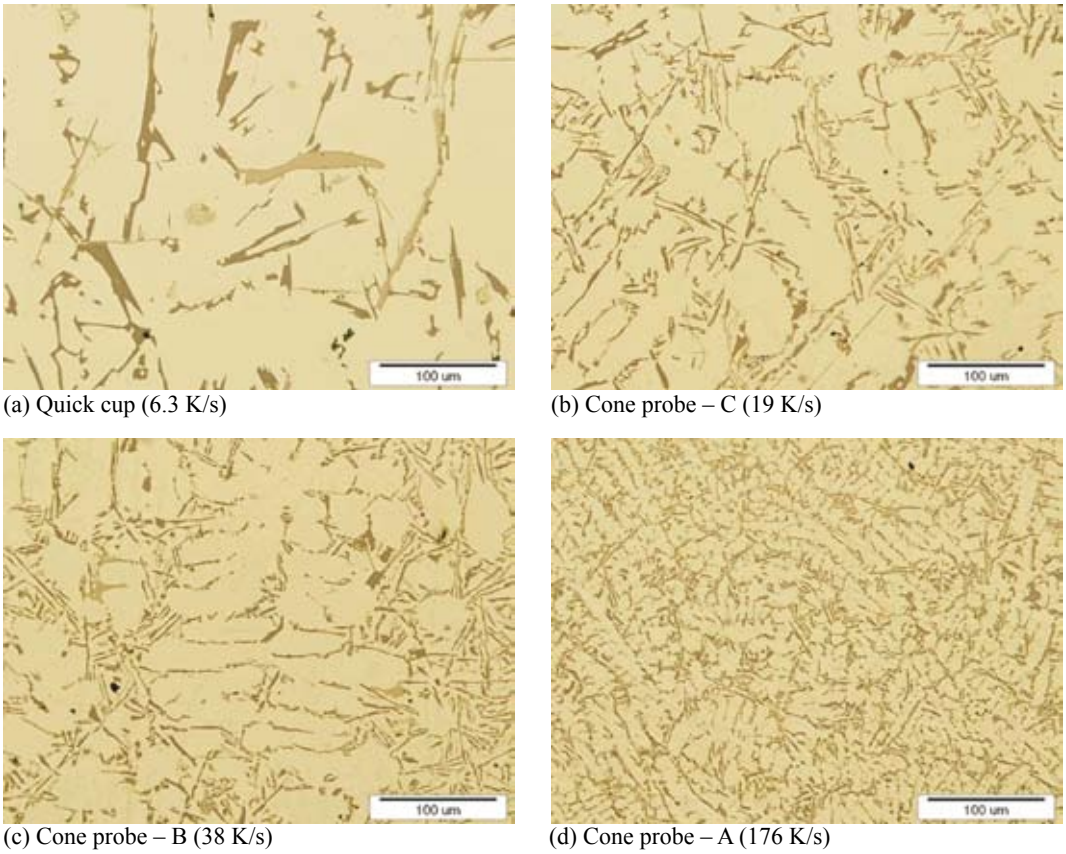

(a) Quick cup (6.3 K/s)

(b) Cone probe – C (19 K/s)

(c) Cone probe – B (38 K/s)

(d) Cone probe – A (176 K/s)

Figure 10. Microstructure of the sample Vz.1 (basic alloy)

As a result two diagrams are showing the relationship between largeness of the microstructural constituents and the cooling rate for the range of 6 K/s to 176 K/s. Figures 12 and 13 are showing relationship between largeness of the crystals and of the eutectic silicon particles as the function of the cooling rate. We also calculated the physical model for the grain size reduction and the eutectic silicon particle reduction as the function of the cooling rate. Fitted exponential curves are also shown on Figures 13 and 14. Equations and parameters of the fitted curves are collected in Table 7.

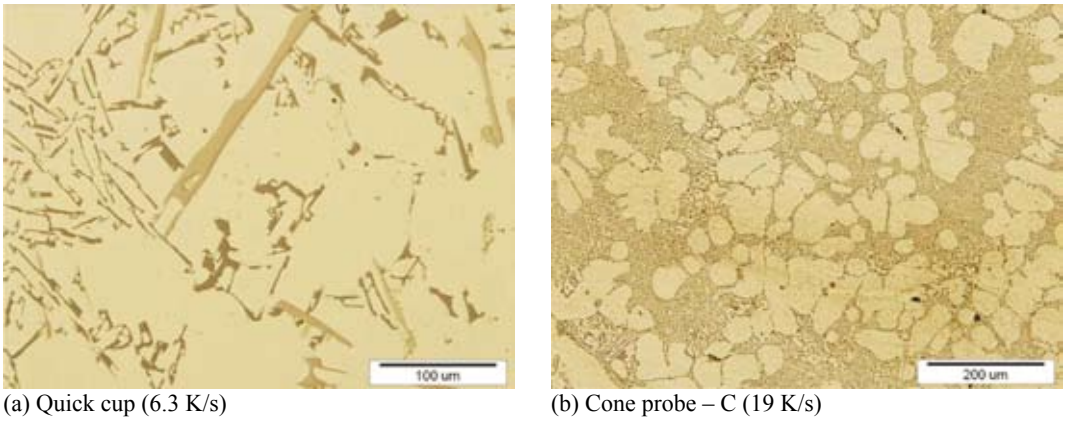

(a) Quick cup (6.3 K/s) (b) Cone probe – C (19 K/s)

(c) Cone probe – B (38 K/s) (d) Cone probe – A (176 K/s)

Figure 11. Microstructure of the specimen Vz.4 (grain refined with B, modified with Sr)

Table 7. Equations and parameters of the calculated physical models

Grain size	Model	R^2	y0	A1	t1
Vz.1	y=A1exp(-x/t1)+y0	0.99999	307.41226 +/-4.21092	4080.72927 +/-40.58991	7.55081 +/-0.09232
Vz.4		0.97071	97.10749 +/-0.47917	142.64657 +/-4.3781	17.38183 +/-0.63481
Vz.11		0.97292	262.866 +/-1.97866	1079.5082 +/-24.6731	14.59254 +/-0.35247
Particle length					
Vz.1	y=A1exp(-x/t1)+y0	0.99044	5.52465 +/-0.61155	34.20882 +/-19.42654	5.17144 +/-2.49776
Vz.4		0.99994	0.52289 +/-0.02266	8.84548 +/-0.13965	9.12575 +/-0.20775
Vz.11		0.86737	0.54676 +/-0.20373	0.89092 +/-0.37989	25.70911 +/-22.90963

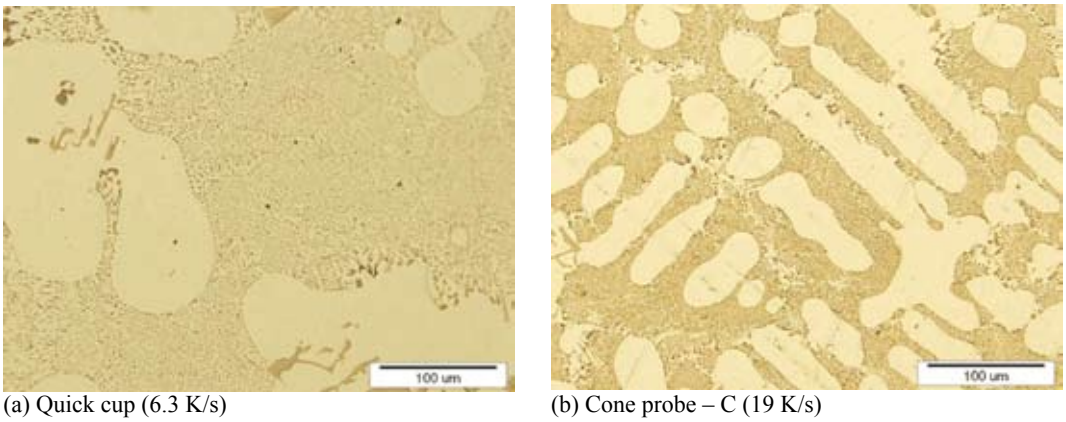

(a) Quick cup (6.3 K/s)
(b) Cone probe – C (19 K/s)
(c) Cone probe – B (38 K/s)
(d) Cone probe – A (176 K/s)

Figure 12. Microstructure of the specimen Vz.11 (grain refined with Ti, modified with Na)

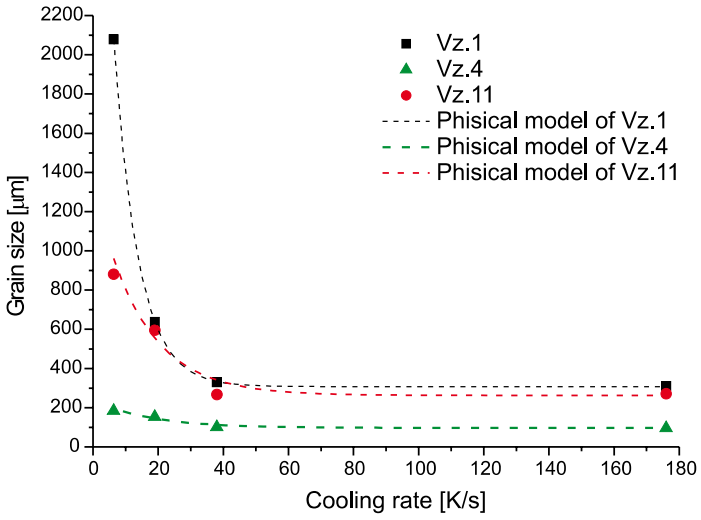

Figure 13. Grain size of the primary α_{Al} crystals as the function of the cooling rate at the solidification and the calculated physical models

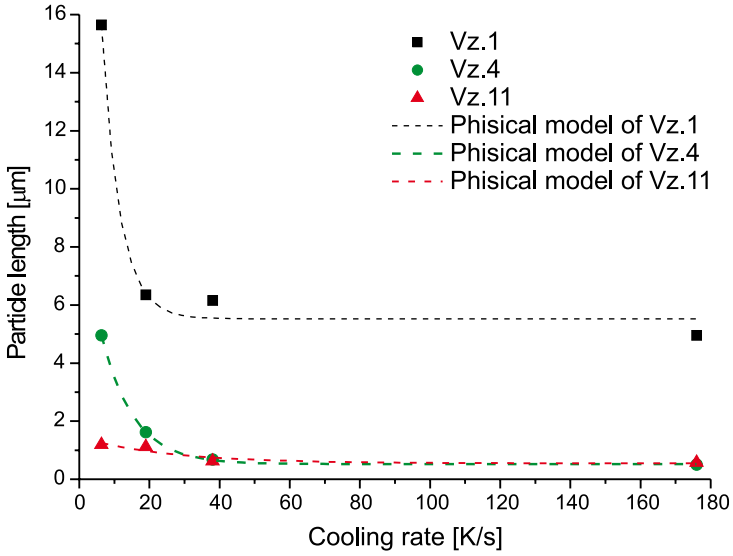

Figure 14. Silicon particle length as the function of the cooling rate and the calculated physical models

Conclusions

»In situ« thermal analysis is very good and simple tool to predict the microstructure of the Al-Si alloys. This method gives also the informations of the nucleating potential of an alloy and is measured from the liquidus and the solidus temperature on the cooling curve after the thermal analysis. Both criterions show the levels of the grain refinement and modification.

From measurement in quick cup measuring cell we determined liquidus temperatures and the recalescences at the primary solidification and the eutectic temperatures and the recalescences at eutectic solidification. Liquidus temperature in the specimen grain refined and modified with B and Sr is about 11 °C higher than in unmodified alloy and there is no recalesccence. At specimen grain refined and modified with Ti and Sr the liquidus temperature is 5.5 °C higher than in unmodified alloy and recalescence of 0.3 °C is occurring. Higher liquid temperature and the lower recalescence at the primary solidification is a good sign of well done grain refinement.

In modified alloys the eutectic temperature is usually lower and the higher recalescence is occurred. In the specimen grain refined and modified with B and Sr the eutectic temperature is 6 °C lower than in unmodified alloy and the recalescecnce is 2.8 °C. In the unmodified specimen the recalescence is only 0.5 °C. In the specimen grain refined and modified with Ti and Na the liquidus temperature is 7 °C lower and recalescence is 1.8 °C. These are also good signs of a well modified alloy.

These findings are also confirmed by the microstructural analysis. The biggest grain size is in the unmodified alloy. It is in range from 2.1 mm at lowest cooling rate to 330 µm at highest one. In the grain refined specimen

with B the grain size is from 185 μm to 96 μm and in the grain refined specimen with Ti the grain size is from 881 μm at lowest cooling rate to 271 μm at highest one.

Similar results are with length of the eutectic silicon. The length has shortened from 15 μm in the quick cup measuring cell of the unmodified alloy to 0.5 μm in the Sr modified alloy at highest cooling rate.

This research is applicable in industry at the high-pressure die-casting and at the gravity die-casting where the thickness of the castings is not unique and the cooling rates are different. In thick parts of the castings the largeness of the eutectic silicon particles and the grain size are bigger so it would be necessary to use the grain refinement and modification. From the calculated diagrams and the fitted physical models it is possible to determine the level of the grain refinement and modification.

Povzetek

Vpliv udrobnevanja, modificiranja in ohlajevalne hitrosti na mikrostrukturo zlitine AlSi10Mg

Namen preiskave je bil ugotoviti učinkovitost različnih udrobnilnih sredstev in modificirnih sredstev za pridobitev finejših zmesnih kristalov α_{Al} in vlaknatega evtektskega silicija. Preiskave smo izvedli na podevtektski zlitini AlSi10Mg, pri čemer smo oplemenitenje oziroma modificiranje (udrobnitev zmesnih kristalov α_{Al} in modificiranje evtektika (α_{Al} + β_{Si}) izvedli z različnimi udrobnilnimi in/ali modificirnimi sredstvi. Zlitino smo talili v indukcijski peči, nato pa smo dodajali različne količine udrobnilnih in modificirnih sredstev.

Za oceno udrobnitve primarnih zmesnih zrn α_{Al} in modificiranja evtektskega silicija smo uporabili naslednje analize: enostavno termično analizo in metalografsko analizo, pri čemer smo vzorce opazovali v svetlem polju in polarizirani svetlobi.

Analizirali smo tri vzorce. Prvi je bil osnovna, neoplemenitena zlitina, drugi je bil modificiran z borom in stroncijem in tretji s titanom in natrijem.

Vzorce smo ulili v dve merilni celici. Prva je bila narejena po postopku Croning, druga pa je bila tako imenovana stožčasta proba iz sive litine. Med strjevanjem smo izvedli »in situ« enostavno termično analizo in iz zbranih podatkov dobili ohlajevalne krivulje in izračunali ohlajevalne hitrosti.

S pomočjo računalniške simulacije smo izračunali polnjenje livne votline stožčaste probe in strjevanje litine. Prav tako smo izračunali tudi ohlajevalne hitrosti na mestih meritve. Izračunani in eksperimentalno dobljeni podatki se dobro ujemajo. Izračunane ohlajevalne hitrosti so bile na mestu meritve A znašajo 176 K/s, na mestu B 38 K/s in na mestu C 19 K/s.

Pri opisu makro in mikrostrukture smo določili velikosti izločenih primarnih zmesnih kristalov α_{Al} in delcev evtektsko izločenega silicija. To smo izvedli s pomočjo svetlobnega mikroskopa in računalniškega programa analySIS 5.0 z integriranim standardom ASTM E 112 – 96. Za določevanje velikosti primarnih zrn smo vzorce opazovali v polarizirani svetlobi, za določevanje ve-

likosti delcev evtektskega silicija pa smo vzorce opazovali v svetlem polju.

Iz podatkov smo izdelali dva diagrama, ki podajata odnos med ohlajevalno hitrostjo in velikostjo zmesnih kristalov in delcev evtektskega silicija. Na podlago teh podatkov in dobljenih krivulj smo izračunali še fizikalni model, ki podaja eksponentno padajočo odvisnost med velikostjo kristalnih zrn in delcev evtektskega silicija ter ohlajevalno hitrostjo. Iz njih je razvidno, da so v primeru neoplmenitene zlitine (vzorec Vz.1) pri počasnem ohlajanju (6,3 K/s), zrna v povprečju velika približno 2 mm. Pri zlitini udrobneni z B (vzorec Vz.4) so pri enaki ohlajevalni hitrosti zrna stokrat manjša in pri vzorcu udrobnenem s Ti (vzorec Vz.11) so zrna velika približno 880 μm. Z večjo ohlajevalno hitrostjo se velikost zrn v vseh primerih zmanjša, največji učinek pa ima leta pri osnovni zlitini. Pri največji ohlajevalni hitrosti (167 K/s) so ta velika cca. 310 μm, v vzorcu Vz.4 so velika samo 96 μm in v vzorcu Vz.11 le 270 μm. Iz teh podatkov je jasno, da je zelo dobro udrobnilno sredstvo Ti, prav tako tudi B, slaba stran slednjega pa je, da talina postane nagnjena k poroznosti. Učinek udrobnenja teh sredstev se še poveča z večjo ohlajevalno hitrostjo.

Na velikost in obliko izločanja evtektskega silicija prav tako vplivajo ohlajevalna hitrost in modificirna sredstva. Z večjo ohlajevalno hitrostjo in z dodatkom modificirnih sredstev se delci evtektskega silicija β_{Si} izločajo bolj fino in zaobljeno. Pri vzorcu osnovne, neoplemenitene zlitine (vzorec Vz.1), se pri počasnem ohlajanju lamele izločajo s povprečno dolžino cca. 15 μm in razmerjem med dolžino in širino 3,7. Pri najvišji ohlajevalni hitrosti pa je dolžina delcev 5 μm razmerje med dolžino in širino 2,4. Vzorec modificiran s Sr (vzorec Vz.4) ima dolžino lamel pri majhni ohlajevalni hitrosti cca. 5 μm in razmerje med dolžino in širino 3,6, pri najvišji ohlajevalni hitrosti pa 0,2 μm in razmerje 1,8. Pri vzorcu modificiranem z Na (vzorec Vz.11) so delci evtektskega silicija najmanjši pri vseh ohlajevalnih hitrostih. Delci so pri najmanjših ohlajevalnih hitrostih dolgi le 0,9 μm in razmerje med dolžino in širino 1,8. Pri velikih ohlajevalnih hitrostih pa delci dosegajo 0,2 μm razmerje pa se malce poveča zaradi prečne usmerjenosti vlaken evtektskega silicija na mestu meritve.

References

[1] Davis, J.R.. ASM Specialty Handbook, Aluminium and Aluminium Alloys. ASM International, 1993, pp. 220 – 224.

[2] Terčelj, Milan, Kugler, Goran, Turk, Radomir. Temperature na drsni površini orodja med toplo ekstruzijo aluminija. V: VIŽINTIN, Jože (ur.), BEDENK, Janez (ur.), KALIN, Mitjan (ur.). *Zbornik predavanj posvetovanja o pogonskih in alternativnih gorivih, tribologiji in ekologiji*. Ljubljana: Slovensko društvo za tribologijo: = Slovenian Society of Tribology, 2004, 2004, 171-187 f.

[3] Trbižan, Milan, Smolej, Anton, Turjak, Igor. Termična analiza podevtektskih AlSi zlitin. Zbornik referatov, 35. livarsko posvetovanje, Portorož, 1994, pp. 180-189.

[4] Mrvar Primož, Medved Jožef, Modifikacija slitine AlSi10Mg s Ti, B i Sr i kontrola nukleacijskog potencijala. Ljevarstvo 47, 2005.

[5] Ruddle, W., Ronald. Grain refinement. Proceedings of The conference on thermal analysis of moltem aluminium, Illinois 11.-12.12. 1985, str. 77-100.

[6] Bäckerud, Lenart, Król, Eva, Tamminen, Jarmo. Solidification characteristic of aluminium alloys: volume 1: wrought alloys. Norway: Tangen Trykk, 1986, str. 30-36.

[7] Pan, E.N., Cherng, Y.C., Lin, C.A., Chiou, H.S.. Roles of Sr and Sb on Silicon Modification of A356 Aluminium Alloys. Transactions of the American foundry Society, vol. 102, Illinois 1.-4.5. 1994, str. 609-629.

[8] Mrvar, Primož, Trbižan, Milan, Medved, Jože. Solidification of aluminium cast alloys investigated by the dilatation analysis. *Metalurgija (Sisak)*, 2001, god. 40, br. 2, str. 81-84.

Temperature field analysis of tunnel kiln for brick production

J. Duraković, S. Delalić

University of Zenica, Faculty of Metallurgy and Materials Science,
Travnicka cesta 1, 72000 Zenica, BiH;
E-mail: jusuf.durakovic@famm.unze.ba

Received: September 25, 2006 **Accepted**: November 14, 2006

Abstract: Today researches in the field of brick production mostly deal with problem of fuel consumption. Average specific fuel consumption in brick production lines is approximately 2100 kJ per 1kg of the product. Such values are in engineering praxis considering as very high.

Ovens in ceramics industry are optimized according to requested quality of products which ought to be made with minimal fuel consumption. This can be successfully achieved only if the burners are supplied with sufficient amount of energy and if energy of burned materials are connected or included into the process of increasing supplied energy thus affect the sintering curve.

This work is an approach of determination of temperature fields in tunnel kiln for brick production.

Keywords: Brick production, Tunnel kiln, Temperature field

Introduction

Uneven distribution of temperature through the sections of material layers, starting from the bottom then all over to the top of the kiln, is a very common occurrence in brick production.

Hence, row bricks material at the lower sections normally stay at lower temperature, while upper sections of materials do with sharp increasing temperature. Thus the temperature curves of raw materials in this temperature area show some differences. To some extent, equalizing of the temperature across the heigh of raw clay might be adequately done by using circulatory equipment. As a consequence, relatively significant differences in temperature field occur in that area, primarily due to the energy set up by fuel combustion. Top sections of clay are exposed to high temperature level for some time. Middle and lower sections are also subjected to sharp temperature increasing during the heating process. Process optimization described by mathematical model should offer reliable proof about parameters with strongest influence on desired values. Modeling is required for those parameters that significantly affect the production process. Others should be included by correlations[1-3].

Energy balance mostly consists of flue gas energy then, temperature of the product at the kiln exit, preheated air temperature, maximal temperature of sintering process, additional volume of air used as a heat transfer medium and possible volume of air pull out of the cooling area[4-6]. Heat transfer

Scientific paper

direction regarding the kilt conveyer direction of movement in tunnel kiln might be of less interest then the vertical heat transfer which forms mechanism of heat transfer by a lateral convection[7].

MATHEMATICAL MODEL

Fuel consumption by unit of a product in brick production considerably affects the price of a final product. Hence the final goal of any brick manufacturer is a production by optimal fuel consumption and at the same time with required and satisfactory quality of product. Thus the different approaches and possibilities of decreasing specific fuel consumption have been investigated.

For mathematical analysis of all significant parameters that affect the fuel consumption in tunnel kiln, it is necessary to define temperature field inside kiln. Main heat transportation medium in the kiln is fuel gas, so in order to get the relationship that define temperature field in kiln, current state and conditions inside it must be taken into consideration[8]. According to these conditions appropriate partial differential equation has to be set up. Modified partial differential equation that describes heat transfer is as follows[9]:

$$M \cdot \frac{\partial^2 U(x,y,z,t)}{\partial t^2} + H \cdot \frac{\partial U(x,y,z,t)}{\partial t} - K^2 \cdot \nabla^2 U(x,y,z,t) = F(x,y,z,t) \tag{1}$$

where are:

- M, mass of the medium,
- U, spatial coordinate and time dependent function connects physical meaning of parameters M, H, and K^2, and function F(x, y, z, t),
- H, heat transfer resistant factor or specific force that cause change in velocity of field U by time t,
- K, specific force that cause change in acceleration of field U by spatial variable Fexternal force cause changes in field state, and $\nabla^2 U$, Laplace's operator.

If M is too small comparing to H, and if field U is independent of time t, changing only when the spatial coordinates are changing, then finally if we assumed that area of interest for consideration is of quadrilateral shape and negligible comparing to overall length L of tunnel kiln, expression (1) became:

$$-K^2 \cdot \frac{\partial^2 U(x)}{\partial x^2} = F(x) \tag{2}$$

In this case U(x) means temperature and can be replaced by abbreviation for absolute temperature T(x). Boundary conditions are $U_{(0)}=u_0$, $U_{(L)}=u_L$.

Solution is obtained in three phases.
First, since the U(x) depends only of x coordinate, partial derivation can be expressed as a ordinary derivation:

$$\frac{d^2U(x)}{dx^2} = -\frac{F(x)}{K^2} \tag{3}$$

Which means that G(x) function whose second derivation is G"(x) have to be found by integration as follows:

$$G(x) = \int \left\{ \int \left[-\frac{F(x)}{K^2} \right] dx \right\} dx \tag{4}$$

Second, desire field function U(x) is obtained by equation (5):

$$U_{(x)} = G_{(x)} + A \cdot x + B \tag{5}$$

where A and B are the random constants.
A and B are defined according to boundary conditions of field function U(x), that are: $U_{(0)}=u_0$, $U_{(l)}=u_{L.}$

$$U(x) = G(x) + \left[uL - u0 - G(L) + G(0) \right] \cdot \frac{x}{L} + u0 - G(0) \tag{6}$$

If upon the temperature field acts external force F(x), it cause "echo", so the temperature field U(x) has obtained form. Function U(x) is echo function of temperature field equilibrium (the balance of thermal state of the system). Function U(x) is produced through the balance of external force F(x) and force that causes changes in U(x) field only when x variable is changing time independent. This working regime is characteristics for many heat aggregates. While keeping the temperature during the time, thermal aggregate is in state of equilibrium. This state became stationary after some time of oven heating. To determine real U(x) function all before mentioned parameters must be defined: the length L, then U_0 and $U_{L.}$.

The most important step is determination of parameter K– giving its value followed by dimension and unit. H function influence on equilibrium state might be negligible since it is assumed that U is time independent function, so it can be written that H = 1. Function F(x) depends of heat conducted into the kiln. The discretization above aimed to enable easier computer modeling and calculation, but also form step approximation of function F(x). Sense of the discretization is to replace all functions $F_{(t,T,x,y,z)}$ which depend of time, spatial coordinates and place inside the kiln, with set of discrete values.

Equilibrium function

Starting point is assumption that there exists a relationship between final product characteristics and factors such as: temperature field regime inside the kiln, refractory linings, carriage and product. This relationship is very complex by its nature (affected by nature of factors by itself as well as by number of different influencing factors). Manufacturing process essentially is a mechanism that realizes mentioned relationships in a way that each product is accompanied by values of certain campaign for which temperature equivalent of heating the chamber, that is actually fuel consumption per 1 kg of product, can be measured.

Temperature equilibrium data has been presented by measured heating curve (Figure 1) from which values of the coordinates x and

Table 1. Measuring points and temperatures in the chamber

T_1 (0.0 m, 30 ^{0}C)	T_2 (3.9 m, 65 ^{0}C)	T_3 (19.9 m, 400 ^{0}C)	T_4 (25.1 m, 440 ^{0}C)
T_5 (30.8 m, 460 ^{0}C)	T_6 (36.9 m, 600 ^{0}C)	T_7 (43.2 m, 710 ^{0}C)	T_8 (45.8 m, 780 ^{0}C)
T_9 (48.4 m, 825 ^{0}C)	T_{10} (51.0 m, 860 ^{0}C)	T_{11} (53.6 m, 865 ^{0}C)	T_{12} (56.2 m, 865 ^{0}C)
T_{13} (58.8 m, 865^{0}C)	T_{14} (61.4 m, 865 ^{0}C)	T_{15} (71.6 m, 800 ^{0}C)	T_{16} (82.6 m, 710 ^{0}C)
T_{17} (88.0 m, 660 ^{0}C)	T_{18} (118,0 m, 60 ^{0}C)		

Abbreviated as Ti ($de_{[i]}$, $ve_{[i]}$), i = 1,2,...,18.

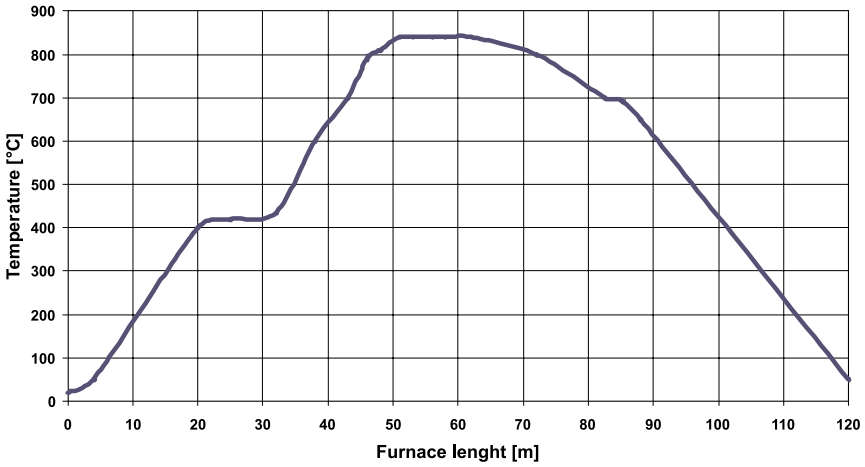

Figure 1. Measured heating curve

y were taken: x (distance from starting point or enter into the chamber) and y (temperature equivalent of the external force).

From the diagram in Figure 1, 18 points with their coordinates have been taken and separately presented in Table 1.

External force function is unknown since the K value is also unknown. But values of the temperature given in Figure 1 might be taken as a thermal energy equivalent used to obtained force F. Then, external force is presented as:

$$F_x = \begin{cases} V_{[i]} & if\ x = de_{[i]} \\ & i = 1,2,3.. \\ 0 & if\ x \neq de_{[i]} \end{cases} \quad (7)$$

where is $V_{[i]} = ve_{[i]}/(K^2)$.

Desired function $G_{(x)}$ for which is $G_{(x)}=F_{(x)}$ or

$$G'(x) = \int_{de[i]}^{x} F(x)dx \quad . \quad (8)$$

Integration results in:

$$G_{(x)} = V_{[i]} \text{ for } de_{[i]} \leq x \leq de_{[i+1]},\ i = 1,2,3.... \quad (9)$$

And finally:

$$Gi_{(x)} = ci \cdot x + ci, \text{ for } de_{[i]} \leq x \leq de_{[i+1]},\ i = 1,2,3 \quad (10)$$

Function of the temperature field is expressed as:

$$T_{(x)} = Gi_{(x)} + c_{i1} \cdot x + c_{i2}, \text{ for } de_{[i]} \leq x \leq de_{[i+1]},\ i = 1,2,3.... \quad (11)$$

Following conditions must be fulfilled:

$$T(de_{[i]}) = V_{[i]}, \qquad i = 1,2,3.... \tag{12}$$

and:

$$Gi(de_{[i]}) = g(i) = g = g_{(i+1)} = Gi(de_{[i+1]}), \qquad i = 1,2,3.... \tag{13}$$

And the last step is to obtain values for $T_{(x)}$:

$$T_{(X)} = V_{[i]} + \frac{(V[i+1] - V[i])}{(de[i+1] - de[i])} \cdot (x - de[i]) \tag{14}$$

It is clear that $T(de_{[i]}) = V_{[i]}$ i $T(de_{[i+1]}) = V_{[i+1]}$, for i = 1,2,3....

Equation (14) describes the function of temperature equilibrium and thus the temperature field in a chamber after longer heating process.

The way in which temperature field in chamber has been generated, is shown in Figure 2. Computer program was developed on Delphi 3 programming language base at Faculty of Metallurgy and Materials Science, University of Zenica.

Results

For the determination of temperature field inside the kiln chamber it is common to use term "temperature equivalent of heat"[10]. Then, in initial Equation (1) instead of temperature, the heat that can be expressed by temperature, mass and specific heat, was included. This explain the reasons for usage of the temperature as a heat equivalent. Area closed by temperature curve and horizontal axis (Figure 2) represents the total heat necessary for achieving requested temperature

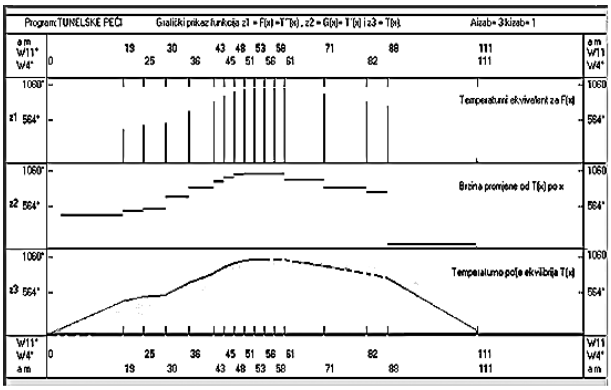

Figure 2. Temperature field output - testing case

inside the kiln. This enables determination of temperature equivalents in kiln as well as heat capacity.

The diagram (Figure 2) consists of three parts. Third part (Z_3) illustrates T(x) function. It is clear that this part match completely to the curve which is used for determination of T(x) function (Figure 1). This verify that temperature field inside the kiln can be obtained theoretically.

First part of the diagram (Z_1) represents temperature equivalent of the external force which is calculating according to expression $F(x) = T''(x)$. Finally, the second part of the diagram (Z_2) shows the rate of temperature change T(x) if x coordinate is changing. Function $G'(x) = T'(x)$ is also presented on this part of diagram.

CONCLUSIONS

In our work presented and discussed mathematical model is appropriate for analysis and checking of a stationary temperature field in brick products and in the furnace. Using developed software, it is possible to execute a simulation of temperature distribution in furnace during a brick production process in real conditions.

REFERENCES

[1] L. M. FARG: Evaluation and optimization of an Egyptian tunnel kiln, Ziegelindustrie International, 9/2003.

[2] W. HOFFMANN: Mathematische Grundlagen und Modellierung, Keramische Zeitschrift, 54/2003.

[3] H. SCHMIDT: Maβnahmen zur Begegnung von Schadesbildungen an Ziegeln beim Bremen, Ziegelindustrie International, 33/1991.

[4] W. LEISENBERG: Reduzierung des Gesamtwearmeverbrauches im Ziegelwerk durch Mabnahmen am Ofen, Keramische Zeitschrift, 11/1985

[5] F. PAVLIN, B. KOSEC, M. BIZJAK, M.C. FERFOLJA: Temperature Profil Measurements in Wellman Type Annealing Furnaces, RMZ – Materials and Geoenvironment, 46 (1999) 1, 86 – 87.

[6] R. JESCHAR, H.G. BITNER: Possibilities for the optimization of tunnel kiln processes in the brick and tile industry Quality improvement and reduction in energy consumption, Ziegelindustrie International, 10/1989.

[7] R. JESCHAR, H.G. BITTNER: A Mathematical Model for Layout and Optimization of Tunnel Furnace Processes in the Field of Ceramic Industry, 12th IMACS World Congress on Scientific Computation,Conference proceedings, 1988

[8] Y.V. DESHMULH: Industrial Heating, Taylor & Francis, Boca Raton, 2005.

[9] R. JESCHAR, K. JUNGE: Heat transfer in counter-flow kilns, Gas Wearme International, 5/1980.

[10] L. MICHALSKI, K. ECKERSDORF, I. MCGHEE: Temperature Measurement, John Wiley &Sons, Chichester, 1991.

Autor's Index, Vol. 53, No. 3

(NEW) INSTRUCTIONS TO AUTHORS (from Sep. 2003)

RMZ-MATERIALS & GEOENVIRONMENT (RMZ- Materiali in geookolje) is a periodical publication with four issues per year (established 1952 and renamed to RMZ-M&G in 1998). The main topics of contents are Mining and Geotechnology, Metallurgy and Materials, Geology and Geoenvironment.
RMZ-M&G publishes original Scientific articles, Review papers, Technical and Expert contributions (also as short papers or letters) **in English**. In addition, evaluations of other publications (books, monographs, …), short letters and comments are welcome. A short summary of the contents in Slovene will be included at the end of each paper. It can be included by the author(s) or will be provided by the referee or the Editorial Office.
**** Additional information and remarks for Slovenian authors:***
English version with extended "Povzetek", and additional roles (in Template for Slovenian authors) ***can*** *be written. Only exceptionally the articles in the Slovenian language with summary in English will be published. The contributions in English will be considered with priority over those in the Slovenian language in the review process.*

Authorship and originality of the contributions. Authors are responsible for originality of presented data, ideas and conclusions as well as for correct citation of data adopted from other sources. The publication in RMZ-M&G obligate authors that the article will not be published anywhere else in the same form.

Specification of Contributions

Optimal number of pages of full papers is 7 to 15, longer articles should be discussed with Editor, but 20 pages is limit.
Scientific papers represent unpublished results of original research.
Review papers summarize previously published scientific, research and/or expertise articles on the new scientific level and can contain also other cited sources, which are not mainly result of author(s).
Technical and Expert papers are the result of technological research achievements, application research results and information about achievements in practice and industry.
Short papers (Letters) are the contributions that contain mostly very new short reports of advanced investigation. They should be approximately 2 pages long but should not exceed 4 pages.
Evaluations or critics contain author's opinion on new published books, monographs, textbooks, exhibitions …(up to 2 pages, figure of cover page is expected).
In memoriam (up to 2 pages, a photo is expected).
Professional remarks (Comments) cannot exceed 1 page, and only professional disagreements can be discussed. Normally the source author(s) reply the remarks in the same issue.

Supervision and review of manuscripts. All manuscripts will be supervised. The referees evaluate manuscripts and can ask authors to change particular segments, and propose to the Editor the acceptability of submitted articles. Authors can suggest the referee but Editor has a right to choose another. **The name of the referee remains anonymous**. The technical corrections will be done too and authors can be asked to correct missing items. The final decision whether the manuscript will be published is made by the Editor in Chief.

The Form of the Manuscript

The manuscript should be submitted as a complete hard copy including figures and tables. The figures should also be enclosed separately, both charts and photos in the original version. In addition, all material should also be provided in electronic form on a diskette or a CD. The necessary information can conveniently also be delivered by E-mail.

Composition of manuscript is defined in the attached Template

The original file of Template is temporarily available on E-mail addresses:
joze.pezdic@ntfgeo.uni-lj.si, joze.pezdic@guest.arnes.si
barbara.bohar@ntf.uni-lj.si

References – can be arranged in two ways:
- first possibility: alphabetic arrangement of first authors – in text: (Borgne, 1955),
or
- second possibility: [1] numerated in the same order as cited in the text: example[1]

Format of papers in journals:

Le Borgne, E. (1955): Susceptibilite magnetic anomale du sol superficiel. *Annales de Geophysique*, 11, pp. 399-419.

Format of books:

Roberts, J. L. (1989): Geological structures, *MacMillan, London*, 250 p.

Text on the hard print copy can be prepared with any text-processor. The electronic version on the diskette, CD or E-mail transfer should be in MS Word or ASCII format.
Captions of figures and tables should be enclosed separately. **Figures (graphs and photos)** and tables should be original and sent separately in addition to text. They can be prepared on paper or computer designed (MSExcel, Corel, Acad)
Format. Electronic figures are recommended to be in CDR, AI, EPS, TIF or JPG formats. Resolution of bitmap graphics (TIF, JPG) should be at least 300 dpi. Text in vector graphics (CDR, AI, EPS) must be in MSWord Times typography or converted in curves.
Color prints. Authors will be charged for color prints of figures and photos.
Labeling of the additionally provided material for the manuscript should be very clear and must contain at least the lead author's name, address, the beginning of the title and the date of delivery of the manuscript. In case of an E-mail transfer the exact message with above asked data must accompany the attachment with the file containing the manuscript.
Information about RMZ-M&G:
Editor in Chief prof. dr. Jože Pezdič (tel. ++386 1 4704-633) or
Secretary Barbara Bohar Bobnar, un. dipl. ing. geol. (++386 1 4704-630),
Aškerčeva 12, Ljubljana, Slovenia

or at E-mail addresses:
joze.pezdic@ntfgeo.uni-lj.si, joze.pezdic@guest.arnes.si
barbara.bohar@ntf.uni-lj.si

Sending of manuscripts. Manuscripts can be sent by mail to the **Editorial Office** address:
- RMZ-Materials & Geoenvironment
  Aškerčeva 12,
  1001 Ljubljana, Slovenia

or delivered to:
- **Reception** of the Faculty of Natural Sciences and Engineering (for RMZ-M&G)
  Aškerčeva 12, Ljubljana
- E-mail – addresses of Editor and Secretary
- You can also contact them on their phone numbers.

These instructions are valid from September 2003

TEMPLATE

The title of the manuscript should be written in bold letters (Times New Roman, 14, Center)

Name Surname[1], …. , & Name Surname[X] (Times New Roman, 12, Center)

[x]Faculty of ... , University of ... , Address…, Country, e-mail: ... (Times New Roman, 12, Center)

THE LENGTH OF FULL PAPER SHOULD NOT EXCEED TWENTY (20, INCLUDING FIGURES AND TABLES) PAGES (OPTIMAL 7 TO 15), SHORT PAPER FOUR (4) AND OTHER TWO (2) WITHOUT TEXT FLOWING BY GRAPHICS AND TABLES.

Abstract(Times New Roman, Bold/Normal, 11): The text of the abstract is placed here. The abstract should be concise and should present the aim of the work, essential results and conclusion. It should be typed in font size 11, single-spaced. Except for the first line, the text should be indented from the left margin by 10 mm. The length should not exceed fifteen (15) lines (10 are recommended).

Key words: a list of up to 5 key words (3 to 5) that will be useful for indexing or searching. Use the same styling as for abstract.

Introduction (Times New Roman, Bold, 12)

Two lines below the keywords begin the introduction. Use Times New Roman, font size 12, Justify alignment.

There are two (2) admissible methods of citing references:

1. by stating the first author and the year of publication of the reference in the parenthesis at the appropriate place in the text and arranging the reference list in the alphabetic order of first authors; e.g.:
   "Detailed information about geohistorical development of this zone can be found in: Antonijević (1957), Grubić (1962), ..."
   "… the method was described previously (Hoefs, 1996)"
2. by consecutive Arabic numerals in square brackets, superscripted at the appropriate place in the text and arranging the reference list at the end of the text in the like manner; e.g.:
   "... while the portal was made in Zope[3] environment."

Results and discussion (Times New Roman, Bold, 12)

Tables, figures, pictures, and schemes should be incorporated (inserted, not pasted) in the text at the appropriate place and should fit on one page. Break larger schemes and tables into smaller parts to prevent extending over more than one page.

Conclusions (Times New Roman, Bold, 12)

This paragraph summarizes the results and draws conclusions.

Acknowledgements (Times New Roman, Bold, 12, Center - optional)

This work was supported by the ****.

References (Times New Roman, Bold, 12)

Regardless of the method used, in the reference list, the styling, punctuation and capitalization should conform to the following:

FIRST OPTION – in alphabetical order

Casati, P., Jadoul, F., Nicora, A., Marinelli, M., Fantini-Sestini, N. & Fois, E. (1981): Geologia della Valle del'Anisici e dei gruppi M. Popera – Tre Cime di Lavaredo (Dolomiti Orientali). *Riv. Ital. Paleont.*; Vol. 87, No. 3, pp. 391-400, Milano.

Folk, R. L. (1959): Practical petrographic classification of limestones. *Amer. Ass. Petrol. Geol. Bull.;* Vol. 43, No. 1, pp. 1-38, Tulsa.

SECOND OPTION – in numerical order

[1] Trček, B. (2001): *Solute transport monitoring in the unsaturated zone of the karst aquifer by natural tracers.* Ph.D. Thesis. Ljubljana: University of Ljubljana 2001; 125 p.

[2] Higashitani, K., Iseri, H., Okuhara, K., Hatade, S. (1995): Magnetic Effects on Zeta Potential and Diffusivity of Nonmagnetic Particles. *Journal of Colloid and Interface Science 172*, pp. 383-388.

Citing the Internet site:

CASREACT-Chemical reactions database [online]. Chemical Abstracts Service, 2000, updated 2.2.2000 [cited 3.2.2000]. Accessible on Internet:<http://www.cas.org/CASFILES/casreact.html>.

Povzetek (Times New Roman, 12)

A short summary of the contents in Slovene (up to 400 characters) can be written by the author(s) or will be provided by the referee or by the Editorial Board.

TEMPLATE for Slovenian Authors

The title of the manuscript should be written in bold letters (Times New Roman, 14, Center)

Naslov članka (Times New Roman, 14, Center)

Name Surname[1], …. , & Name Surname[X] (Times New Roman, 12, Center)
Ime Priimek[1], …, Ime Priimek[X] (Times New Roman, 12, Center)

[x]Faculty of ... , University of ... , Address…, Country; e-mail: ... (Times New Roman, 12, Center)
[X]Fakulteta…, Univerza…, Naslov…, Država; e-mail: … (Times New Roman, 12, Center)

THE LENGTH OF ORIGINAL SCIENTIFIC PAPER SHOULD NOT EXCEED TWENTY (20, INCLUDING FIGURES AND TABLES) PAGES (OPTIMAL 7 TO 15), SHORT PAPER FOUR (4) AND OTHER TWO (2) WITHOUT TEXT FLOWING BY GRAPHICS AND TABLES.
DOLŽINA IZVIRNEGA ZNANSTVENEGA ČLANKA NE SME PRESEGATI DVAJSET (20, VKLJUČNO S SLIKAMI IN TABELAMI), STROKOVNEGA ČLANKA ŠTIRI (4) IN OSTALIH PRISPEVKOV DVE (2) STRANI.

Abstract(Times New Roman, Bold/Normal, 11): The text of the abstract is placed here. The abstract should be concise and should present the aim of the work, essential results and conclusion. It should be typed in font size 11, single-spaced. Except for the first line, the text should be indented from the left margin by 10 mm. The length should not exceed fifteen (15) lines (10 are recommended).

Izvleček(TNR, B/N, 11): Kratek izvleček namena članka ter ključnih rezultatov in ugotovitev. Razen prve vrstice naj bo tekst zamaknjen z levega roba za 10 mm. Dolžina naj ne presega petnajst (15) vrstic (10 je priporočeno).

Key words: a list of up to 5 key words (3 to 5) that will be useful for indexing or searching. Use the same styling as for abstract.

Ključne besede: seznam največ 5 ključnih besed (3-5) za pomoč pri indeksiranju ali iskanju. Uporabite enako obliko kot za izvleček.

Introduction – Uvod (Times New Roman, Bold, 12)

Two lines below the keywords begin the introduction. Use Times New Roman, font size 12, Justify alignment. All captions of text and tables as well as the text in graphics must be prepared in English and Slovenian language.

Dve vrstici pod ključnimi besedami se začne Uvod. Uporabite pisavo Times New Roman, velikost črk 12, z obojestransko poravnavo. Naslovi slik in tabel (vključno z besedilom v slikah) morajo biti pripravljeni v slovenskem in angleškem jeziku.

There are two (2) admissible methods of citing references – obstajata dve sprejemljivi metodi navajanja referenc:

1. by stating the first author and the year of publication of the reference in the parenthesis at the appropriate place in the text and arranging the reference list in the alphabetic order of first authors; e.g.:
1. z navedbo prvega avtorja in letnice objave reference v oklepaju na ustreznem mestu v tekstu in z ureditvijo seznama referenc po abecednem zaporedju prvih avtorjev; npr.:
   "Detailed information about geohistorical development of this zone can be found in: Antonijević (1957), Grubić (1962), ..."
   "… the method was described previously (Hoefs, 1996)"
2. by consecutive Arabic numerals in square brackets, superscripted at the appropriate place in the text and arranging the reference list at the end of the text in the like manner; e.g.:
2. z zaporednimi arabskimi številkami v oglatih oklepajih na ustreznem mestu v tekstu in z ureditvijo seznama referenc v številčnem zaporedju navajanja; npr.;
   "... while the portal was made in Zope[3] environment."

Results and discussion – Rezultati in razprava (Times New Roman, Bold, 12)

Tables, figures, pictures, and schemes should be incorporated (inserted, not pasted) in the text at the appropriate place and should fit on one page. Break larger schemes and tables into smaller parts to prevent extending over more than one page.

Tabele, sheme in slike je potrebno vnesti (z ukazom Insert, ne Paste) v tekst na ustreznem mestu. Večje sheme in tabele je potrebno ločiti na manjše dele, da ne presegajo ene strani.

Conclusions – Sklepi (Times New Roman, Bold, 12)

This paragraph summarizes the results and draws conclusions.
Povzetek rezultatov in zaključki.

Acknowledgements – Zahvale (Times New Roman, Bold, 12, Center - optional)

This work was supported by the ****.

References - Viri (Times New Roman, Bold, 12)

Regardless of the method used, in the reference list, the styling, punctuation and capitalization should conform to the following:
Ne glede na uporabljeno metodo pri seznamu citiranih referenc upoštevajte naslednjo obliko:

FIRST OPTION – in alphabetical order (v abecednem zaporedju)

Casati, P., Jadoul, F., Nicora, A., Marinelli, M., Fantini-Sestini, N. & Fois, E. (1981): Geologia della Valle del'Anisici e dei gruppi M. Popera – Tre Cime di Lavaredo (Dolomiti Orientali). *Riv. Ital. Paleont.*; Vol. 87, No. 3, pp. 391-400, Milano.

Folk, R. L. (1959): Practical petrographic classification of limestones. *Amer. Ass. Petrol. Geol. Bull.;* Vol. 43, No. 1, pp. 1-38, Tulsa.

SECOND OPTION – in numerical order (v numeričnem zaporedju)

[1] Trček, B. (2001): *Solute transport monitoring in the unsaturated zone of the karst aquifer by natural tracers.* Ph.D. Thesis. Ljubljana: University of Ljubljana 2001; 125 p.

[2] Higashitani, K., Iseri, H., Okuhara, K., Hatade, S. (1995): Magnetic Effects on Zeta Potential and Diffusivity of Nonmagnetic Particles. *Journal of Colloid and Interface Science 172*, pp. 383-388.

Citing the Internet site:

CASREACT-Chemical reactions database [online]. Chemical Abstracts Service, 2000, updated 2.2.2000 [cited 3.2.2000]. Accessible on Internet:<http://www.cas.org/CASFILES/casreact.html>.

Citiranje internetne strani:

CASREACT-Chemical reactions database [online]. Chemical Abstracts Service, 2000, obnovljeno 2.2.2000 [citirano 3.2.2000]. Dostopno na svetovnem spletu: <http://www.cas.org/CASFILES/casreact.html>.

Povzetek – Summary (Times New Roman, 12)

An extended summary of the contents in Slovene (from one page to approximately 1/3 of the original article length).
Razširjeni povzetek vsebine prispevka v Angleščini (od ene strani do približno 1/3 dolžine izvirnega članka).

Citation and indexing of RMZ-Materials and geoenvironment
(Število citatov in indeksiranja člankov RMZ-M&G)
(prepared by Pezdič, J. - from search done by Šercelj, M., CTK Ljubljana

Citation index according to Web of Science 1970 –2006:

110 papers have 165 citations (4x before 1998, max. 49x in 2004)
(110 člankov je bilo citirano 165 krat – 4x pred 1998; največ 49x v letu 2004))

No. of indexing of RMZ- M&G in singular Databases
(Število indeksiranih člankov iz RMZ- M&G v posameznih bazah)

	Database Name	Total		before 1998
1:	Civil Engineering Abstracts	773	770	3
2:	CA SEARCH® - Chemical Abstracts® (1967- present)	760	475	285
3:	Inside Conferences	313	237	76
4:	Materials Business File	253	253	
5:	METADEX®	164	38	126
6:	ANTE: Abstracts in New Technologies and Engineering	158	158	
7:	GeoRef	154	30	124
8:	Aluminium Industry Abstracts	36	9	27
9:	PASCAL	30		30
10:	Energy Science and Technology	27		27
11:	TEME - Technology and Management	27		27
12:	Ei Compendex®	13		13
13:	CSA Aerospace & High Technology Database	12	12	
14:	Computer and Information Systems	10	10	
15:	Mechanical & Transportation Engineering Abstracts	8	7	
16:	Engineered Materials Abstracts®	3		3
17:	Corrosion Abstracts	3	3	
18:	Analytical Abstracts	1		1
19:	FLUIDEX	1		1
20:	Solid State and Superconductivity Abstracts	1	1	
21:	Electronics and Communications Abstracts	1	1	
		2748	**2004**	**744**

- Total No. of Databases (število vseh baz): 21
- No. of new bases in RMZ-M&G after 1998 (število novih baz v RMZ-M&G po 1998): **7**
- Total No. of indexing (število indeksov skupaj): 2748
- No. of indexing after 1998 (število indeksov po 1998): 2004
- No. of indexing between 1970-1998 (število indeksov med 1970-1998): 744

RMZ - Materials and Geoenvironment

RMZ-M&G, Vol. 53, No. 3 pp. 285-417 (2006)

Contents